THE AMERICAN UNIVERSITY IN CAIRO

SCHOOL OF SCIENCES AND ENGINEERING

Development and characterization of biodegradable biorenewable polymeric nanocomposites for food packaging applications

A Thesis Submitted to

The Chemistry Master's Program with Specialization in Food Chemistry

in partial fulfilment of the requirements for

the degree of Master of Science

By:

Samar Mohamed Ahmed Fadl

Under the supervision of

Prof. Tarek Madkour

5/25/2015

Acknowledgement

As I look back to the beginning of this journey, I realize that what I have achieved would have been impossible without the help and support of multitude people.

First and foremost, I would like to express my sincere appreciation to my supervisor, Professor Dr. Tarek Madkour, for all his support, mentoring and suggestions throughout the course of this research and particularly towards the end of this work. I especially acknowledge him for his patience and his unceasing encouragements to me and to my colleagues.

Special thanks are given to Dr. Nahed Yacoub for her encouragement, support, and trust. She is such a devoted professor, I am grateful I met such a decent person. I would like also to thank Dr. Shahinaz Abd El Rahman for giving me the opportunity to volunteer as a teacher assistant under her supervision. This opportunity has polished my skills and has paved the way to many challenging prospects. A special thank is also dedicated to Dr. Adham Ramadan for giving us the chance to enjoy the nanotechnology classes. Attending Dr. Adham's classes is such pleasant and challenging, I have learnt a lot by attending only two of his classes.

I would like to convey my heartfelt appreciation to Mr. Mahmoud Abd El Moez, Mr. Emad Raafat, and Mr. Samir Nabhan. I would like to express my deepest appreciation to Mr. Ahmed Omia for his utter dedication, his diligence, and his continuous help to the graduate students at the Chemistry and the Nanotechnology programs. I would like also to thank Eng. Ihab Salama and Eng. Ahmed Ghazaly at the STRC Center and my colleague Ahmed Khalifa at the STA program for their kind help and support. I am also grateful to the young research assistants Mostafa Shaheen and Zeinab Hamid for their help and dedication during this research work.

I would also like to express my deepest gratitude to my dearest brother Denis Mutiibwa, for his absolute support, without his devotion, guidance, and encouragement I would not have embarked on this journey. I would like also to wholeheartedly thank Dr. Nicholas Lees-Gayed for his kind support, his trust, and his guidance.

I would like to specially thank my father Mohamed Fadl, my mother Madiha Mahgoub, my sisters, and my brother. They are the inspiration for making me what I am and they will always be the motivation for what I will ever be. A very special thank is dedicated to my elder sister Sylvia Fadl for her genuine support, encouragement, patience, devotion, guidance, prudence, care and love throughout my life. No words can express my gratitude to her. I am also grateful to my brother in law, Mohamed Elsayed Ismail for his kind support and guidance throughout this journey. It is hard to express my gratitude to my husband, Samual Daoud for his endless love, encouragement, patience, and guidance. I would like also to thank my colleagues and friends for their continuous encouragement and support.

 Last but not least, this work would have been impossible without the generous fellowship provided by Mo Ibrahim Foundation. A special thank is dedicated to Dr. Mohamed Ibrahim and Dr. Ahmed Ibrahim for their kind attention and encouragement. A special thank is also dedicated to Charles Bailey Fellowship for their kind support during the last year.

Abstract

During the last 10 decades, plastic products have dominated humans' lives with various applications in different fields, and particularly in food packaging industry. The fact that plastics do have numerous desirable characteristics does not conceal their detrimental effect on the environment and on human health. In order to overcome these problematic issues and to contribute to sustainable development in the future, other alternatives represented in employing biorenewable biodegradable polymers are implemented for plastics production.

Poly (lactic acid) (PLA) is one of the most common employed biopolymer owing to its interesting characteristics. However, PLA exhibits poor mechanical and barrier properties. Natural plasticizers and nano-reinforcement are incorporated into PLA matrix in order to overcome its brittle nature and to improve its barrier properties, particularly for the purpose of food packaging applications.

This research focused on two parts: (i) improving the toughness and flexibility of PLA by investigating the effect of addition of three different plasticizers, namely, polyethylene glycol (PEG), tri n-butyl citrate (TBC), and triacetin (TA) of different concentrations using cast solution method, and (ii) PLA/TA 10%, the best investigated combination among all in terms of mechanical properties, was then chosen as the base system to further investigate the effect of incorporating four different nano-reinforcements, namely, carbon nanotubes (CNT), COOH functionalized carbon nanotubes (CNTCOOH), graphene platelets (GNP), and COOH functionalized graphene nanoplatelets (GNPCOOH) of different concentrations for fabrication of PLA nanocomposites. The physical, chemical, and barrier properties of all prepared samples were investigated through the stress-relaxation measurements, DSC, TGA, Mercury Porosimetry, biodegradability, water absorption, oxygen permeability, and water vapour transmission.

GNPCOOH nanocomposites exhibited the best mechanical behaviour among all samples, while TGA analysis revealed that it had no effect on the thermal stability. Results obtained by Hg porosimetry have shown that the total porosity has tremendously decreased by incorporation of the investigated nanofillers. The biodegradation of PLA nanocomposites in natural compost was investigated and it was observed that the incorporation of nanofillers had no specific effect on biodegradation of PLA nanocomposites. Water absorption test revealed that the functionalized nanofillers showed relative increase in water absorption as compared to pristine nanofillers. Oxygen permeability test showed that lower concentrations of GNPCOOH had higher oxygen diffusion, while higher concentrations revealed a remarkable decrease in oxygen permeability. Water vapour transmission test showed that the incorporation of nanofillers has considerably decreased the rate of water vapour transmission.

Table of Contents

List of Tables

List of Figures

List of Abbreviations

BP	biopolymers
CNT	Carbon nanotubes
CNTCOOH	carboxylic group-functionalized carbon nanotubes
DCM	Dichloromethane
DSC	Differential Scanning Calorimetry
DWCNT	Double-wall carbon nanotubes
EPO	Epoxidized Palm Oil
FT-IR	Fourier Transform Infra-Red Spectroscopy
GNP	Graphene Nanoplatelets
GNPCOOH	Carboxylic group-Functionalized Graphene Nanoplatelets
GO	Graphene Oxide
MWCNT	Multi-Wall Carbon Nanotubes
NG	Natural Graphite
PBS	Phosphate-Buffered Solution
PCBs	polychlorinated biphenyls
PCL	ε-Caprolactone
PDLA	Poly (D-Lactic Acid)
PHAs	Polyhydroxyalkanoates
PLA	Poly (Lactic Acid)
PLLA	Poly (L-lactic acid)
PNC	Polymer Nanocomposites
POP	Polycyclic Aromatic Hydrocarbons
PVA	poly vinyl alcohol
rGO	Reduced Graphene Oxide
SWCNTs	Single-Wall Carbon Nanotubes
TEM	Transmission Electron Microscopy
TGA	Thermogravimetric Analysis
WVTR	Water Vapour Transmission Rate

1. Introduction

During the last one hundred years, polymeric materials, more commonly known as plastic products dominated humans' everyday lives. It is estimated that 280 million tons of plastic were produced globally in 2012 *(1)*. Plastic products have applications in many different areas including automotive, construction, electronics, furniture, household, and medical devices. However, the largest contribution of plastic products is in the field of food packaging *(2)*. It has been reported that the first use of polymeric materials for food packaging was in 1960s in a pursuit of overcoming the limitations of other materials used for packaging such as glass, metal, and paper board *(3)*. The shift from using traditional materials such as metal and glass to plastics, particularly in packaging applications is attributed to the unique specifications of the latter, such as low cost, lightweight, fracture and chemical resistance, as well as ease of molding and processing *(4)*.

Although plastic products have many desirable aspects, they do have many drawbacks; one of the main disadvantages of plastic materials is being manufactured of depleting resources. The majority of plastic products nowadays are derived from petroleum-based materials, which are known to be non-renewable resources. Plastics production consumes 8% of the total world oil production of which 4% of oil being used as feedstock and 3% to 4% of the oil being consumed as energy during plastics manufacturing. This estimation is expected to increase in the future due to the annual increase of plastics production *(5)*. Another drawback that accompanies the usage of fossil-based polymers is the fact that they are non-degradable materials. Plastic products are considered as one of the most noxious materials that have a deleterious effect on the environment. According to statistical studies, plastic pollutants accumulate in the environment as their degradation is estimated to range from hundreds to thousands of years *(6)*. Not only traditional plastics are harmful to the economy and to the environment, but to human health as well. Different types of additives are known to be added to plastic products in order to improve their properties. However, there is increasing doubt regarding the safety of these additives, and there is a growing interest in studying the effect of additives leaching on human health *(5)*. Therefore, in order to overcome the obstacles associated with traditional plastics usage such as the limited

fossil resources, environmental pollution, and health risks, scientists are determined to find other alternatives that contribute to sustainable development in the future *(7)*.

One of the suggested solutions for the problematic issues resulted from using synthetic polymers was employing biodegradable polymers as environmentally friendly materials. Unlike traditional polymers, biopolymers are derived from natural sources that are renewable, they do not tend to accumulate in the environment as they are biodegradable, and they do not pose any risk on human heath since they are based on natural resources *(8)*. Natural-based polymers found applications in different fields including food packaging; it has been reported that they have desirable features such as providing better food preservation as well as enhancing the shelf-life for packaged food *(9)*. Biodegradable polymers can be categorized into natural polymers represented in polynucleotides, polysaccharides, proteins and polyamides, and synthetic biopolymers such as aliphatic polyesters, polyether, as well as polyvinyl esters among others *(8)*.

Although biodegradable polymers demonstrate some unique features that favor their usage over the currently used traditional plastics, they in fact exhibit poor mechanical properties as well as poor barrier properties that limit their usage in many fields *(10)*. Different approaches have been implemented in order to overcome the disadvantages of employed biopolymers; this included copolymerization, blending, plasticization, as well as incorporation of small amounts of nanofillers *(11, 12)*.

The brittle nature of biopolymers can be overcome by employing different concentrations and various types of natural plasticizers *(11)*. In order to be effective in improving the mechanical properties of biopolymers, the employed plasticizers must have specific characteristics that markedly reduce the glass transition of the biopolymer under investigation. For food packaging applications, the employed plasticizers must have other properties such as lack of leaching or migration as well as lack of toxicity *(13)*.

On the other hand, fabrication of nano-biocomposites also improves the physical properties for biopolymers. Nanofillers incorporated in the manufacturing of nano-biocomposites can either be nanoparticles, nanofibers, nanowhiskers, or nanoplatelets. Currently, solid layered inorganic clays are used to develop nano-biocomposites for food packaging

applications thanks to their ease of processing and low production cost *(14)*. Moreover, biodegradability, antimicrobial activity, mechanical, and thermal properties of biopolymers can all be improved by introducing nano-reinforcemnets into the polymeric matrix *(15)*.

2. Literature Review

2.1. Food Packaging

The process of packaging is an indispensable stage in the world's industry. Different products including drugs, cosmetics, detergents, and food need to be packaged before being distributed to the markets. Of all mentioned commodities, food and beverage products attract most attention when discussing the importance of packaging. In United States alone, $55 - 65\%$ of the estimated \$ 130 billion packaging industry is mainly allocated to foods and beverages packaging *(16)*. The main purpose of food packaging is not limited to containment of the product, but also providing protection, promotion and information for the product, reducing food waste, and tracking processed food *(16-19)*.   .

2.2. Polymers as Food Packaging Materials

It is reported that the first use of plastics as packaging materials was in the 1960s, where it emerged as a means to overcome the limitations of other materials used for packing such as impermanence towards light, liquid, and undesirable flavours, high cost, heavyweight or fragility *(20, 21)*. Polymers are synthetic materials derived from hydrocarbons, the basic components of crude oil and natural gas *(22, 23)*. Different polymers are produced through the polymerization of various monomers *(24)*. Plastics became the most reliable and widely used material for food packaging in recent decades; this shift towards plastic packages is accounted for their unique features including low-cost, light-weight, as well as fracture and chemical resistance. Furthermore, plastics can be easily molded to produce different shapes and sizes of food contact materials such as bottles, jars, films or wrappers. They are heat sealable and can be incorporated into the production line in a way that facilitates forming the desired shape of plastic, filling it with food, then sealing it, all in the same production line *(17)*.

2.3. Adverse Aspects of Plastics as Packaging Materials

Plastic products have recently earned a notorious reputation for claims of imposing health risks as well as the fact that they are a source of environmental pollution. While plastic impact on environment is highly perceptible, its impact on human health is still a subject of controversy. Although scientists have been investigating the safety of plastics and its

impact on human health for more than five decades, their safety is still indecisive and further research remains to be sought.

2.3.1. Plastics and Health Risks

Plastics are known to include different types of additives such as fillers, plasticizers, colorings, flame-retardants, and/or antioxidants. All these additives impart plastic products desirable properties for different applications, however, they raise doubts whether plastics are safe materials for human consumption. Additives, which migrate from plastics to food items, disrupt the endocrine system of human beings whenever they exist in levels that exceed the legislated values *(25, 26)*. Furthermore, they have a negative impact on male reproductive system, which results in developing abnormal sperms characteristics and may end up in testicular cancer diseases *(27, 28)*. In addition, not only additives are questioned, but also the monomeric building blocks that constitute the polymers in general are questioned *(27, 29)*. For example, bisphenol A is also considered as an endocrine disrupting chemical and was reported as estrogen mimicking molecule that can bind to estrogen receptors *(30-32)*.

2.3.2. Plastics and Environmental Pollution

Plastic wastes are major pollutants since they accumulate in the environment due to their longevity that is estimated to range from hundreds to thousands of years *(33)*. Reports show that $60 - 80\%$ of marine debris are fossil-oil based plastics *(33-35)*. First reports addressing plastic pollution were collected during 1960s from seabird carcasses and it soon became noticeable that the plastic debris extended from shoreline to deep sea and from the Equator to the poles *(33, 36)*. Plastic wastes are not only destroying the aesthetic value of the surroundings but also posing a threat to economic activities including tourism and marine industries *(37)*. The impact of plastic debris on marine life has drawn much attention as it is reported that more than 100,000 marine animals and 1 - 2 million sea birds are perished yearly due to plastic wastes entanglement, ingestion or suffocation (Figure 1) *(34, 37, 38)*.

Figure 1: Stork entangled in a plastic bag

The problem of plastic pollution even exacerbates by fragmentation and formation of meso- and micro-plastics. Microplastics are problematic because they were reported to concentrate contaminants found in the surroundings on their surfaces. Metals as well as persistent organic pollutants (POP) such as polycyclic aromatic hydrocarbons, polychlorinated biphenyls (PCBs), and organochlorine pesticides are adsorbed to the surface of microplastics in high concentrations *(33, 39-41)*. By ingestion, these toxic substances are transported from microplastic fragments to the food web *(42)*.

2.4. Biorenewable Biodegradable Polymers

In order to contribute to sustainable development and to address the problematic issues stemmed from employing conventional plastic polymers, researchers are now adopting a new approach, namely, utilization of biorenewable biodegradable polymers, which are expected to pave the way for safe plastic products and green environment *(43)*. Although biopolymers (BP) have not yet dominated the plastic market due to high-cost production and underperformed properties, it is estimated that the market of these environmentally friendly materials will expand by 10 - 20% per year *(44)*. Biodegradable polymers are derived from either natural or synthetic sources. Natural biopolymers are divided into four subcategories: Polynucleotides (e.g. DNA and RNA), Proteins and polyamides (e.g. gelatin, casein, and collagen), Polysaccharides (e.g. starch, cellulose, and chitosan), and other biopolymers (e.g. natural rubber and lignin) *(43)*. On the other hand, synthetic biopolymers include aliphatic polyesters, polyethers, polyamides, and polyvinyl alcohols. Synthetic BP are either obtained from petroleum sources such as poly (ε-caprolactone)

(PCL) and poly vinyl alcohol (PVA) or from renewable sources, (e.g. wood, cellulose, and corn) such as polylactic acid (PLA) and polyhydroxyalkanoates (PHAs) *(43, 45)*. Synthetic biopolymers are more favorable due to their ease of processability and better mechanical properties *(43)*.

2.4.1. Advantages of Biopolymers

Biopolymers are gaining much credit at the expense of traditional polymer owing to their advantageous properties. Unlike oil-based polymers, biopolymers are derived from renewable resources; this tribute offers an alternative path to maintain sustainable development of ecologically and economically promising technology. Moreover, by using renewable sources for plastics production, fossil-based raw materials are directed to serve other substantial purposes that are mainly dependent on this depleting source. Furthermore, processing of bio-polymeric materials requires less energy; this significantly reduces the carbon dioxide emission, leads to less greenhouse effect, and consequently alleviates the global warming phenomenon. On the other hand, biopolymers are biodegradable materials that tend to decompose naturally into non-toxic materials, namely, water, carbon dioxide, biomass, and inorganic compounds as a result of enzymatic activity of microorganism. Compostability is another advantage of biopolymers; in other words, biopolymers can safely be degraded in compost medium; this can also lead to substantial reduction in plastic garbage in the environment *(44)*.

2.4.2. Disadvantages of Biopolymers

The fact that biodegradable polymers have many desirable advantages does not conceal their limitations *(46, 47)*. One of the main drawbacks of biopolymers is their poor mechanical properties. Poly (lactic acid), for example, is known to be a naturally brittle biopolymer having an elongation at break that does not exceed 10% *(46)*. Although PLA is analogous to poly (ethylene terephthalate) (PET) with respect to tensile strength and elastic modulus, its brittleness and fragility confine workability as well as end-use applications that require plastic deformation at high stress levels such as cable insulation, flooring, and food packaging applications *(46, 48, 49)*. In order to overcome the stiffness of biopolymers, different scientific attempts that ranged from copolymerization and blending to surface modifications and plasticization were implemented to improve the

mechanical properties of biopolymers *(48, 50)*. Plasticizers are defined as non-volatile, low molecular compounds that are used as additives in polymers industry. The fundamental function of plasticizers is to give brittle polymers flexibility and processability during thermoformation by lowering the glass transition temperature (T_g) of the investigated polymer *(47)*. Plasticizers have the ability to decrease hardness, viscosity, density, and the electrostatic charge of polymers *(47)*. In addition, plasticizers affect polymer crystallinity, optical clarity, as well as biological degradation of investigated biopolymers *(51)*.

2.4.2.1.   Plasticizers: Attributes and Performance

Most of utilized plasticizers are found to be linear or cyclic carbon chains of high boiling point liquids *(47)*. Having low molecular weight that ranges from 300 to 600 g.mol^{-1}, permits the plasticizer to pervade the intermolecular voids between polymer chains. As a result, the secondary forces among polymer chains are minimized; this leads to a smoother chain motion and hence, reduced glass transition temperature of the investigated polymer. It was proved that T_g value is dependent on the mobility of polymer chains. Restricted motions of polymer chains is associated with high T_g while flexible motion of the chains results in decreasing the value of T_g *(52)*. Employing the appropriate plasticizers depends on a number of factors such as compatibility between polymers and plasticizers, plasticizer concentration, resistance to migration and volatility, desired properties in the end product, toxicity, and effective cost *(53, 54)*.

2.4.2.2.   Shift towards Natural Plasticizers

The continuous growth of plastic industry was associated with an increase in the production and utilization of different plasticizers. There is currently a growing trend towards replacing traditional phthalate-based plasticizers with natural-based plasticizers made from biodegradable and/or renewable resources. Currently, natural plasticizers include epoxidized triglyceride vegetable oil from sunflower oil, castor oil, soybean oil, and fatty acid esters *(55)*.

2.4.3. Poly (Lactic Acid) as a Biorenewable Biodegradable Polymer

Poly lactic acid (PLA) (Figure 2) is a promising biopolymer with various applications in numerous fields, and is considered as one of the most studied thermoplastic biopolymers *(45)*.
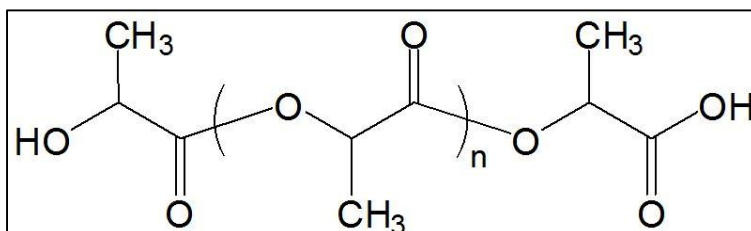
Figure 2: Chemical structure of poly (lactic acid)

The building block of PLA is (2-hydroxy propionic acid) (Figure 3), which is commonly known as lactic acid *(45)*.   .
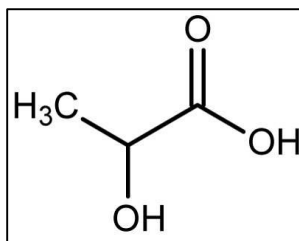
Figure 3: Chemical structure of lactic acid

Poly (lactic acid) is an aliphatic thermoplastic polyester that exists in two optical arrangements, resulting in the production of two types of PLA: amorphous or semi-crystalline states. The two optical arrangements of PLA are (L-lactic acid) (PLLA) and (D-lactic acid) (PDLA) where the former is the most common and is preferred to D-stereoisomer as it produces higher yields as well as better properties *(45, 56)*. On the other hand, PDLA is incorporated into PLLA to modify the crystallization characters for specific applications *(45)*. PLA has found applications in many fields particularly in medical industry as sutures and in food industry as disposable utensils *(56)*. It is worth mentioning that although PLA has drawn much attention recently, it is not considered as a new polymer; it was first synthesized in 1845 by Théophile-Jules Pelouze through condensation of lactic acid *(57)*. In 1932, Carothers *et al.* developed a new method to polymerize PLA using cyclic dimers (lactides) *(43, 57)*. Cargill Dow Company, currently known as

"NatureWorks" took the lead to reduce the production costs of PLA and started marketing it under the brand name "Ingeo" *(43, 58)*. Production of poly (lactic acid) on large scales started in 1997, when Cargill Dow Production of PLA was conducted through two synthetic approaches, (i) polycondensation of lactic acid and (ii) through the ring-opening polymerization of lactide dimers *(45)*.

2.4.3.1.   Hydrolytic Degradation of Poly (Lactic Acid)

The term hydrolysis or "solvolysis" indicates the cleavage of C-X bond by the help of water molecule, where the polymer chain is cleaved into two sub chains *(43, 45)*. As Amar pointed out *(45)*, hydrolysis process takes place randomly at the ester linkage in the polymer chain resulting in a reduction of molecular weight of the polyester. There is a number of factors that affect the rate of hydrolysis reaction including water concentration, temperature, morphology of the polymer, and the presence of acid or base catalysts *(45)*.

According to Fischer *et al. (43)* the hydrolytic degradation of semi-crystalline polyesters has found to be more complicated than that of amorphous ones. It was reported that the hydrolysis reaction takes place through two phases. In the first phase, water molecules diffuses to the amorphous regions leading to cleavage of ester bonds. This can be accompanied by the increase of degree of crystallinity. The second phase takes place when all the amorphous regions have undergone degradation; at this point, the degradation starts from the edges towards the center of crystalline regions. It worth mentioning that there are inconsistent views regarding the effect of crystallinity on the rate of degradation; while most of the published studies reported that crystallinity reduces hydrolytic degradation, other researchers pointed out that the increase of polymer crystallinity is associated with an increase in the degree of degradation *(43)*.

2.4.3.2.   Naturally Plasticized Poly (Lactic acid)

For food packaging applications, PLA has been plasticized with a wide range of biodegradable plasticizers. Plasticizers approved for food packaging applications must meet specific characteristics. For example, a plasticizer has to be non-toxic, non-volatile during processing, have lack of tendency to migrate to matrix surface, and it has to be miscible with the polymer *(50)*. According to a study published by Sinclair, lactide

monomer can be used to plasticize PLA. Achieved results demonstrated a remarkable increase in the elongation at break. However, lactide was found to migrate to the surface of the polymer due to its low molecular weight, this resulted in stiffening of PLA at the long term *(46)*. In order to overcome the problematic issue of plasticizer migration, oligomeric plasticizers of relatively large molecular weights have been investigated. Martin and Averous studied the plasticizing effect of oligomeric lactic acid, PEG, PEG monolaurate, glycerol, as well as citrate esters. According to their published results, oligomeric lactic acid and low molecular PEG demonstrated satisfactory effects. Citrate esters having molecular weight that ranged between 276 and 402 g.mol^{-1} showed a significant increase in the elongation at break that was accompanied with a remarkable reduction in tensile strength. On the contrary, glycerol was the least efficient plasticizer for PLA *(59)*. Based on a study performed by Ljungberg and Wesslen using triacetin and tributyl citrate, different loads of the plasticizers were employed, and were successfully able to lower T$_g$ values of the polymer to 10 °C at a concentration of 25%. However, for higher loads, phase separation took place *(60)*. In further study by Rasal *et al.*, triacetin and tributyl citrate were reported to migrate to the polymer surface during long periods of storage due to their low molecular weights *(46, 61)*. Thus, in order to address the problematic migration of low molecular weight plasticizers during storage, researchers synthesized tributyl citrate oligomers; however, this plasticizer also was found to migrate to matrix surface *(62)*. It was also pointed out that high molecular weight plasticizers tend to result in phase separation even at low concentrations *(63)*. In a further study that was published by Ljungberg and Wesslen, it was proved that the incorporation of triacetin and tributyl citrate was associated with a reduction in the glass transition temperature. For long storage durations, they observed an increase in PLA film crystallinity; this behaviour occurred because the glass transition temperature that was around the room temperature permitted the rearrangement of polymer chains. As a result, both plasticizers migrated to the surface of the matrix during long storage and led to the stiffening of PLA films *(61)*. Other studies addressed the problematic issue of plasticizers migration by grafting plasticizers such as citrates or poly (ethylene glycol) to the surface of PLA using reactive extrusion techniques *(64, 65)*.

2.5. Nanotechnology in Food Packaging

In food industry, food packaging is the field that witnessed the greatest interaction with nanotechnology as compared to other fields such as nanofood production or food processing. To ensure food safety, food spoilage due to microbial activity can be detected through nanotechnology by employing nanosensors. A nanosensor is composed of arrays of thousands of nanoparticles that have the ability to fluoresce with different colours when they are in contact with food pathogens. Nanosensors proved to be successful in reducing the time needed for pathogen detection from days to hours or even minutes. Currently available nanosensors can be embedded within the packaging material where they act as "electronic tongue" or "electronic nose" to detect released gases or chemical compounds due to microbial activity within food *(66, 67)*. This type of packaging is known as "intelligent food packaging" as the package is designed to sense food spoiling and alert the customer to avoid spoiled food *(66)*.

On the other hand, "active food packaging" is an innovative packaging that aims at releasing additives or preservatives such as flavours, colourants, antioxidants or nutritional supplements to inhibit food spoilage, avoid loss of nutrients, and extend the shelf-life of food products. Active packaging can also include oxygen scavengers within the package to prevent the oxidation of fatty acids and suppress the development of undesirable food textures, off-flavours, or off-odours. This type of smart packaging demonstrates promising success because the release of the active compound from the nanocapsules within the package itself can be tuned or controlled. Currently, this technique has been applied to a number of biopolymers including gelatin, chitosan, and poly lactic acid *(66, 67)*. Another application in the field of food packaging is the development of edible nanocoatings. This type of edible nanocoating can be used to protect fast foods, confectionary, fruits and vegetables, and many other products. These nanocoatings act as gas and moisture barriers and as vehicles to deliver colours, flavours, enzymes and anti-browning agents; thus, extending the shelf-life of food products even after the package is open *(68, 69)*. Nanomaterials also are used as reinforcements for biodegradable polymers to improve their features. Nanotechnology has developed nanofillers that can enhance the mechanical, thermal, biodegradable, and barrier properties of biopolymers. Nanofillers that can be used

as reinforcements include nanofibers, nanowhiskers, nanotubes, and layered inorganic clays. Inorganic nanoclays are currently the one being used in food packaging thanks to their low cost and ease of processing *(67)*. Improving physical and chemical properties of food packaging materials can be implemented through the fabrication of polymer nanocomposites.

2.6. Nanocomposites

The term "nanocomposites" reflects the dispersion of nanofillers (in the range of 10^{-9} m) within certain matrices (e.g. polymers, metal, or ceramics) to improve physical and chemical properties of the material under investigation *(70, 71)*. Nanofillers could either have one (e.g. nanotubes), two (e.g. nanoplatelets) or all three dimensions (e.g. nanoparticles) in the range of nanometer *(70, 72)*. It must be noted that the properties of the fabricated nanocomposites are not only dependent on the properties of the precursors from which the nanocomposites are prepared, but also on the interfacial and morphological features of the prepared nanocomposites *(71)*. Polymer Nanocomposites (PNC) has gained much attention during the last few years; in this case, the nanocomposites contain a polymer or a copolymer that could be either elastomeric, thermoplastic, thermoset polymer with nanofillers that range from nanoparticle and nanoplatelets to nanofibers and nanotubes dispersed within the polymeric matrix. It worth mentioning that the nanofillers influence the characteristics of the nanocomposites at very low concentrations. This behaviour stems from three factors: (i) nanofillers have very small inter-particle distance, (ii) the transformation of large fraction of the polymer near their surface into an interphase of different characteristics, and (iii) the alteration of the morphological features of the nanocomposites, all due to massive surface area to volume ratio that they possess as compared to normal size macroscopic particles *(71)*.

2.6.1. Advantages and Disadvantages of Nanocomposites

Advantageous properties of using nanofillers in polymeric matrices include improving the mechanical properties such as stiffness, toughness, and tensile strength, improving thermal expansion and thermal conductivity, enhancing dimensional stability, decelarating erosion and attrition, and promoting gas and moisture barrier properties. Alternatively, usage of nanofillers limits the processability of nanocomposites due to the exponential increase in

viscosity. Furthermore, the interfacial interaction and the compatibility between the nanofillers and the matrix could be challenging, and this might hinder the uniform distribution of nanofillers within the matrix resulting in sedimentation or agglomeration of the nanofillers. Some nanocomposites can also show problematic optical properties *(71)*.

2.6.2. Biodegradable Polymer Nanocomposites

In pursuit of developing and employing eco-friendly polymeric materials to achieve sustainable development, scientific research is now shifting from petroleum-based nanocomposites to bio-based nanocomposites *(70, 73)*. In general, biopolymer nanocomposites have applications in many different fields, particularly in development of biodegradable food packaging and edible films *(70, 73)*. Research in food packaging focuses on improving gas and moisture barrier properties, thermal stability, and mechanical properties *(74, 75)*.

2.6.3. Carbon Nanotubes (CNTs) as Nano-reinforcements

CNTs created great interest among engineers and scientists due to their extraordinary physical properties *(76)*. CNTs proved to have outstanding thermal stability, high electrical conductivity, high strength, and high modulus. These unique features along with the fact that they have very low density rendered CNTs as the strongest and lightest material known today and suggested employing this material in enormous applications with bionanotechnology and nanoengineering being in the lead *(77)*.

2.6.3.1.   Structure of Carbon Nanotubes

Carbon nanotubes (CNTs) were first discovered in 1973 by M. Endo, however, they attracted more attention when Sumio Iijima reported them while studying fullerene materials *(78)*. Carbon nanotubes are known to have a one-dimensional cylindrical hollow structure. They are formed of hexagonal carbon atoms, covalently bonded to each other *(79, 80)*. They are similar to graphite structure in that they have sp^2 hybridization where each carbon atom is attached to three other carbon atoms in a honeycomb array *(81)*. CNTs diameter can be extended only for few nanometer, however, its length can extend to tens of microns or even centimeters with half of a fullerene-like molecule cap at its ends *(78, 79)*. Whilst CNTs are all made of the same graphite sheet that is rolled into cylindrical

structures, they have various structures that differ in thickness, length, layers number, as well as types of spiral *(77)*. CNTs can either be made of single-wall carbon nanotubes (SWCNTs) or a number of concentric carbon nanotubes (MWCNTs) depending on the number of graphite sheets rolled up *(70)*. The concentric cylinders that exhibit the "Russian Doll" structure of the MWCNTs are bound together due to weak van der Waals forces *(80)*. Double-wall carbon nanotubes (DWCNTs) are considered as a special case of MWCNTs, where the cylindrical structure of the double-wall CNT is only composed of two concentric cylinders *(79, 81)*. CNTs have three different morphologies: (i) armchair, (ii) zigzag, and (iii) chiral (Figure 4). These different morphologies are mainly dependent on the tube axis orientation relative to the hexagonal lattice *(79, 82)*.
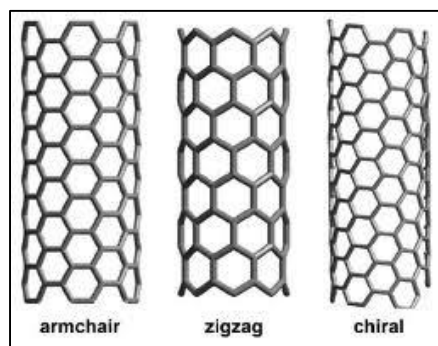
Figure 4: Different geometries of carbon nanotubes

2.6.3.2. Modification of Carbon Nanotubes

Dispersion of CNTs within a polymeric matrix is challenging; this is attributed to the tendency of CNTs to agglomerate as they have very large surface area. Researchers attempted to find solutions to disperse CNTs within polymer matrices using various techniques such as mechanical mixing and sonication to ensure homogenous dispersion during nanocomposites fabrication. Another approach that proved to permanently disperse CNTs to prepare homogenous nanocomposites was found to be "surface functionalization of CNTs". Among the techniques used for CNTs functionalization are non-covalent (physical) functionalization as well as covalent (chemical) functionalization *(78, 81)*. Covalent functionalization is attained by introducing functional groups using oxidizing agents to create hydroxyl or carboxyl groups on the surface of CNTs *(78)*. Research studies showed that carboxylic functionalized CNTs had enhanced stability in water due to its ability to form hydrogen bonds between the nanotube and water molecules

for more than 100 days *(78, 79)*. According to the literature, acid functionalization of CNTs proved to have significant enhancement of the interfacial interaction between CNTs and polymer matrix. This results in improving young's modulus and other mechanical properties of the nanocomposites *(78)*.

2.6.3.3. Poly (Lactic acid)/Multi-Wall Carbon Nanotubes Nanocomposites

First report on the preparation of PLA/MWCNTs nanocomposites was in 2005 *(76)*. Moon *et al.*, used two different techniques to prepare the PLA nanocomposites. The first method entailed preparing 10 wt% PLA/chloroform solution. Then, previously dispersed MWCNTs in chloroform solution was added to the PLA/chloroform solution and sonicated for 6 hours to ensure complete dispersion of MWCNTs in PLA matrix. The other technique included the tearing of previously prepared nanocomposites into small pieces. These small pieces of nanocomposites film was then stacked between two metal plates and then hot pressed for 15 minutes at 150 kgf/cm^2 and 200 °C. Moon *et al.* concluded that the physical properties of the host matrix can be significantly altered by incorporating MWCNTs, and proved that MWCNTs could be uniformly dispersed in PLA matrix *(76)*.

In 2006, Zhang *et al.*, prepared PLA/MWCNTs nanocomposites using solution blending and precipitation method and they investigated electronic, thermal, and biocompatibility properties of the prepared samples. They reported that the interaction between MWCNTs and PLA occurred through the more hydrophobic group C - CH$_3$. They also concluded that MWCNTs act as a plasticizer for the PLA; this was confirmed as the glass transition, crystallization, and melting temperatures had lower values compared to pristine PLA. Furthermore, the biocompatibility test demonstrated that the presence of MWCNTs in the matrix inhibited the growth of fibroblast cells, and it was suggested that this might be due to the unfavorable attachment of cells to the PLA/MWCNTs surface *(83)*.

In a further study, Kobashi *et al.* investigated the liquid sensing properties of PLA/MWCNTs nanocomposites in which, the electric properties changed when the nanocomposites came to contact with solvents. The nanocomposites were prepared by melt processing using different loads of MWCNTs between 0.5 wt% and 2.0 wt%. TEM characterization showed that MWCNTs formed a conductive network structure, which is essential for determining the liquid sensing properties of nanocomposites. Kobashi *et al.*

studied the electrical resistance of nanocomposites in solvent immersion/drying cycles. It was reported that lower loadings of MWCNTs demonstrated larger electrical resistance changes but with higher signal noises. This result suggested that the conductive MWCNTs network tended to disconnect since lower loadings of MWCNTs retain lesser dense structures compared to nanocomposites that incorporate higher loadings of MWCNTs. Kobashi *et al.* successfully detected number of solvents in their investigation. They proved that PLA/MWCNTs nanocomposites can sense poor solvents for PLA such as water, ethanol, and n-hexane as well as good solvents such as dichloromethane, tetrahydrofuran, chloroform, and toluene. Kobashi *et al.* came to the conclusion that PLA/MWCNTs nanocomposites are potential candidates for solvents leakage detection applications *(84)*.

Bourbigot *et al.* published a study, where PLA and PLA/MWCNTs nanocomposites were both prepared based on reactive extrusion technique via ring opening polymerization of L,L-lactide monomer. Bourbigot's group studied the flame retardancy of PLA/MWCNTs and compared it with that of virgin PLA. It was revealed that the flame spread for PLA/MWCNTs nanocomposites is much slower than that of virgin PLA. It was observed that virgin PLA tended to flow, drip, and burn on a higher rate compared to PLA/MWCNTs that did not flow or drip. This behaviour was attributed to the fact that incorporation of MWCNTs into PLA matrix increased the viscosity of the material, and hence, retarded the process of dripping and resulted in slower flame spread *(85)*.

Based on a study performed by Kuan *et al.*, MWCNTs was used as reinforcement nanofillers for low-crystalline as well as high-crystalline PLA to investigate the electrical and thermal characteristics of the prepared nanocomposites. Furthermore, in order to improve compatibility of MWCNTs with low-crystalline PLA matrix, Kuan *et al.* modified MWCNTs using maleic anhydride to create maleic anhydride-grafted-MWCNTs (MA-g-MWCNTs). It was pointed out that grafted nanotube enhanced the interfacial interaction between PLA and MWCNTs due to increased physical and chemical bonding between the nanofillers and the polymer matrix, consequently, MWCNTs were better dispersed within the PLA matrix. In their work, Kuan's group revealed that the degree of crystallinity of PLA strongly affected the electrical properties of the nanocomposites. It was also reported that higher electrical conductivity can be achieved at lower loadings of CNTs. Kuan *et al.*

also studied the effect of incorporating MWCNTs on the mechanical properties of low- and high-crystalline PLA. In both cases, the tensile strength increased, however, for high-crystalline PLA, the addition of MWCNTs resulted in a slight increase of the tensile strength, while in case of low-crystalline PLA, adding the same amount of modified MWCNTs caused the tensile strength to have higher increase up to 14.4%. Kuan *et al.* attributed this behaviour to the better dispersion of the MWCNTs in PLA matrix in case of low-crystalline PLA; in other words, homogeneously distributed MWCNTs enhanced the interface bonding as well as increased the shear stress between the PLA and the modified carbon nanotubes, thus, resulted in an increased tensile strength *(86)*.

Kuan *et al.* has also reported the improvement in the interfacial adhesion of MWCNTs to PLA matrix. They applied water-crosslinking technique to create silane-grafting system. Crystalline, thermal, and mechanical properties of the prepared nanocomposites were investigated under different carbon nanotubes loads and different water-crosslinking time. According to their published results, the addition of 1 phr MWCNTs enhanced the tensile strength by 13% as compared to that of neat PLA. Furthermore, the heat deflection temperature of PLA/MWCNTs nanocomposites was improved by almost 40 °C after 7 hours of water-crosslinking reaction. Kuan *et al.* also reported that applying water-crosslinking techniques improved the thermal degradation temperature by 12 °C and 20 °C, with and without addition of MWCNTs, respectively *(87)*.

In a study performed by Wu *et al.*, the crystallization and biodegradation behaviour of PLA/MWCNTs nanocomposites were investigated. In their published paper, Wu *et al.* reported that although the presence of the carbon nanotubes hindered the crystal growth dynamically, MWCNTs also exhibited nucleating effect on cold as well as melt crystallization. In other words, MWCNTs played a dual role in PLA crystallization: a physical barrier as well as a nucleating agent; the dominant role was found to be dependent on the employed crystallization conditions. Wu *et al.* also revealed that the rate of PLA biodegradation was impeded when carbon nanotubes are added due to the inhibition effect of the added MWCNTs, and that amorphous samples demonstrated higher rates of degradation compared to crystalline ones. Wu *et al.* also compared the degradation levels for samples with melt crystallization history and those with cold crystallization history; it

was found that degradation on surface and inside the melt crystallization history is lower than that of those with cold crystallization history. It was concluded that the biodegradation is mainly dependent on the crystallization histories of investigated samples *(88)*.

According to a research study conducted by Kim *et al.*, the thermal degradation of PLA/MWCNTs was explored through the determination of mechanical properties, molecular weight, and weight loss during non-isothermal and isothermal degradation. For non-isothermal process, it was reported that PLA/MWCNTs exhibited an increased thermal degradation peak and onset temperature compared to neat PLA. Kim *et al.* also proved that the PLA/MWCNTs nanocomposites showed more enhanced thermal stability than that of neat PLA; this was based on the fact that PLA/MWCNTs nanocomposites had higher molecular weight compared to neat PLA. Furthermore, PLA/MWCNTs nanocomposites of higher loads of the carbon nanotubes demonstrated improved mechanical properties as well as higher activation energy of thermal degradation when compared to those of lower CNTs loads *(89)*.

Dong *et al.* conducted a study on stereocomplex-type based on PLLA/PDLA (different loads of PDLA) with MWCNTs through melt compounding method, and compared the obtained results with PLLA/MWCNTs nanocomposites. Dong *et al.* investigated the degree of MWCNTs dispersion within the polymer matrix, crystallization, mechanical, and hydrolytic degradation properties. According to their published results, it was reported that the dispersion of MWCNTs in PLLA/PDLA20/MWCNTs nanocomposites was significantly improved compared to PLLA/MWCNTs that exhibited MWCNTs aggregates. This observation was attributed to the increased shear stress during melt mixing in case of PLLA/PDLA20/MWCNTs. Dong *et al.* pointed out that the increased shear stress overcame the van der Waals and electrostatic forces that led to filler agglomeration in case of PLLA/MWCNTs. DSC analysis of prepared samples demonstrated that the crystallization time for PLLA/MWCNTs samples was less than that of neat PLLA; this result was consistent with previous studies and was attributed to the nucleating effect of MWCNTs nanofillers. It was also observed that the incorporation of PDLA significantly shortened the crystallization time with increased loads of PDLA compared to PLLA/MWCNTs and neat PLLA. DMA analysis of prepared samples showed that storage

modulus value at temperatures above glass state (80 - 90 °C) for neat PLLA, PLLA/MWCNT, PLLA/PDLA5/MWCNTs, PLLA/PDLA10/MWCNTs, PLLA/PDLA20/MWCNTs were 4.0, 5.2, 14.0, 21.9, 92.6 MPa, respectively. This behaviour indicated that the addition of PDLA induced the reinforcement effect of incorporated nanofillers. Dong *et al.* also investigated the hydrolytic degradation rates of neat PLLA as well PLLA nanocomposites. It was observed that the rate of hydrolytic degradation increased in PLLA/MWCNTs compared with neat PLLA. Dong *et al.* pointed out that the observed increase in hydrolytic degradation was consistent with a previous research study conducted by Qiu *et al.* Further increase in the rate of hydrolytic degradation was observed with the incorporation of PDLA of different loads; this was attributed to the formation of *in situ* stereocomplex crystals within the polymer matrix when PDLA was incorporated *(90)*.

Based on a study performed by Mai *et al.*, a monitoring system for *in situ* degradation for biodegradable material was first reported. Mai *et al.* stated that monitoring the degradation level for biodegradable product during its lifetime is of great importance. Hydrolytic degradation test was investigated in many scientific researches to evaluate the degradation of PLA in human body and in soil *(91)*. Degradation of biopolymers is affected by two factors: external such as temperature, moisture, and acidity and internal factors such as crystallinity, molecular weight, branched structures, and crosslinking *(90)*. Mai *et al.* developed PLA/MWCNTs nanocomposites system that was capable of monitoring biodegradation. The experimental work was conducted using two different media for degradation, namely, water and phosphate-buffered solution (PBS). The hydrolytic degradation rate of the PLA/MWCNTs composite was found to be higher in case of PBS than in water since it is easier for PLA oligomers produced to be easily swollen and solubilized in sodium salts to undergo further degradation. As Mai *et al.* pointed out, changes in electrical resistivity was successfully accounted for based on biopolymer degradation. It was also revealed that, in contrast to other stimuli reported in previous work, *in situ* biodegradation of samples resulted in electrical conductivity. Mai *et al.* also demonstrated that nanocomposites of lower concentrations of MWCNTs displayed increased sensitivity and stronger signal change towards degradation compared to nanocomposites of higher MWCNTs loads. These behaviours were accounted for the

elimination of amorphous domains during biodegradation process and the increase of the nanofillers network density *(91)*.

Researchers also investigated the effect of introducing carboxylic-functionalized MWCNTs to PLA matrix. Wu *et al.* studied the effect of adding pristine MWCNTs, MWCNTs-OH, and MWCNTs-COOH to PLA matrix. TEM images revealed that the dispersion of MWCNTs-COOH with in the PLA matrix was more homogenous compared to MWCNTs-OH and pristine MWCNTs. This was attributed to the neat affinity between the carboxylic groups on the surface of the nanotubes and the PLA matrix. TGA analysis was used to study the effect of pristine and functionalized MWCNTs on thermal stability, it was revealed that no significant enhancement of thermal stability was recorded during the first stage of degradation; however, during the progress of degradation, MWCNTs and MWCNTs-COOH hindered the thermal decomposition of PLA due to thermal conductive effect and barrier effects, respectively *(92)*.

In another study performed by Mina *et al.*, PLA/MWCNTs and PLA/MWCNTs-COOH nanocomposites were both prepared. Mina *et al.* employed treated pristine MWCNTs with acid and heat to introduce a carboxylic functional group to the surface of the CNTs. Mina *et al.* revealed that incorporation of pristine and functionalized MWCNTs of very low concentrations is associated with increments in tensile strength and tensile modulus. This was attributed to the formation of crystalline structures within PLA and the interaction of the polymer molecules with CNTs. Investigating surface resistivity, Mina *et al.* reported that by addition of very small loads of MWCNTs, the surface resistivity can be reduced significantly by a factor of (10^{13}) compared to neat PLA. This was accounted for by the high surface area to volume ratio of CNTs and the many π bonds, which can easily drive the electrons within the PLA/CNTs nanocomposites. Furthermore, XRD analysis suggested that lower contents of MWCNTs favors the formation of orthorhombic α-crystal in PLA, while higher MWCNTs favors the formation of orthorhombic β-crystal, which is less stable *(93)*.

In another research published by Mina *et al.*, MWCNTs were modified via three different methods, namely, annealing, oxidation at 500 °C, and acid treatment. It was reported that acid treated carbon nanotubes exhibited better mechanical properties as compared to heat-

treated CNTs due to increased crystallinity and better interaction between CNTs and PLA matrix. DSC results revealed high crystallization of PLA by incorporation of treated MWCNTs during heating/cooling process. However, neat PLA remained amorphous during the cooling process. TGA analysis demonstrated a decrease in thermal degradation with higher loads of CNTs due to increased thermal conductivity *(94)*.

Chrissafis *et al.*, applied solvent evaporation method to prepare PLA/MWCNTs-COOH of different CNTs loadings. SEM images confirmed the homogeneous distribution of functionalized CNTs within the matrix. Mechanical properties was reported to be improved by addition of functionalized CNTs. This behaviour was attributed to the favourable formation of hydrogen bonding between the hydroxyl end groups at PLA and the carboxylic groups on MWCNTs. This bond formation was confirmed through the use of FT-IR analysis. The melting point of PLA proved to slightly increase by addition of MWCNTs-COOH; this was accounted for on the basis that MWCNTs acts as a nucleating agent, which increased the degree of crystallization *(95)*.

2.6.4. Graphene Nanoplatelets as Nano-reinforcements

2.6.4.1. Graphene Nanoplatelets (GNP)

Graphene (Figure 5) is a single layer of sp^2-hybridized carbon atoms arranged in a two-dimensional hexagonal lattice where each carbon atom in the lattice is bonded to two other neighboring carbon atoms with a bond length of 0.142 nm *(96)*.
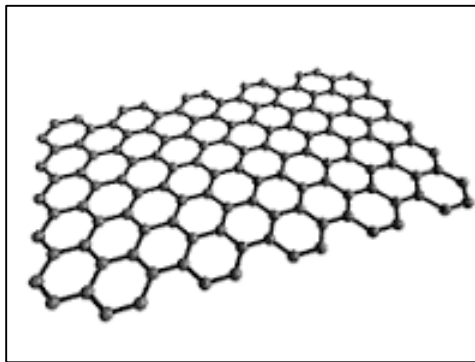
Figure 5: Structure of graphene nanoplatelets

It was first discovered in 2004 when Geim and co-workers were able to define the single layers of graphene while conducting a simple experiment. This discovery refuted the theory that graphene has a thermodynamically unstable structure and that it cannot exist under

ambient conditions *(97, 98)*. Graphene is considered as the "thinnest material in the universe" and has superior characteristics that qualify it to be employed in a wide spectrum of applications including sensors, electronic circuits, electrodes for solar cells, and ultra-thin carbon films *(98)*. It has been proved that graphene surpasses other nanofillers such as expanded graphite, carbon nanotubes, and carbon nanofibers thanks to its extraordinary transparency, flexibility, electrical, mechanical, and thermal properties *(96, 98)*. Graphene is reported to demonstrate the highest thermal conductivity (six times more than copper) recorded in the scientific literature *(99)*. It is also known for its high electric conductivity that is parallel to that of copper metal even though it has only one-fourth the copper density and an array of properties that exceeds steel by 50 times *(99)*. Additionally, graphene is comparable to nanoclays in terms of platelet structure and low price. Furthermore, unlike carbon nanofibers and carbon nanotubes, which have thin and long structure, the lamellar structure of graphene eliminates the issue of entanglement; thus, reducing the tendency of graphene to aggregate *(99)*.

2.6.4.2. Poly (Lactic Acid)/Graphene Nanocomposites

The outstanding properties of graphene suggested the use of graphene to improve the physical properties such as flame retardancy and gas permeability of polymers through the fabrication of polymer/graphene nanocomposites *(98)*. Scientific researches have reported that graphene can even demonstrate better electrical and mechanical properties compared to those of clays and other carbon nanocomposites *(98)*. However, it is important to note that superior properties of polymer/graphene nanocomposites is strongly influenced by the distribution of the graphene within the polymer matrix as well the interfacial interaction between the nanofillers and the polymer. It has been reported that virgin graphene is incompatible with organic polymers and tends to form non-homogeneous nanocomposites. In order to overcome this issue, researchers proposed the incorporation of graphene oxides, which are highly oxygenated graphene that include functional moieties such as carboxyl, hydroxyl, ketone, and diol groups. The presence of these groups can effectively relieve the van der Waals interaction and improve the compatibility of the graphene with the organic polymer. However, graphene oxides are known to be dispersed in aqueous solution only depending on their features. This fact created a further problem that needs to be solved as most organic polymers cannot be dissolved in aqueous solutions *(98)*.

Kim *et al.* performed a research study that compared natural graphite (NG)/PLA composites and graphene nanoplatelets (GNP)/PLA nanocomposites in terms of structural, thermal, mechanical, and electrical properties. Kim *et al.* prepared the graphene nanoplatelets from the natural graphite using Staudenmaier technique. XRD analysis revealed that a characteristic peak that corresponds to natural graphite was clearly observed even at low concentrations of NG; this confirmed that NG do not tend to exfoliate during melt compounding. On contrary, PLA/GNP nanocomposites showed no characteristic peak of GNP in XRD patterns; this supported the assumption that GNP layers were completely intercalated within the polymer matrix. These findings were also confirmed by SEM images. Kim *et al.* employed TGA technique to study the thermal behaviour of the samples. It was reported that PLA/NG composites showed no effect on thermal stability compared to neat PLA; however, PLA/GNP nanocomposites displayed an increase in thermal stability with incorporation of GNP. This was attributed to the behaviour of GNP, which acts as mass transfer barrier that hinder the thermal degradation of nanocomposites. For mechanical properties, the Young's modulus for both PLA/NG and PLA/GNP demonstrated an increment in moduli values, however, the increment in Young's modulus of PLA/GNP was greatly increased compared to PLA/NG. On the other hand, the electrical resistivity studies revealed that the percolation threshold of PLA/NG was achieved at high loads of NG (10 wt% - 15 wt%) counter to PLA/GNP nanocomposites, which reached the percolation at much lower loads of GNP (3 wt% - 5 wt%). The extraordinary effect of GNP on electrical resistivity is ascribed to the well dispersion of the nanofillers within the polymer matrix, a feature that went unnoticed for PLA/NG composites due to the crystalline state of NG sheets *(100)*.

Narimissa *et al.*, fabricated PLA/GNP nanocomposites using melt blending and dry mixing methods to investigate their morphological, mechanical, and thermal properties. XRD technique was employed to study the morphology of the nanocomposites and it was observed that melt blending technique applied was not completely efficient in separating graphite layers, which led to the formation of GNP aggregates; this finding was presumably due to the strong bonding between graphite platelets that complicated the process of GNP exfoliation within the polymer matrix. TEM images were also examined and it was reported that the dispersion of GNP is considered as "sufficient". However, the observed

single exfoliated layers shown by TEM images cannot be viewed as indicative of complete delamination of GNP within the polymer matrix. Narimissa *et al.*, also inspected the variation in mechanical characteristics when GNP were incorporated. It was reported that the Young's modulus values have remarkably increased by the addition of GNP. Samples that consisted of 3 wt% showed maximum increase in Young's modulus values, while nanocomposites with higher loads of GNP demonstrated lesser increase in Young's modulus. The gradual decrease in mechanical properties that associated the increase of GNP loads was ascribed to the agglomeration of GNP at higher loads as confirmed by TEM images. On the other hand, tensile strength showed a gradual decrease by incorporation of GNP due to the existence of loops at close proximity within the weak regions in filler-matrix system. In addition, at nanofillers concentrations higher than 3%, GNP tends to exist within the interface resulting in a decrease in the tensile strength. The elongation at break was also found to show a similar behaviour to that observed for tensile strength. Narimissa *et al.*, reported that thermal properties of PLA/GNP nanocomposites revealed no difference as compared to the neat PLA, and that GNP do not act as a nucleating agent *(99)*.

Based on study performed by Pinto *et al.*, nanocomposites of poly (lactic acid) and graphene (GNP) as well as graphene oxides (GO) were prepared using solvent-casting technique. The prepared samples were dried under two various conditions; room temperature and vacuum oven. Samples dried at room temperature contained 3 wt% of solvent that acted as a plasticizer. Investigation of mechanical properties revealed that Young's modulus and yield strength both increase significantly for plasticized samples when GNP and GO are incorporated. However, it began to decrease at higher loads of the nanofillers due to aggregation. Moreover, it was demonstrated that elongation at break was independent of the concentration of the incorporated nanofillers. On the other hand, vacuum-dried samples showed a significant reduce in elongation at break when compared to room temperature-dried samples (from 200% for plasticized to 4% for non-plasticized samples). In the same manner, Young's modulus as well as yield strength both increased for vacuum-dried samples by the incorporation of GNP and GO nanofillers (optimum loading 0.4%). Further addition of nanoplatelets resulted in a decrease in Young's modulus and yield strength value. Pinto *et al.* also examined the gas permeability properties for the prepared samples with respect to two different gases, namely, oxygen and nitrogen. It was

reported that by addition of GNP and GO as nanofillers, the gas permeability for the two types of gases has decreased by three-folds and four-folds for oxygen and nitrogen, respectively, when 0.4 wt% of the two fillers was incorporated. This was attributed to the tortuous effect created by the added nanofillers *(101)*.

In another study published by Pinto *et al.* in 2013, PLA/GNP and PLA/GO nanocomposites were examined to investigate their biocompatibility and to determine whether chemical composition, topography, wettability, or surface charge would mostly impact cellular response to implanted surfaces for biomedical applications. Pinto *et al.* concluded that surface topography and wettability have both changed when 0.4 wt% of GNP and GO were incorporated into PLA matrix. However, cell proliferation experienced no change compared to the neat PLA except for nanocomposites that contained GO and were incubated for 24 hours. This was ascribed to the creation of more favourable surface morphology and the increase of film hydrophilicity that favoured cell adhesion and proliferation due to the presence of GO within the nanocomposites. Nanocomposite films also demonstrated no cytotoxicity; thus, small amounts of GNP and GO can be incorporated into nanocomposites to improve their mechanical properties for biomedical applications without risking patients' lives *(102)*.

Pinto *et al.*, also studied the effect of biodegradation for 6 months on the PLA/GNP nanocomposites. It was observed that Young's modulus and tensile strength have both increased by the incorporation of graphene nanoplatelets. After being subjected for biodegradation for 6 months, it was reported that the nanocomposites toughness has decreased slightly compared to neat PLA which demonstrated a decrease in the same property by about 10 folds; it was concluded that addition of GNP greatly minimizes the effect of biodegradation on mechanical properties of PLA/GNP nanocomposites *(103)*.

In a research study by Chieng *et al.*, PLA was plasticized with epoxide palm oil (EPO) and PLA-EPO/GNP nanocomposites samples were prepared through melt blending method. XRD patterns showed a peak characteristic to GNP; this peak indicates that graphene sheets were not completely separated and that they existed in the form of stacks. The intense of the peak further increased with the increase of GNP loads. Chieng *et al.* revealed that the mechanical properties were significantly improved with addition of small concentration of

GNP. Maximum values of tensile strength and elongation at break were obtained at 0.3 wt% of GNP, further increase of GNP loads were associated with decrease in these two values due to stacking of GNP sheets *(104)*.

Chieng *et al.*, have also reported the thermal properties of the prepared PLA-EPO/GNP nanocomposites. According to their findings insertion of GNP into plasticized PLA had no significant effect on the degree of crystallinity of the prepared samples, which was also confirmed by XRD analysis. It was reported that the observed decrease in T_g was due to the addition of 0.3 wt% of GNP to the plasticized PLA and was associated with an increase in the elongation at break of the nanocomposites. However, a further increment of GNP loadings resulted in an increase in T_g value owing to the failure of the plasticizer to interact with PLA molecular chains as plasticizer molecules became trapped within the GNP spacing. TGA analysis revealed that thermal stability is enhanced when GNP is added to plasticized PLA as GNP acts as heat insulator that impede the escape of volatile products formed during decomposition process *(97)*.

Chieng *et al.* also conducted a research study to examine the effect of GNP increment on plasticized PLA. The utilized plasticizer was poly (ethylene glycol) (PEG). Diffraction patterns showed demonstrated a distinctive peak related to the presence of GNP within the plasticized PLA matrix. It was also observed that the plasticized PLA had an amorphous structure, and that by addition of GNP, the degree of crystallinity started to slightly increase. On the other hand, the tensile strength showed an increment with the addition of GNP to PLA/PEG blend; this increment reached maximum at 0.3 wt%, and started to decrease with further addition of the nanofillers. This finding is presumably due to the aggregation of nanoplatelets sheets at higher loads. Furthermore, DSC thermograms revealed that there is a limited increase in crystallinity, which was consistent with results obtained from XRD. TGA curves suggested the increase in thermal stability of the prepared PLA-PEG/GNP nanocomposites *(105)*.

Chieng *et al.*, conducted a study on plasticized PLA/ GNP as well as plasticized PLA/rGO (reduced graphene oxide) nanocomposites using melt blending technique. Two types of plasticizers, namely, polyethylene glycol (PEG) and epoxidized palm oil (EPO) were employed. XRD analysis revealed that the rGO nanofillers were fully exfoliated within the

matrix and existed as a single layer graphene that did not experience any type of aggregation compared to the GNP; this finding was also confirmed through the TEM images. Chieng *et al.*, also revealed that the incorporation of rGO into either neat PLA or plasticized PLA remarkably increased the tensile strength without compromising the elasticity of the samples compared to GNP nanofillers. This result was accounted for the fact that rGO shows better exfoliated individual graphene layers compared to GNP leading to higher aspect ratio as well as enhanced interfacial interaction between the nanofillers and the polymer matrix. On the other hand, TGA analysis showed an increase in thermal stability for PLA nanocomposites and for PLA-EPO nanocomposites compared to neat PLA. On the contrary, PLA-PEG nanocomposites showed a decrease in the thermal stability; this decline in thermal stability is ascribed to the tendency of PEG to distribute around the polymer and to break the polymer - polymer bonding *(106)*. Furthermore, rGO showed better thermal stability compared to GNP nanofillers due to the high aspect ratio of well exfoliated graphene sheets of rGO *(97)*.
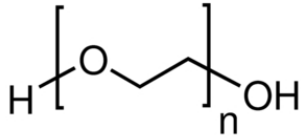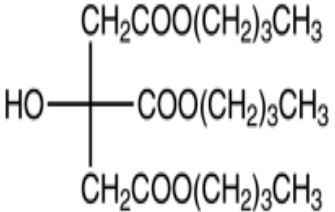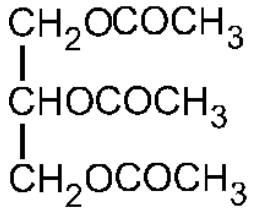
According to a study conducted by Li *et al.*, GNP was prepared by liquid-phase exfoliation method from graphite powder. According to Li *et al.*, this technique is a benign, facile, and of low-cost compared to other methods that require oxidation in strong acidic media or interaction with alkali metal. Exfoliated graphene (GNP) was then introduced into PLA matrix to prepare PLA/GNP nanocomposites. The diffraction patterns of the nanocomposites showed no peak for the GNP, suggesting a complete exfoliation of the prepared GNP with no stacking or aggregations of the graphene layers. Li *et al.* proved through TGA thermograms that the thermal stability increased by addition of GNP to PLA matrix due to the strong interfacial interaction between the polymer and the nanofillers. Furthermore, dynamic mechanical analysis (DMA) demonstrated a dramatic increment in tensile strength properties (from 36.64 MPa to 51.14 MPa) for PLA/GNP nanocomposites compared to neat PLA when 1.0 wt% GNP was incorporated into the polymer *(107)*.

3. Experimental Procedures

3.1. Materials

Poly (lactic acid) (PLA) pellets with a commercial name "Ingeo" grade 4043D, was purchased from NatureWorks LLC, Minnetonka, USA. Ingeo 4043D had a density of 1.24 g/cc, a relative solution viscosity (RV) of 4.0 ± 0.10, and a D-isomer level of $4.25 \pm 0.55\%$. Plasticizers selected for this study were all chosen to be biocompatible with PLA, have no known toxicity, and are classified as (GRAS) (Generally Recognized as Safe). Polyethylene glycol (PEG) was purchased from Loba Chemie, Mumbai, India. Molecular weight of PEG was about 400 g.mol^{-1}. Tri-n-butyl citrate (TBC) and triacetin (also known as glycerol triacetate) were supplied by Alfa Aesar, Karlsruhe, Germany. Both plasticizers had purity of 99%. Plasticizers characteristics are listed in Table (1).

Table 1: Designations and physical properties of used plasticizers

Plasticizer	Designation	Molecular Structure	Molecular Weight (g.mol^{-1})	Boiling Point (°C)	Density (g.cc^{-1})
Polyethylene Glycol	PEG		380 – 420	260	1.13
Tri-n-butyl Citrate	TBC		360.45	325	1.040
Triacetin	TA		218.21	257–259	1.155

Pristine multi-walled carbon nanotubes (CNTs), carboxylic acid functionalized multi-walled carbon nanotubes (CNTCOOH), pristine graphene nanoplatelets (GNP), and carboxylic acid functionalized graphene nanoplatelets (GNPCOOH) were all purchased from Cheap Tubes Inc. Cambridge port, Vermont, USA. Specifications for CNTs in terms of outer diameter (OD), inner diameter (ID), Length (L), COOH content (CC), Purity (P), Ash (A), specific surface area (SA) and for GNPs in terms of diameter (D), average thickness (T_A), number of layers (NoL), COOH content (CC), purity (P), and surface area (SA) are listed in Tables (2 and 3), respectively. Dichloromethane (DCM) solvent was purchased from Sigma Aldrich, Germany. All supplied materials were used as is without further purification.

Table 2: Specifications for carbon nanotubes

Nanofillers	OD (nm)	ID (nm)	L (μm)	CC (wt%)	P (wt%)	A (wt%)	SA (m²/g)
CNT	30 – 50	5 – 10	10 – 20	N/A	>95	< 1.5	>60
CNTCOOH	30 – 50	5 – 10	10 – 20	0.73	>95	< 1.5	>60

Table 3: Specifications for graphene nanoplatelets

Nanofillers	D (μm)	T_A (nm)	NoL	CC (wt%)	P (wt%)	SA (m²/g)
GNP	2	8 – 12	10 – 12	N/A	>97	600 - 750
GNPCOOH	1 – 2	< 3	< 3	7 ± 1.5	>99	>750

3.2. Preparation of PLA Films
3.2.1. Preparation of PLA/Plasticizers Films

Prior to blending PLA with plasticizers, PLA was vacuum dried at 40 °C and 600 mbar for 5 hours. The method that was adopted to fabricate plasticized PLA films was solvent casting method. To prepare PLA/plasticizers blends, 10 wt% PLA/DCM solutions were prepared. 10 wt%, 20 wt%, and 30 wt% of PEG, TBC, and TA plasticizers were added separately to an Erlenmeyer flask with DCM solvent and allowed to stir for 10 minutes to ensure homogeneous mixing of plasticizers and DCM. The pre-dried PLA was then added to the plasticizer/DCM solution and was left to stir for 15 hours until complete dissolution.

The Erlenmeyer flasks were then transferred to water bath sonicator and sonicated for 30 minutes to eliminate air bubbles. PLA/plasticizer blends were then cast on smooth, free of scratches glass plates using a laboratory-designed applicator. The initial thickness of cast solutions was 1 mm that decreased to about 120 µm after evaporation. The cast films were kept in a closed environment to avoid formation of air bubbles and/or deformation of films during evaporation that extended for 24 hours at room temperature. The glass plates were then immersed in distilled water for 10 to 15 minutes to facilitate peeling off the films. To eliminate residual solvent, which also acted as a plasticizer, films were further vacuum dried at 20 °C and 600 mbar for 24 hours.

3.2.2. Preparation of PLA-TA/Nanofiller Nanocomposites Films

Prior to blending PLA with triacetin, PLA was vacuum dried as described in section 3.2.1. The method that was adopted to fabricate PLA-TA/Nanofillers nanocomposites films was solvent casting method. 10 wt % PLA/DCM solutions of 10 wt % TA with 0.1%, 0.5%, and 1.0% of CNT, CNTCOOH, GNP, and GNPCOOH were prepared as follows. First, DCM solvent was divided into two unequal portions (1: 4.4). TA 10 wt% was added to the larger portion of DCM and allowed to stir for 5 minutes, then, pre-dried PLA was added to the mixture and was allowed to stir for 4 hours until complete dissolution. Different concentrations of different nanofillers were added separately to the smaller portion of DCM and were sonicated continuously for 2 minutes using a probe sonicator. Sonicated nanofillers were then added to the completely dissolved PLA/TA/DCM solution and left to stir for 24 hours. The solutions were then transferred to water bath sonicator and sonicated for 10 minutes for degasing. The solutions were then casted, dried, and peeled off as described in section 3.2.1.The initial thickness of cast solutions was 1 mm that decreased to about 90 – 100 µm after evaporation.

3.3. Characterization Methods
3.3.1. Stress-Relaxation Measurements

The stress-strain isotherms of the various samples at room temperature were obtained from casted film specimens. According to ASTM D882 method, samples free of pinholes and air bubbles with specific width, length, and thickness of 1.5 cm x 9 cm x 0.0085 cm, respectively, were cut from the PLA films to evaluate the mechanical response of the samples and the influence of the inclusion of the plasticizers and nanofillers on the mechanical behavior of the samples according to:

$$[f^*] = f/[A^* (\alpha - \alpha^{-2})] \qquad\qquad (1),$$

where $[f^*]$ is the modulus, A^* is the cross-sectional area and α is the elongation. The equilibrium elastic force, f^*, was recorded after the force reading has become constant for at least 15 min. Three replicates of each sample were tested.

3.3.2. Fourier Transform Infra-Red Spectroscopy (FT-IR)

The chemical structures of the prepared samples were investigated to report whether any new bonds or interactions were formed during blending. FT-IR spectra of PLA neat and PLA/plasticizers films were recorded using Thermo Scientific Nicolet 380 FT-IR, Waltham, MA, USA. The spectra were recorded in wavenumber ranged between 450 and 4000 cm^{-1} at room temperature. The investigated films were cut into 2 cm x 2 cm with a thickness of about 85 - 120 µm. The FT-IR measurements were obtained by averaging 32 scans at resolution of 4 cm^{-1}. The FT-IR spectra of pure powdered nanofillers were obtained by KBr pellet technique using the same instrument. The FT-IR spectra of pure plasticizers in the liquid form were obtained using Bruker ATR-FT-IR instrument (Billerica, Massachusetts, USA). The spectra were recorded between 500 and 4000 cm^{-1}.

3.3.3. Differential Scanning Calorimetry (DSC)

To assess the effect of plasticizers and nanofillers on the thermal behaviour of PLA matrix, differential scanning calorimetry instrument (PerkinElmer PYRIS Diamond Autosampler, Waltham, Massachusetts, USA) was employed. The investigated films were cut into small pieces, and around 17 mg of each specimen were weighed into a 50 µL aluminum pan and

sealed with a cover using universal crimper press. Heating-cooling-heating cycles were performed under nitrogen atmosphere. During the DSC experiment, samples were heated from room temperature to 200 °C at a rate of 10 °C/min, where upon, the temperature was held at 200 °C for 10 minutes to remove thermal history. The samples were then cooled from 200 °C to – 20 °C at a rate of 10 °C/min and again held at – 20 °C for 10 minutes. The next step was to reheat the samples from – 20 °C to 200 °C at a rate of 10 °C/min. The glass transition temperature (T_g), cold crystallization temperature (T_{cc}), and melting temperature (T_m) were all determined from the second heating scan. Enthalpy of cold crystallization (ΔH_{cc}) and enthalpy of fusion (ΔH_m) were both determined by integrating the areas (J/g) under the peaks. The degree of crystallinity is then calculated using the following equation *(95, 99)*:

$$X_C \% = (\Delta H_m / \Delta H_m°)\ 100 \qquad\qquad (2),$$

where $\Delta H_m°$ is the theoretical melting enthalpy of 100% crystalline PLA, and is considered to be 93 (J/g) *(95, 99)*.

3.3.4. Thermogravimetric Analysis (TGA)

The thermal stability of prepared films was studied using TA Instruments TGA Q50, Lukens Drive, New Castle, USA. Films were cut into small pieces and about 6 – 10 mg of each sample was weighed into aluminum crucible. An empty aluminum crucible was then used as reference during measurements. Samples were then heated from room temperature to 600 °C at heating rate of 10 °C/min. The analysis was carried out under nitrogen atmosphere with nitrogen flow rate of 50 ml/min. During these scans sample weight change and sample temperature were recorded. The first derivative (DTG) curves were then plotted depending on calculations from TGA curves.

3.3.5. Mercury Intrusion Porosimeter (MIP)

Studies on porosity characteristics for the prepared neat PLA, plasticized PLA and plasticized PLA nanocomposites films were conducted using the automatic PoreMaster mercury intrusion/extrusion porosimeter, Quantachrome Instruments, Florida, USA. To perform the analysis, samples were cut into small pieces (5 mm x 5 mm) with thickness of

85 μm. About 0.15 g were then weighed and were introduced into the penetrometer. The penetrometer with the sample in it was then transferred to the pressure chamber to measure pore properties.

3.3.6. Natural Biodegradation Test

The biodegradability of the prepared films was examined under natural conditions. A plant-based compost (sugarcane compost) was provided by Research Institute for a Sustainable Environment (RISE). The compost pile was prepared using the plant-based, wood shavings, and pigeons' wastes in a glass reservoir. The dimensions of the used pile were 100 cm length, 50 cm width, and 30 cm height. The experiment was conducted for 4 months. Samples were cut into 9 cm x 1.5 cm stripes with their initial weights recorded. The samples were then placed in the compost pile on a depth of 25 cm. The samples were removed from the compost pile every month and re-weighed. The loss in weight due to biodegradation was recorded as an average of 5 replicates for each sample. Temperature and soil humidity were recorded monthly.

3.3.7. Water Absorption Test

Water absorption test was conducted based on the standard method described in ASTM D570 – 98. The "twenty-four hours immersion" method was applied. Samples with smooth edges and a size of 76 mm x 25 mm were cut from original films. The samples were then conditioned in a vacuum oven at 50 °C and 200 mbar for 24 hours and weighed using a balance capable of reading 0.0001 g (W_c). The dried films were then completely immersed in distilled water at 20 °C for 24 hours. The specimens were then removed from distilled water and were wiped off with a tissue paper to get rid of excess water on the surface of the specimen and re-weighed (W_i). The samples were then re-conditioned at the same conditions that were used in the original drying process to test for water-soluble residual if existed (W_r). The water absorption was then calculated based on the weight gain after immersion in water and weight loss after re-conditioning due to presence of water-soluble residuals according to the equations (3, 4, and 5)

wt increase %= [(W$_i$) − W$_c$)/W$_c$] 100 $\qquad$ (3),

Soluble matter lost %= [(W$_c$ − W$_r$)/W$_c$] 100 $\qquad$ (4),

Percentage of water absorbed % = (3) + (4) $\qquad$ (5)

The water absorption percentage values were recorded as an average of three replicates for each sample.

3.3.8. Oxygen Permeability Test (OP)

Oxygen permeability was examined according to ASTM D3985 using GDP-C - Gas Permeability Tester (Brugger Feinmechanik GmbH, Munich, Germany). Samples were examined under optical microscope to ensure absence of pinholes, and were then cut with diameters of about 12 cm to fit into the permeation cell. The thickness of samples was the average of 25 measurements and ranged between 80 and 90 µm. Specimens were tested at 23 °C ± 2 and relative humidity of 50% ± 5.

3.3.9. Water Vapour Transmission Rate Test (WVTR)

Water vapour transmission property for the prepared films was measured gravimetrically according to a modification of standard method ASTM E96/E96M − 12. The "desiccant method" was applied, where CaCl$_2$ was first vacuum-dried at 60 °C and 700 mbar for 19 hours. Specimens free of defects and pinholes were sealed to the opening of an autoclave bottle containing a 1.5 cm of desiccant using paraffin wax. The diameter of the autoclave bottle opening was 4 cm. The thickness of tested films was the average of 6 measures in different positions of the film and was about 85 µm. The assembly was then weighed with an accuracy of 0.0001 g and placed under controlled atmosphere using a dry keeper. Relative humidity was maintained constant at 92% using NaCl saturated solutions *(108)*. Recorded temperatures ranged between 23 °C and 25 °C. The test was conducted for 7 days, and the assemblies were weighed at 24 hours intervals. The autoclave bottles were shaken horizontally every time after weighing. Obtained results were represented in graphs by plotting weight gain against elapsed time.

4. Results and Discussion

4.1. Investigation of the Physical Properties of PLA Plasticized with Different Plasticizers

In order to contribute to sustainable development and to address the depleting oil and gas resources, researchers are now utilizing biorenewable biodegradable polymers as food packaging materials, which should provide safe plastic products and greener environment. However, biopolymers possess poor mechanical properties. Poly (lactic acid) for example, is known to be naturally brittle polymer. In order to overcome stiffness of biopolymers, use of plasticizers and nanofillers is implemented to improve the mechanical properties of the biopolymers.

4.1.1. Stress Relaxation Measurements

Mechanical properties of the prepared samples were reported based on triplicate measurements except for neat PLA samples, which were based on single measurement. PLA was reported to have high elastic modulus and low elongation at break, which significantly restricted its application in packaging field. Natural plasticizers were employed in order to overcome its limitation by increasing its flexibility and deformability *(109)*. The three plasticizers employed in this study were chosen based on their ability to impart flexibility to PLA, their compatibility, their low toxicity, and being "Generally Recognized as Safe" (GRAS) properties. PEG is generally used for pharmaceutical and medical applications, TBC is also used for pharmaceutical applications and is sometimes utilized as an additive in food where TA is generally used as solvent for flavours in food industry *(109)*.

Stress strain isotherms of neat PLA and plasticized PLA using three different types and concentrations are represented in Figures (6 − 13). Additionally, the ultimate mechanical properties such as the maximum elongation (α_m), maximum nominal force (f^*_m), and the maximum energy required to reach maximum nominal stress at maximum elongation (E_m) for the investigated samples were calculated and were reported in Tables (4 − 6). From Figure (6), it was obvious that PLA exhibited high modulus and very low tensile elongation.
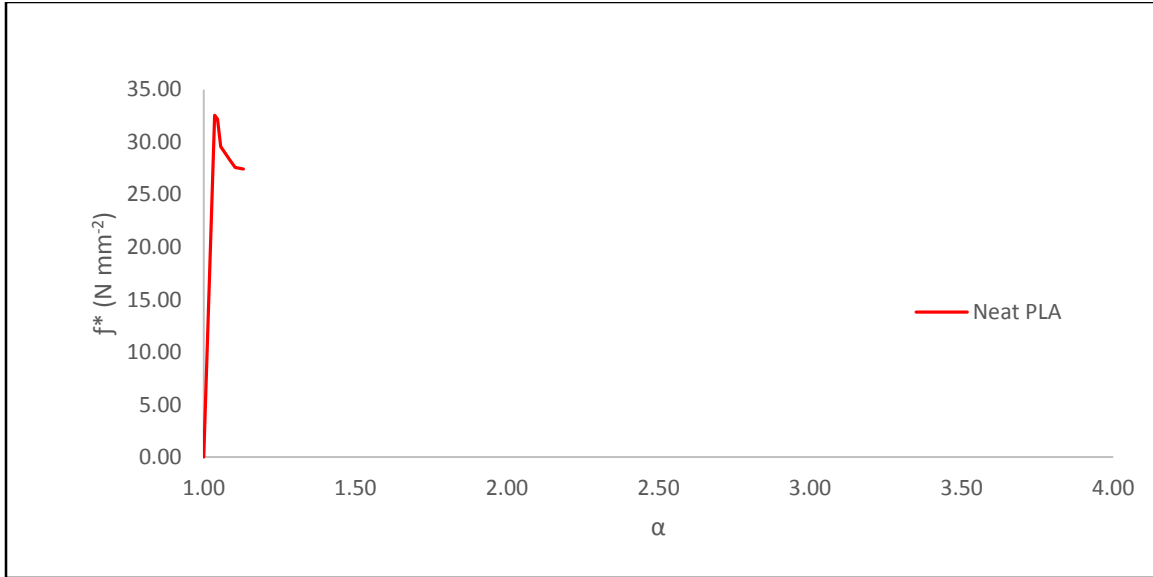
Figure 6: Stress-strain isotherm of PLA: nominal force f* versus elongation α

This behaviour was attributed to the high glass transition of PLA (about 63 °C) as proved by DSC analysis. Below T_g, PLA exhibits rigid behaviour and low mobility that restrict its application to food packaging. As expected, stress relaxation curve Figure (7) showed that the reduced modulus [*f**] is decreases with the increase in elongation in line with Mooney-Rivlin Equation (7)

$$[f^*] = 2C_1 + 2C_2\, \alpha^{-1} \qquad (7),$$

where $2C_1$ and $2C_2$ are constants.

According to the Mooney-Rivlin relationship, the relationship between the reduced force or modulus, [*f**], and the reciprocal elongation, α^{-1}, resembles that of a straight line with the decrease in the reciprocal elongation or increase in the elongation results with a decrease in the modulus.
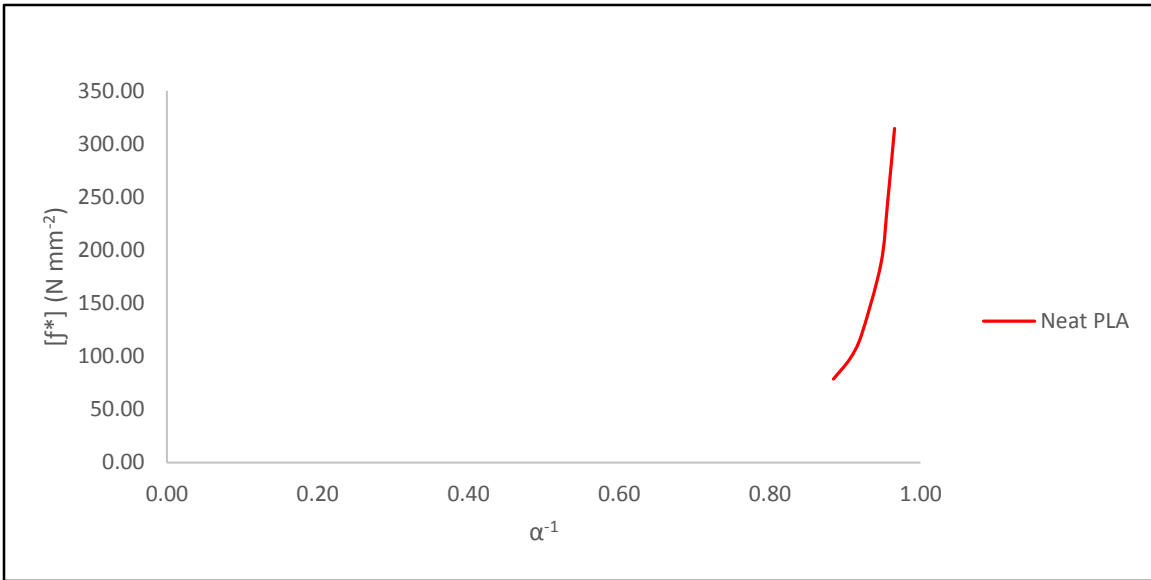
Figure 7: Stress-strain isotherm of PLA: modulus [f] versus reciprocal elongation α^{-1}*

In order to overcome the stiffness of PLA, PEG plasticizer was added in different concentrations to PLA. Figure (8) showed that tensile elongation (α) has slightly increased at the expense of elastic modulus, which showed a significant decrease (by at least 52%) for PEG plasticized samples.

Figure 8: Stress-strain isotherms of PLA/PEG blends at different concentrations: nominal force f versus elongation α*

Figure 9: Stress-strain isotherms of PLA/PEG blends at different concentrations: modulus [f*] versus reciprocal elongation α^{-1}

Further increase of PEG content was expected to increase tensile elongation as was reported elsewhere *(109)*, however, it was observed that increasing PEG concentrations (PEG 20% and 30%) was associated with a decrease in both, tensile elongation and nominal force as compared to PLA/PEG 10% blends. Such behaviour may be attributed to the dissolution of the high crystalline content as observed in the DSC measurements discussed in section 4.1.3. The DSC thermograms indicated that PLA/PEG blends had the highest crystalline content, which reached as much as 20% more than that of other used plasticizers. These highly crystalline blends restricted the motion of the more orderly molecular chains of PLA, thus resulting in the further increase in its stiffness at higher concentrations of PEG. It was also suggested that the strong interactions between the hydroxyl groups of PEG molecules and PLA chains has adversely affected the process of softening the PLA matrix as illustrated by FT-IR analysis in section 4.1.2. This phenomenon is reported in the literature as "antiplasticization effect" and can result in further increase in the rigidity of the polymeric matrix instead of enhancing its flexibility *(110)*. This was also observed for elongation values, which decreased relative to that of neat PLA due to the formation of the strong hydrogen bonding. This has obviously restricted the motion of polymeric chains. Table (4) compares the maximum elongation at break (α_m), maximum nominal force at break ($f*_m$), and amount of energy required to break

39

the sample or reach maximum elongation for neat PLA and PLA/PEG blends of different concentrations.

Table 4: Ultimate mechanical properties for neat PLA and PLA/PEG blends at different concentrations

Material	α_m	f^*_m (N mm^{-2})	E_m (J mm^{-3})
Neat PLA	1.13	27.42	3.47
PEG 10%	1.32 ± 0.09	12.99 ± 0.62	4.03 ± 1.24
PEG 20%	1.10 ± 0.04	10.90 ± 2.33	0.82 ± 0.35
PEG 30%	1.22 ± 0.15	6.71 ± 0.49	1.17 ± 0.95

As can be seen from the listed results in Table (4), the maximum nominal force has significantly decreased by addition of PEG with very slight increase in maximum elongation at break. The low energy required to break neat PLA and PLA/PEG blend samples indicated the high stiffness of the prepared materials. Highly stiffened samples showed low resistance to applied stress due to the inability of molecular chains to move freely, thus, failing to resist stress. Stress relaxation curves for PLA/PEG blends of different concentration showed a normal behaviour as the case in neat PLA. PEG can be considered the less efficient plasticizer as compared to the other two plasticizers. This finding was consistent with Grigale *et al.* published study; it was stated that the structure of PEG was not similar to PLA, thus, its effect as a plasticizer was diminished compared to other plasticizers employed in their study *(109)*.

Unlike PEG plasticizer, TBC plasticizer isotherms (Figures 10 and 11) demonstrated a significant increase in tensile elongation that was associated with the expected decrease in nominal force.
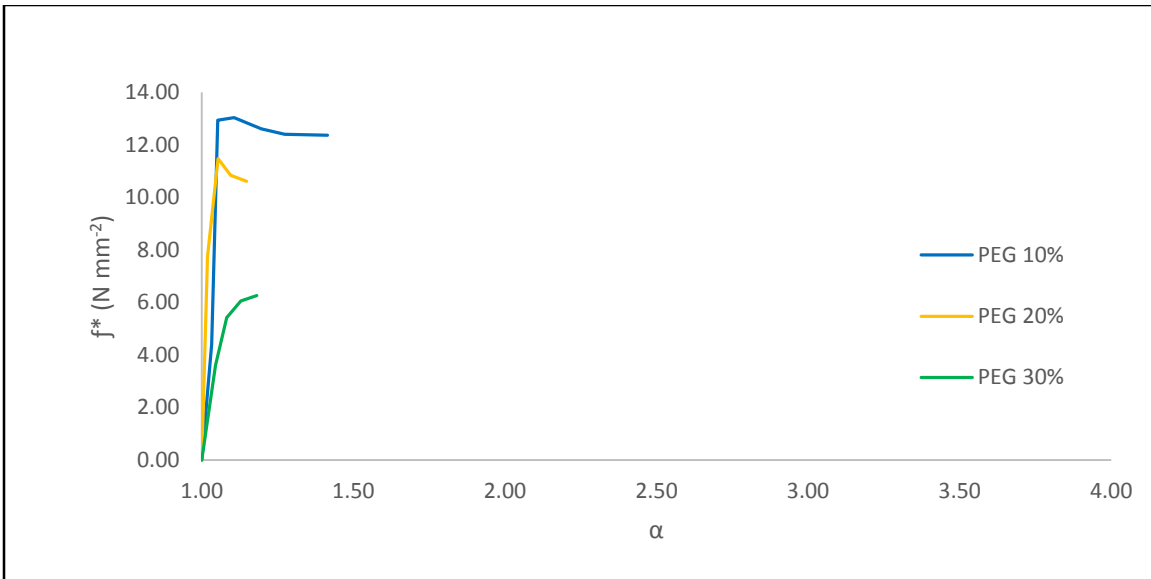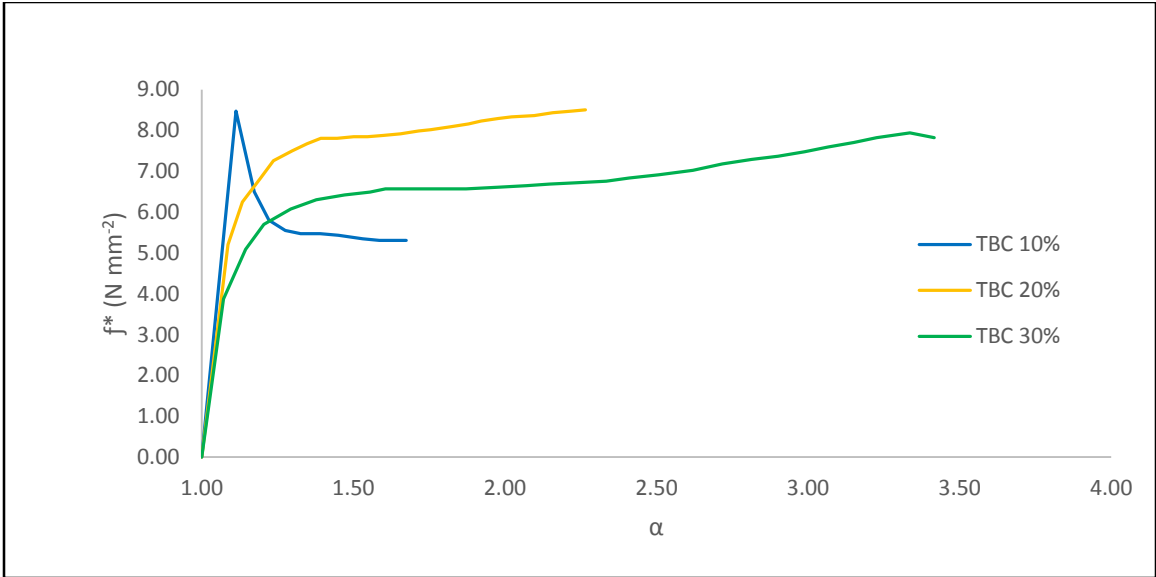
Figure 10: Stress-strain isotherms of PLA/TBC blends at different concentrations: nominal force f* versus elongation α
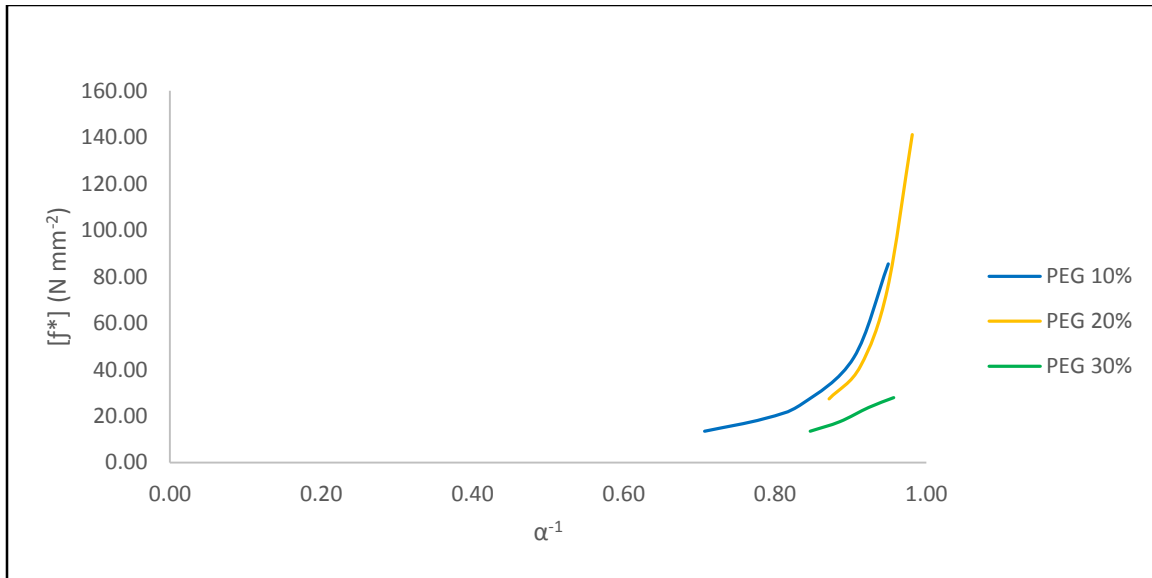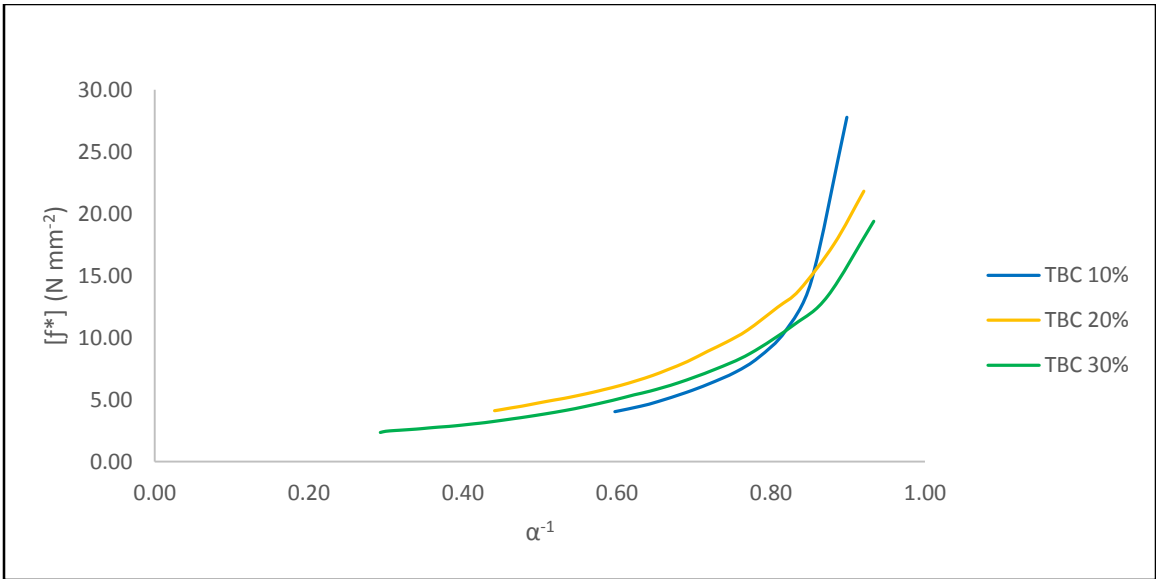

Figure 11: Stress-strain isotherms of PLA/TBC blends at different concentrations: modulus [f*] versus reciprocal elongation α^{-1}

The increase in flexibility by addition of plasticizers was attributed to the decrease of glass transition, which was demonstrated through DSC analysis (section 4.1.3). T_g has decreased from about 63 °C to 43 °C for TBC 10% or even lower values for higher concentrations of TBC. TBC Plasticizer increased flexibility by creating free volumes within PLA matrix;

thus, increased the mobility of PLA molecular chains and decreased T_g values. Table (5) lists the ultimate mechanical properties PLA/TBC blends as compared to neat PLA.

Table 5: Ultimate mechanical properties for neat PLA and PLA/TBC blends at different concentrations

Material	α_m	f^*_m (N mm^{-2})	E_m (J mm^{-3})
Neat PLA	1.13	27.42	3.47
TBC 10%	2.29 ± 0.54	7.91 ± 2.65	7.74 ± 3.02
TBC 20%	2.45 ± 0.20	8.76 ± 0.18	10.82 ± 1.93
TBC 30%	2.54 ± 0.91	5.97 ± 1.95	10.67 ± 8.83

From the table, tensile elongation was reported to increase by 102.65%, 116.81%, and 124.87% for TBC 10%, TBC 20%, and TBC 30%, respectively. On the other hand, the maximum nominal force demonstrated a remarkable decrease with the increase of TBC content that reached 78% in case of PLA/TBC 30% blends. It was also observed that the energy required to break the sample has significantly increased by about 123%, 212%, and 207% for TBC 10%, TBC 20, and TBC 30%, respectively. This remarkable increase in energy was ascribed to the increased toughness of PLA/TBC blends where TBC induced flexibility to PLA matrix by facilitating the motion of the molecular chains to resist the applied stress.

Investigating the effect of adding different concentrations of TA plasticizers to PLA matrix on mechanical properties is represented in Figures (12 and 13).
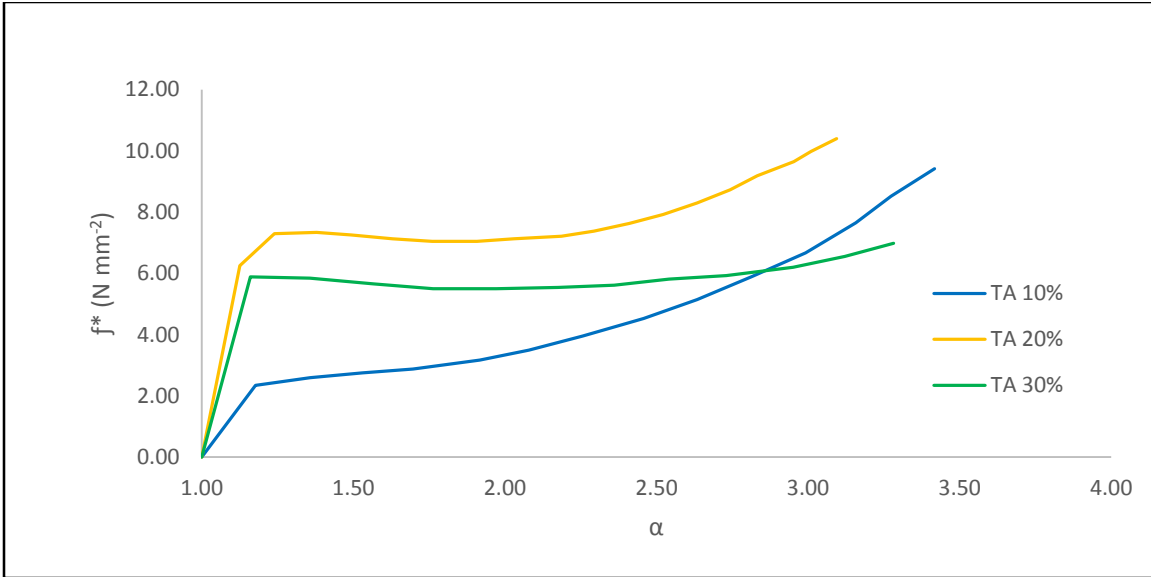
Figure 12: Stress-strain isotherms of PLA/TA blends at different concentrations: nominal force f* versus elongation α
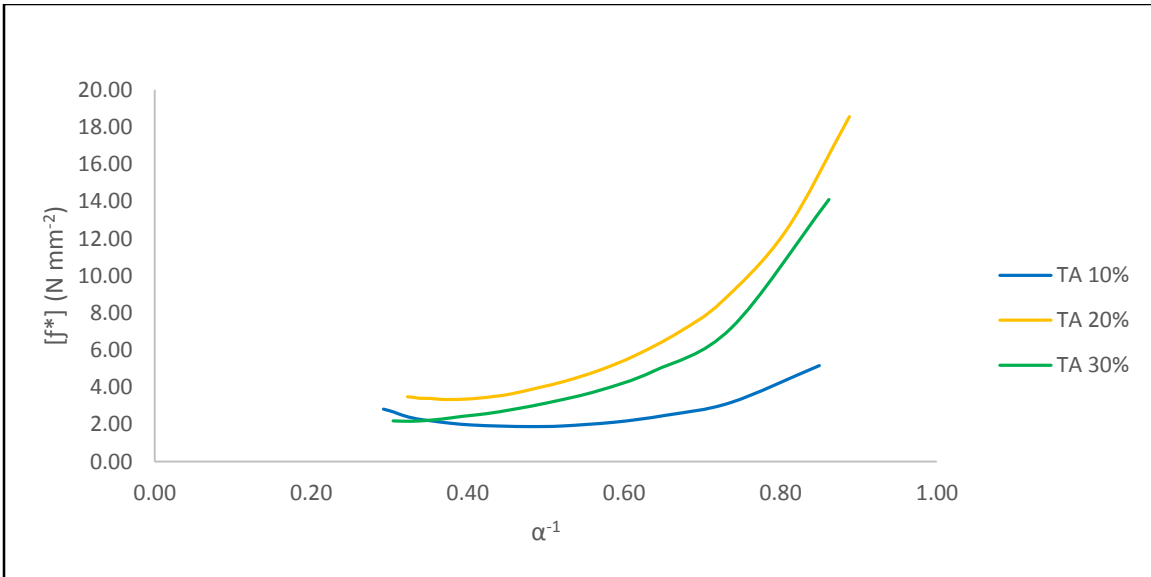
Figure 13: Stress-strain isotherms of PLA/TA blends at different concentrations: modulus [f*] versus reciprocal elongation α^{-1}

As can be seen from the figures, TA increased the tensile elongation by more than 165% for all different loads of TA. The plasticizing effect of TA was proved by DSC analysis, which demonstrated a remarkable decrease in T_g values by more than 10 °C with respect to neat PLA. Compared to PEG and TBC plasticizers utilized in this study, TA proved to be more compatible with PLA. This may be due to the fact that both PLA and TA have

similar structures as they both contain several ester groups. This finding was consistent with Grigale *et al.* whose studies showed that TA had higher elongation efficiency when compared to other PLA plasticizers used to plasticize PLA *(109)*. Table (6) as well as Figure (14) depict the ultimate mechanical properties for PLA/TA blends of different concentrations as compared to neat PLA.

Table 6: Ultimate mechanical properties for neat PLA and PLA/TA blends at different concentrations

Material	α_m	f^*_m (N mm^{-2})	E_m (J mm^{-3})
Neat PLA	1.13	27.42	3.47
TA 10%	3.40 ± 0.13	9.86 ± 0.52	12.41 ± 1.19
TA 20%	3.01 ± 0.24	9.81 ± 1.60	15.18 ± 3.37
TA 30%	3.42 ± 0.15	7.54 ± 0.51	15.28 ± 1.44

From the table, it was observed TA plasticizer showed highest maximum elongation at break among all other studied plasticizers. The maximum nominal force at break was maintained in spite of the increased tensile elongation. This may be attributed to the high compatibility of TA with PLA matrix.
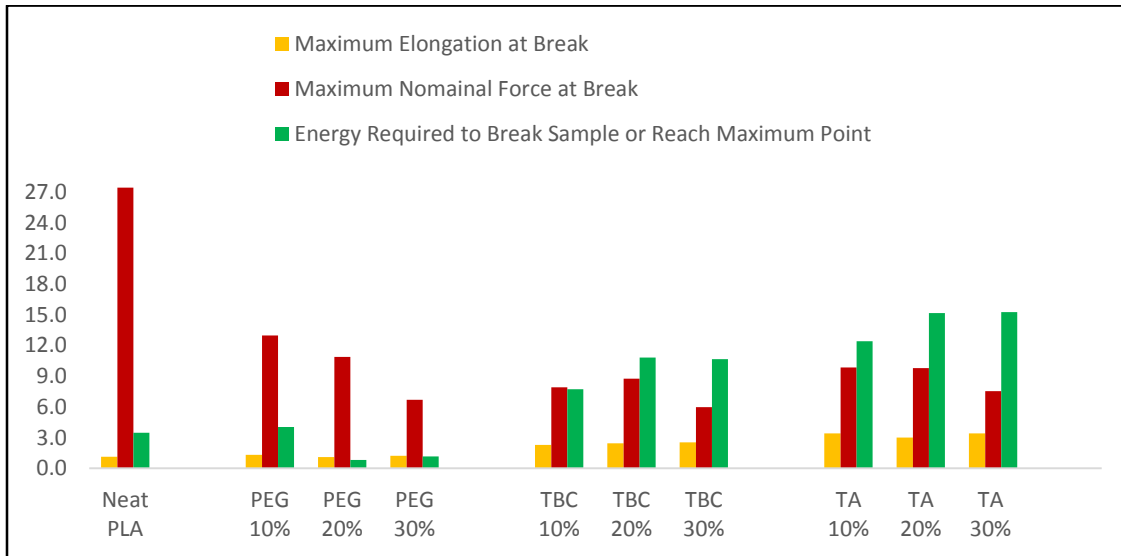
Figure 14: Ultimate mechanical properties for neat PLA and PLA/Plasticizers blends at different concentrations

Furthermore, this behaviour was suggested to also increase PLA/TA blends toughness, which resulted in significantly increasing the amount of energy required to break the

samples. Stress relaxation curves showed normal behaviour for both TA 20% as well as TA 30% where the modulus showed a gradual decrease at higher elongation values. This behaviour is expected since at higher elongation values, the material experiences higher stress that tends to weaken the investigated sample until it reaches the break point. However, for PLA/TA 10% blend, an interesting behaviour was observed. Instead of decreasing continuously with increased elongation values, the modulus had an upturn behaviour as illustrated in Figure (15).
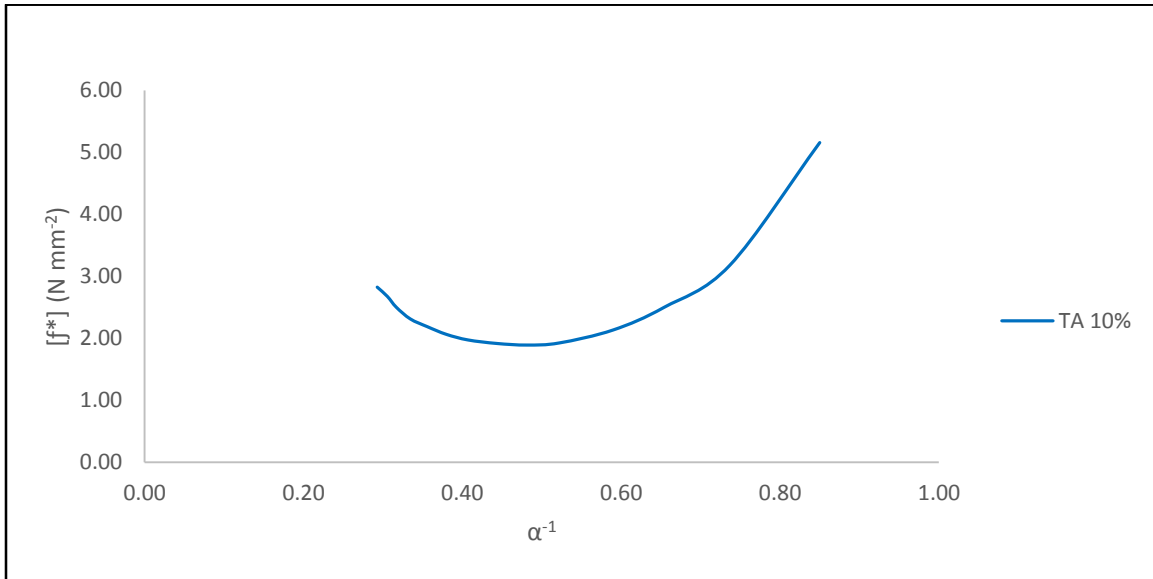
Figure 15: Stress-strain isotherm of PLA/TA 10% blend: modulus [f] versus reciprocal elongation α^{-1}*

This implied that in response to the applied stress, polymeric chains started to strengthen further at these high elongation values. The experienced high toughness as well as high energy required to break PLA/TA 10% samples was accounted for such behaviour *(111)*. This interesting observation could be explained in terms of "strain induced crystallinity" effect, where at higher elongation values, the PLA polymeric chains experience some kind of order which results in formation of small crystallites adding to the total strength of the sample. This behaviour is quite unique to PLA/TA 10% blend in this study. By further increasing the TA plasticizer content to 20% and 30%, the upturn disappeared and both concentrations demonstrated normal behaviour possibly, due to dissolution of any formed crystallites in the presence of high concentration of the plasticizer. Therefore, and due to its enhanced mechanical strength, 10% TA is considered as the optimum concentration for

the PLA blend system and thus PLA/TA 10% blend was chosen as the base system for further studies on the effect of nanofillers on PLA properties. Such performance of PLA/TA 10% is of significant impact particularly in food packaging industry where high flexibility and resistance to tear at high elongations are highly required.

4.1.2. Fourier Transform Infrared (FT-IR) Analysis

As mentioned in section 4.1.1 plasticizers may affect the behaviour of PLA. FT-IR could thus be used to examine the molecular interaction force for better understanding of molecular behaviour. Figure (16 – 19) demonstrate the FT-IR spectra of neat PLA, PLA/PEG, PLA/TBC, and PLA/TA with various concentrations for each plasticizer. For neat PLA (Figure 16), a sharp peak is shown at 3503.6 cm^{-1} indicating the stretching vibration of (O – H) in the hydroxyl and carboxylic groups. The (–CH$_3$) asymmetric and (–CH$_3$) symmetric stretching vibrations have been identified at 3000 and 2945.4 cm^{-1}, respectively. The sharp peak taking place at 1785.9 cm^{-1} is attributed to the stretching of the carbonyl group (C=O) in the carboxyl group. The two peaks at 1460 cm^{-1} and 1228.5 cm^{-1} are assigned to the bending mode of the asymmetric and symmetric vibrations of (–CH$_3$), respectively. The spectrum also displays characteristic peaks at 956.1 cm^{-1} and 894.9 cm^{-1} that could be ascribed to the stretching vibration of (O – C=O) (ester) bond. These assignments were similar to those shown in literature *(105, 112, 113)*.

Figure 16: FT-IR spectrum for neat PLA

Furthermore, the FT-IR spectrum of pure liquid of PEG 400 (spectrum is not shown) demonstrated three distinctive peaks at 3465.36 cm^{-1}, 2866.12 cm^{-1}, and 1294.87 cm^{-1}. These peaks were attributed to the stretching vibrations of (O – H), (-CH$_2$), and (C – O – C) functional groups, respectively *(114, 115)*. However, for the FT-IR spectra (Figure 17) of PLA/PEG blends, a strong broad band in the range of 3200 cm^{-1} to 3700 cm^{-1} was observed for the three spectral analyses of various concentrations of PEG plasticizer. The appearance of this sharp broad band may be attributed to the formation of strong hydrogen bonding between the (O – H) groups found on both the PLA matrix and the PEG plasticizer, which caused broadening in the observed (O – H) vibrational bands *(110)*.
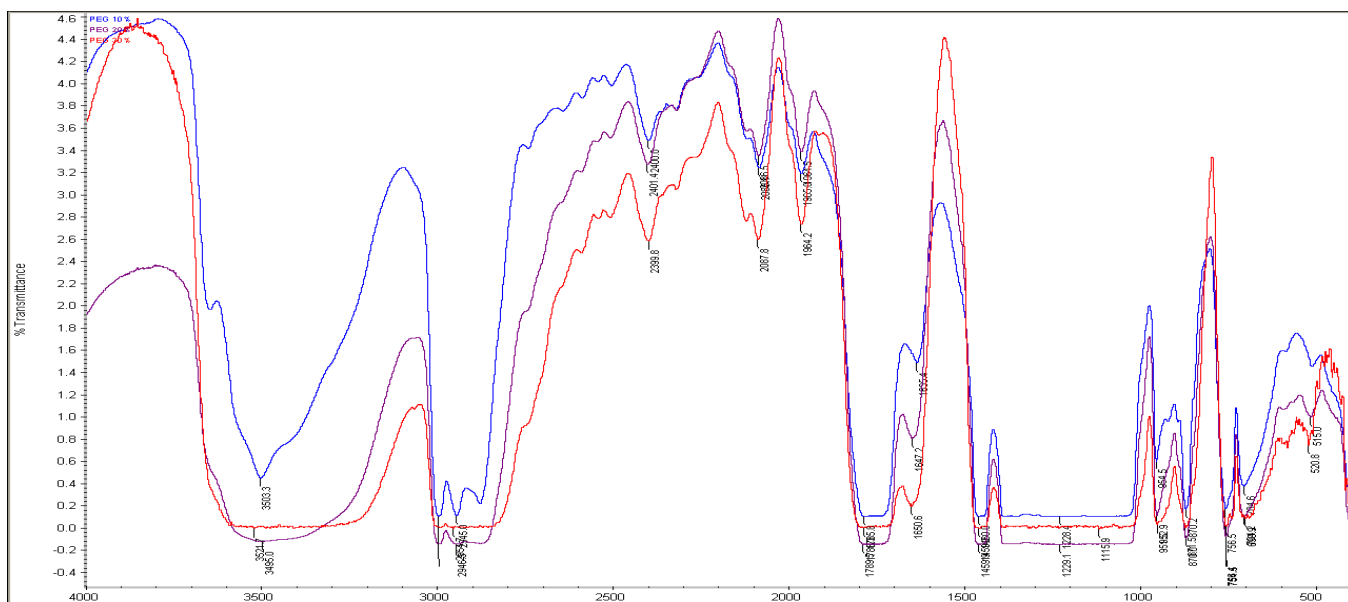
Figure 17: FT-IR spectra for PLA/PEG blends at different concentrations

For pure liquid of TBC (spectrum is not shown), the spectral analysis showed characteristic peaks at 3516.49 cm^{-1} (O – H), 2960.48 cm^{-1} (-CH$_3$), 2874.02 cm^{-1} (-CH$_2$), 1740 cm^{-1} (C=O), and 1178.45 cm^{-1} (C – O) (1 – 4). The FT-IR for PLA/TBC blends (Figure 18), all showed the same spectra that was also consistent with the spectrum of neat PLA. This consistency proved that no new functional groups were formed and that the plasticizer was only physically interacting with the biopolymer rather than forming new chemical bonds.
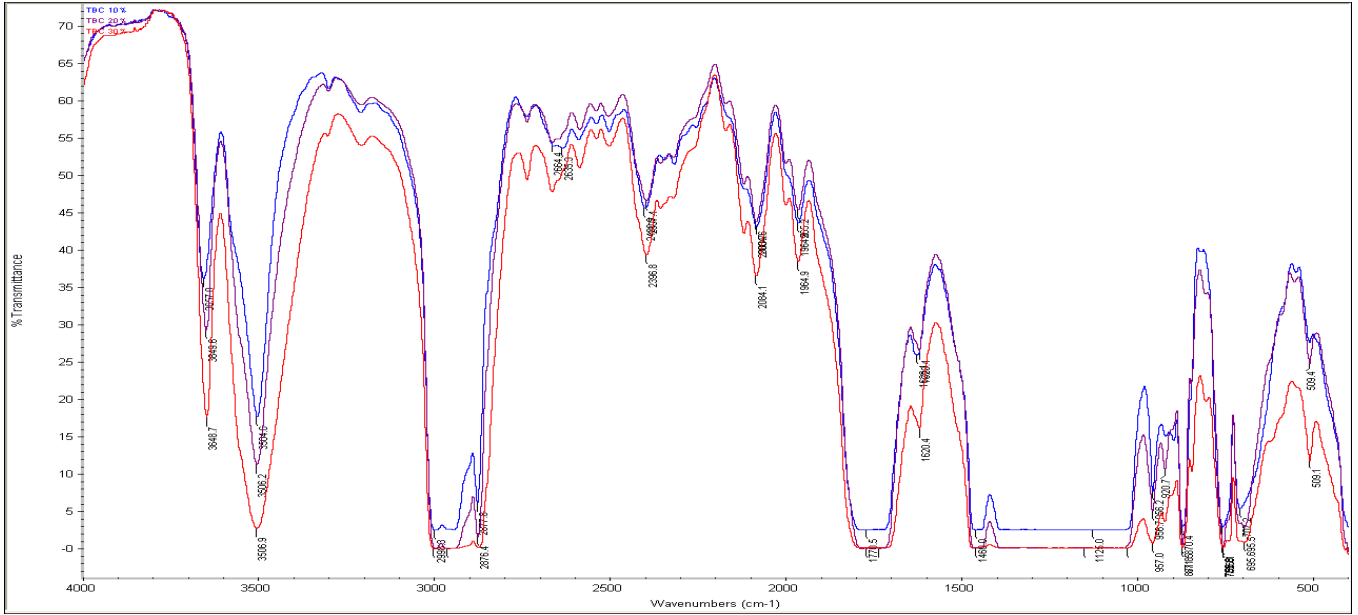
Figure 198: FT-IR spectra for PLA/TBC blends at different concentrations

For pure liquid of TA (spectrum is not shown), the FT-IR chart showed peaks at 3038.06 cm^{-1} and 2962.16 cm^{-1} that were corresponding to asymmetric and symmetric stretching of (–CH$_3$). The spectra also demonstrated a peak at 1647.34 cm^{-1} that was assigned for the carbonyl group (C=O) stretching, peaks at 1438.69 cm^{-1} and 1370.29 cm^{-1} that were attributed to the (C – H) bending modes, as well as a peak at 1098.92 cm^{-1} assigned for the (O – C=O) stretching vibration of the ester group *(116)*. Similar to PLA/TBC blends, plasticizing PLA using triacetin did not result in the demonstration of any new bands.
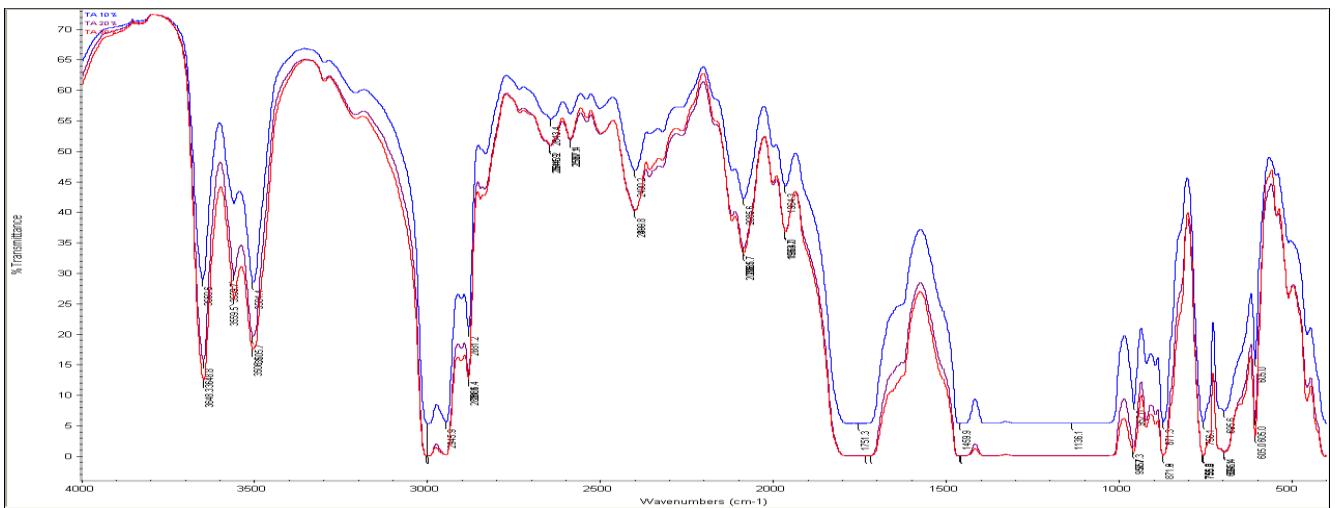
Figure 189: FT-IR spectra for PLA/TA blends at different concentrations

48

This indicated that no chemical interaction was taking place when PLA was plasticized with triacetin.

4.1.3. Differential Scanning Calorimetry Analysis (DSC)

The influence of the plasticizer on the crystalline nature of PLA could further be investigated using DSC technique. The second heating cycles of neat PLA as well as plasticized PLA are depicted in Figures (20 – 22). First heating and cooling cycles are not shown. Figure (20) compares PLA, which was plasticized with different concentrations of PEG to neat PLA.
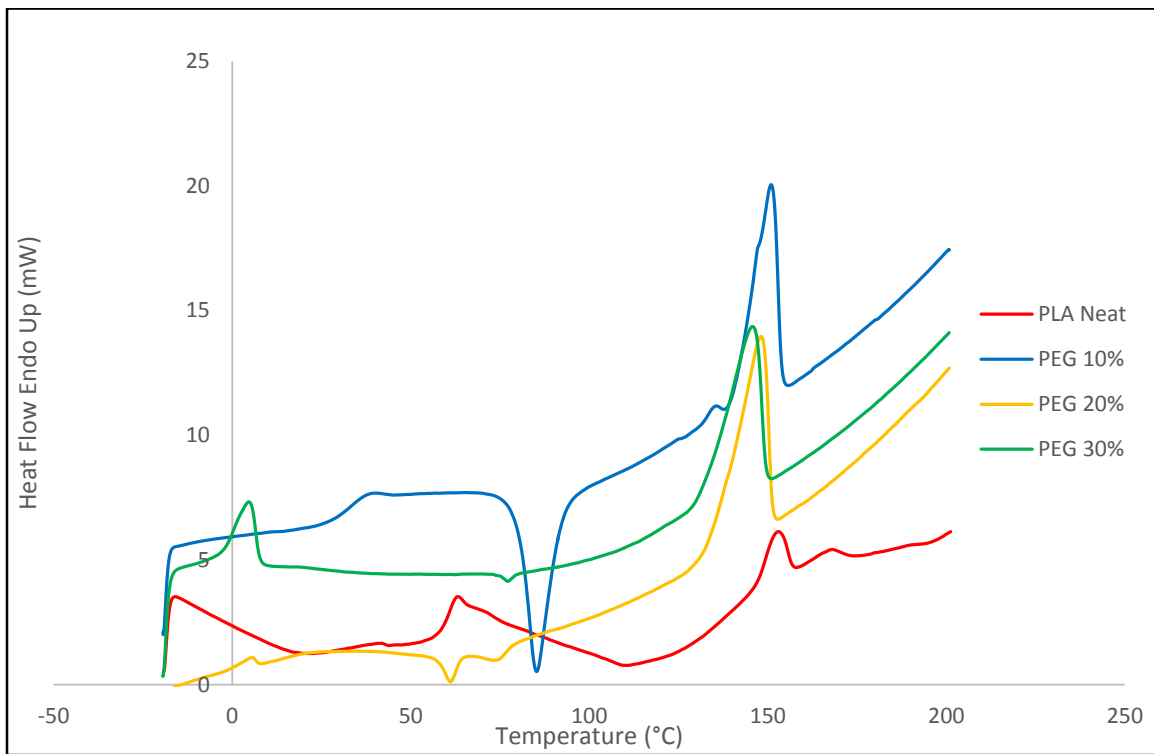
Figure 20: DSC thermograms for neat PLA and PLA/PEG blends at different concentrations

It was observed that neat PLA has a small melting peak (T_m) at 152.99 °C, and a glass transition temperature (T_g) at 63.23 °C. DSC curves also showed that neat PLA has no peak that represents cold crystallization temperature (T_{cc}). This indicated that neat PLA has slow crystallization kinetics, and it may remain in amorphous state under standard processing conditions *(59, 109)*. The amorphous state of neat PLA was also confirmed by the absence of crystallization peak during cooling cycle (cooling curves are not shown) *(117)*. Addition

of PEG with different concentrations to the neat PLA have significantly decreased T_g of neat PLA, and it was revealed that the higher the concentration of PEG, the lower the T_g of plasticized PLA. Furthermore, the melting point (T_m) of neat PLA has shifted to lower temperature when PEG was added; this shift was observed to be more pronounced when PEG content was increased. Additionally, addition of PEG was found to enhance PLA crystallization (T_c), and hence fusion process (T_m) resulting in more intense melting peaks for the plasticized PLA. This was due to the ordering and re-ordering of PLA chains taking place to form new crystals in a process known as crystal perfection. According to previous studies, when PLA was plasticized with different plasticizers, T_{cc} was shifted towards lower temperature by increasing plasticizer content. The obtained results from this study were consistent with literature for PEG 10% and PEG 20%; however, for PEG 30% it demonstrated a small T_{cc} peak at higher temperature rather than a further decrease as expected, which might be due to the dilution effect associated with the by PEG plasticizer *(118)*. PEG 20% and PEG 30% both showed extremely weak cold crystallization peaks compared to PEG 10%. This behaviour was exhibited as higher concentrations of PEG instigated almost complete crystallization of PLA/PEG blend from the molten state during cooling process. This is confirmed by the presence of an exothermic peak around 65 °C and 75 °C for 20% and 30% PEG loads, respectively. Compared to the other two plasticizers investigated in this study, it was observed that the degree of crystallinity for PLA/PEG blends was the highest. This behaviour has obviously affected the mechanical properties of PLA/PEG blends to a great extent as shown in Figure (8) and as described in section 4.1.1. The thermal properties for neat PLA and PLA/PEG blends are shown in Table (7).

Table 7: Thermal properties of PLA and PLA/PEG blends at different concentrations

Material	T_g (°C)	T_{cc} (°C)	T_m (°C)	ΔH_{cc} (J/g)	ΔH_m (J/g)	X_c (%)
Neat PLA	63.23	N/A	152.99	N/A	2.37	2.55
PEG 10%	40.17	85.32	150.89	-17.51	21.27	22.87
PEG 20%	5.52	61.05	148.19	-0.87	22.41	24.10
PEG 30%	4.67	77.19	145.82	-0.33	21.62	23.25

For PLA-PEG 10%, it was observed that the melting endotherm developed a low-temperature peak or "shoulder" that might be due to lamellar re-organization during PLA crystallization *(119, 120)* or due to the formation of less perfect crystals during preparation *(109)*.

Figure (21) demonstrates DSC thermograms for neat PLA against different concentrations of TBC plasticized PLA blends.

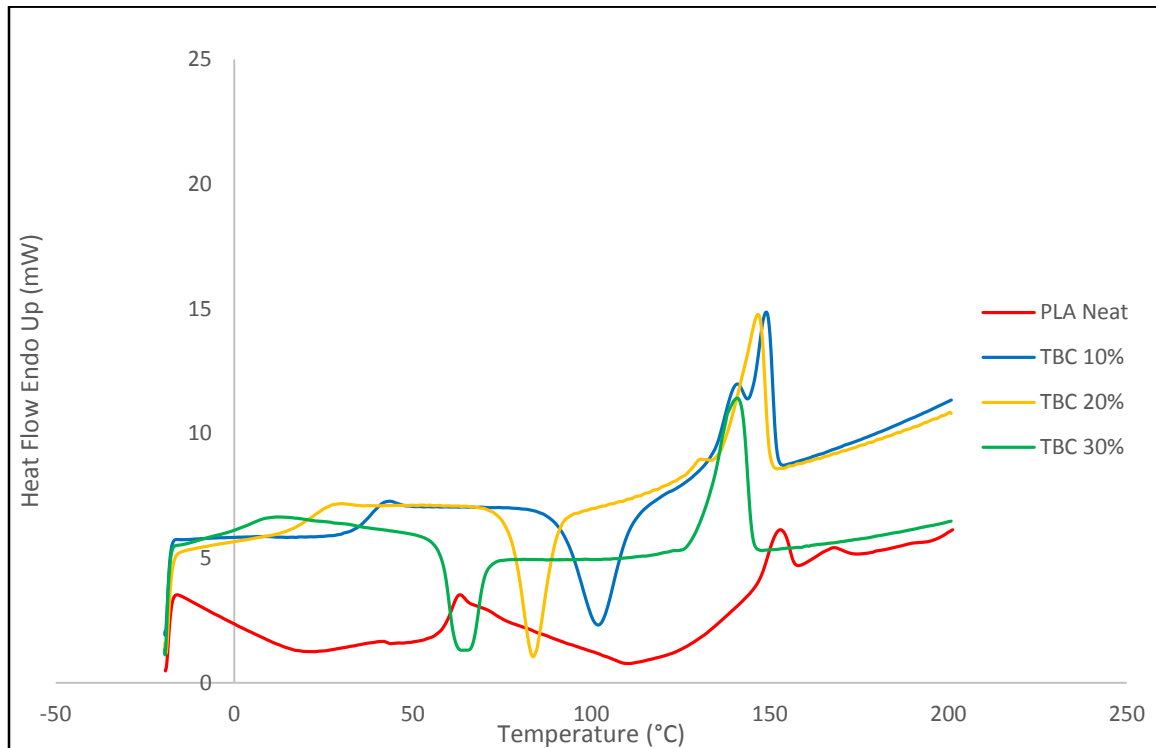*Figure 21: DSC thermograms for neat PLA and PLA/TBC blends at different concentrations*

Like PEG, the addition of different concentrations of TBC revealed a decrease in T_g of TBC plasticized PLA. Table (8) shows that the degree of crystallinity has increased when TBC was added compared to the neat PLA due to the decrease in T_g, which facilitated the crystallization of PLA during storage *(49)*.

Table 8: Thermal properties of PLA and PLA/TBC blends at different concentrations

Material	T_g (°C)	T_{cc} (°C)	T_m (°C)	ΔH_{cc} (J/g)	ΔH_m (J/g)	X_c (%)
Neat PLA	63.23	N/A	152.99	N/A	2.37	2.55
TBC 10%	43.68	101.93	149.02	-18.83	19.08	20.52
TBC 20%	29.89	83.76	146.66	-16.59	15.78	16.97
TBC 30%	12.24	64.38	140.93	-11.65	18.81	20.22

Thus, it can be stated that the incorporation of TBC plasticizer has significantly increased the amount and the size of crystallites within PLA matrix, which is confirmed by the increase of melting point peak intensity of TBC plasticized PLA relative to neat PLA.

Furthermore, DSC traces show a significant decrease in cold crystallization temperatures (T_{cc}) associated with the increase in TBC content *(49, 59)*. This behaviour was ascribed to the fact that PLA crystallizes more easily at lower temperatures due to the increased mobility of PLA chains with increasing plasticizer content; this finding is in agreement with reported results in the literature *(59)*. Unlike TBC 30%, TBC 10% and TBC 20% exhibited low melting points due to reorganization of crystalline structure or formation of two types of crystals.

For TA plasticizer, it was observed that the adequately low boiling point of TA as compared to the glass transition temperature of PLA has remarkably reduced the T_g of the plasticized PLA matrix *(109)*. As for PLA/TBC blends, cold crystallization temperatures of PLA/TA blends were shown to have lower temperatures with respect to neat PLA with increased concentrations of the plasticizer (Figure 22).
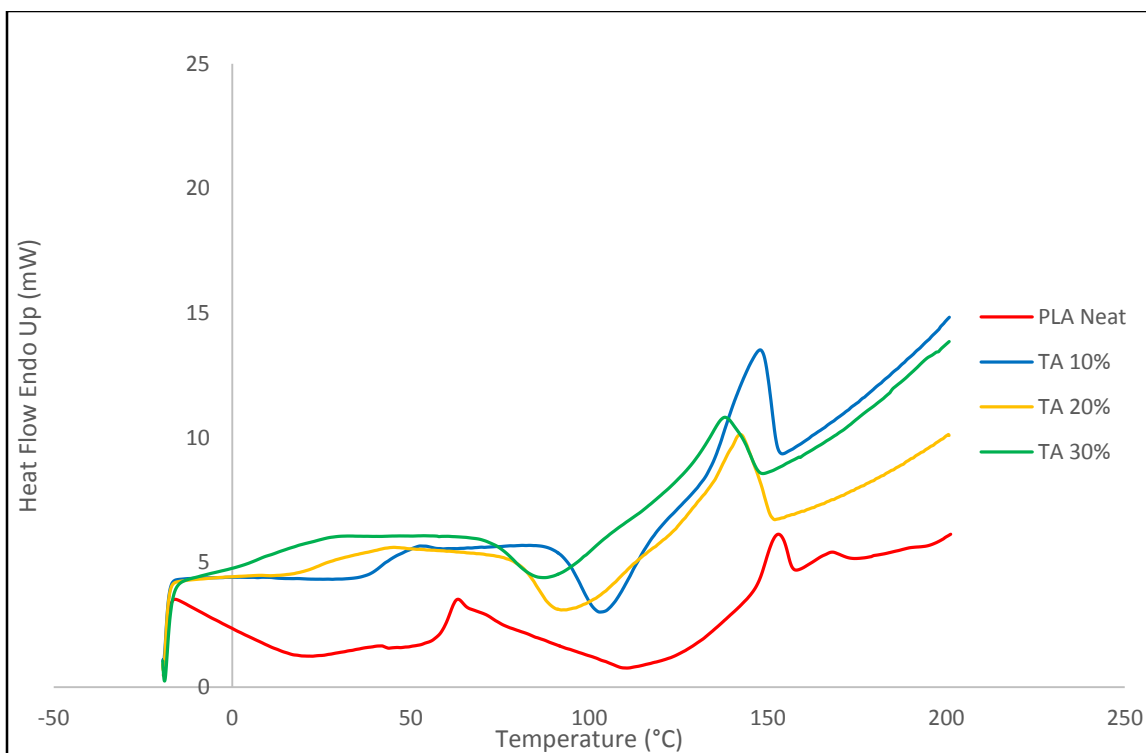
Figure 22: DSC thermograms for neat PLA and PLA/TA blends at different concentrations

The degree of crystallinity, shown in Table (9) has increased as in the case of PEG and TBC plasticizers.

Table 9: Thermal properties of PLA and PLA/TA blends at different concentrations

Material	T_g (°C)	T_{cc} (°C)	T_m (°C)	ΔH_{cc} (J/g)	ΔH_m (J/g)	X_c (%)
Neat PLA	63.23	N/A	152.99	N/A	2.37	2.55
TA 10%	52.62	102.93	147.86	-9.52	14.73	15.84
TA 20%	45.33	92.14	142.28	-12.10	14.99	16.11
TA 30%	32.66	87.45	137.95	-7.59	8.97	9.65

The melting temperatures in PLA/TA blends were observed to shift to lower temperatures by addition of the plasticizers. This is due to the decrease in PLA crystallite sizes, which led to rapid melting of these crystallites at lower temperatures. PLA/TA blends were observed to have the smallest sizes and quantities of crystallites among all used plasticizers. In addition, the increase in the plasticizer content was associated with further decrease in the crystallite sizes.

4.2. Investigation of the Physical Properties of Pristine and Functionalized CNT/ and GNP/ Plasticized PLA Nanocomposites

4.2.1. Stress Relaxation Measurements

Various amounts of different nanofillers were added to the PLA/TA 10% blend in order to enhance its characteristics for food packaging applications. Namely, 0.1%, 0.5%, and 1.0% of CNT, CNTCOOH, GNP, and GNPCOOH nanofillers by weight were used. For notation purposes, CNT 0.1% will refer to PLA/TA 10% mixed with 0.1% CNT nanofillers whereas GNPCOOH 0.5% will refer to PLA/TA 10% mixed with 0.5% COOH functionalized GNP nanofillers and so on for other nanocomposites.

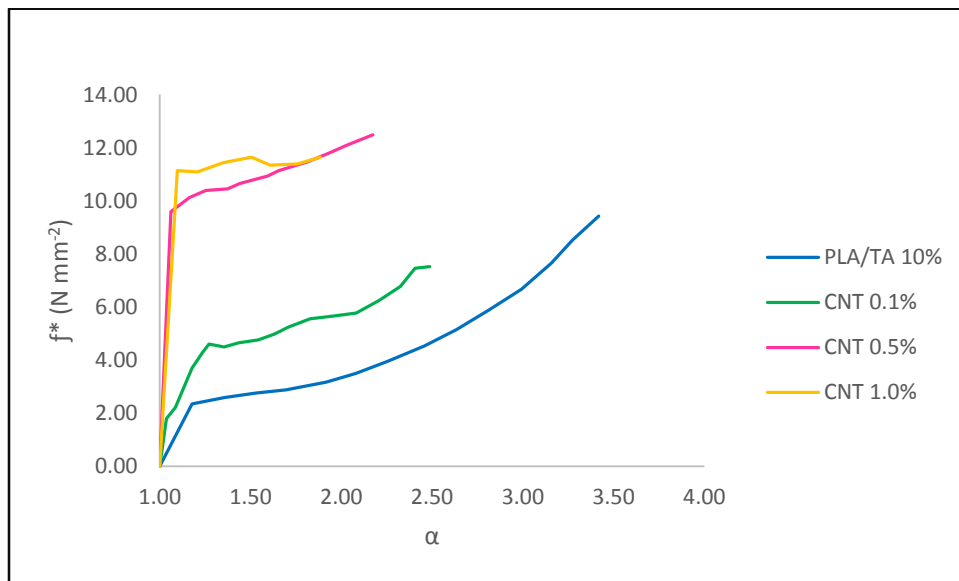Figures (23, 24) show the stress – strain curves for CNT nanocomposites at different concentrations.

Figure 23: Stress-strain isotherms for PLA-TA/CNT nanocomposites at different concentrations: nominal force f versus elongation α

Figure 24: Stress-strain isotherms for PLA-TA/CNT nanocomposites at different concentrations: modulus [f*] versus reciprocal elongation α^{-1}

It was observed that the nominal force has increased at the expense of elongation for all different concentrations of CNT indicating an increased stiffness of the polymeric samples. The decrease in the flexibility of CNT nanocomposites has possibly resulted from the adsorption of polymeric segments onto the surface of the nanofillers leading to a decrease in the length of free segments between the adsorption sites and thus limiting the freedom of the chains. It is worth mentioning that this adsorption is thought of as physisorption not chemisorption since FT-IR spectra did not reveal any change upon the incorporation of the nanofillers. This caused an increase in the samples stiffness and consequently led to more brittle samples. Table (10) compares the maximum elongation (α_m), maximum nominal force (f^*_m), and amount of energy required to break the sample or reach maximum point (E_m) for PLA/TA 10% blend and its CNT nanocomposites of different concentrations.

Table 10: Ultimate mechanical properties for PLA-TA/CNT nanocomposites at different concentrations

Material	α_m	f^*_m (N mm^{-2})	E_m (J mm^{-3})
PLA/TA 10%	3.40 ± 0.13	9.86 ± 0.52	12.41 ± 1.19
CNT 0.1%	2.48 ± 0.13	9.01 ± 1.32	7.88 ± 1.82
CNT 0.5%	2.08 ± 0.10	12.50 ± 0.02	12.31 ± 4.59
CNT 1.0%	1.64 ± 0.21	11.67 ± 0.48	7.46 ± 3.28

According to the data represented in the table, increasing the CNT content was associated with further decrease in maximum elongation values possibly since at higher concentrations of CNT agglomeration of the hydrophobic nanofillers, may take place forming macroscopic clusters or aggregates and disrupting the uniform distribution of the nanofillers as was observed during visual inspection of the material. Stress relaxation curves for CNT nanocomposites showed normal behaviour for the reduced force vs reciprocal of elongation. This has implied that the upturn behaviour observed for PLA/TA 10% blend was eliminated by incorporation of the CNT indicating that CNT nanofillers has prevented the strain induced crystallization of the polymeric chains.

CNTCOOH nanocomposites exhibited a behaviour similar to that of CNT nanocomposites (Figure 25).

Figure 25: Stress-strain isotherms for PLA-TA/CNTCOOH nanocomposites at different concentrations: nominal force f versus elongation α

Functionalized CNT was reported to have better dispersion properties as compared to pristine CNT; due to the extensive hydrogen bonding formed between the carboxylic groups of the nanofillers and the carbonyl ester group of polymeric chains thus reducing the aggregation of the nanofillers particles. However, these hydrogen bonds may restrict the mobility of PLA chains even further leading to a reduced mechanical properties in terms of the tensile elongation. Stress relaxation curve for CNTCOOH nanocomposites

(Figure 26) has also demonstrated an elimination of the characteristic upturn observed for PLA/TA 10% at higher values of tensile elongation.
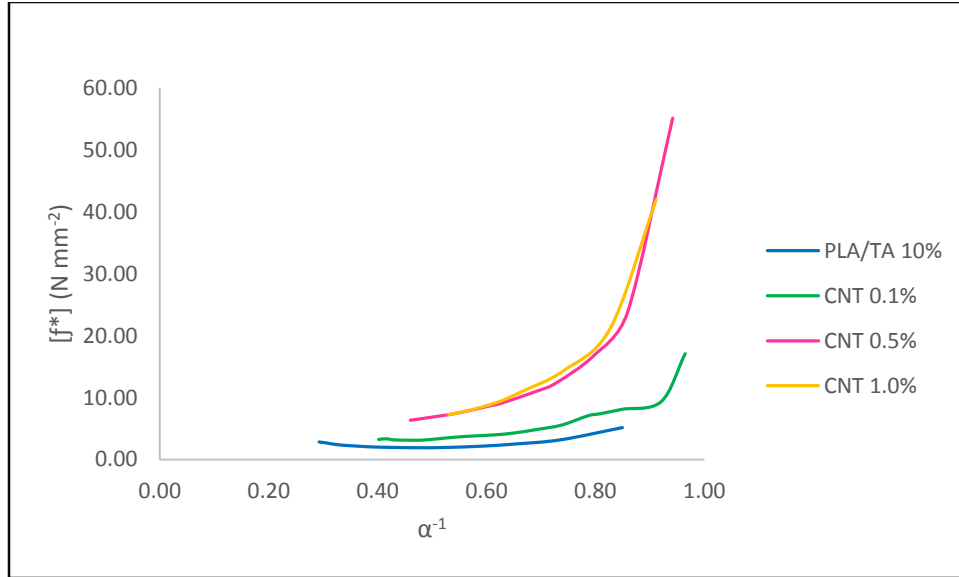

Figure 26: Stress-strain isotherms for PLA-TA/CNTCOOH nanocomposites at different concentrations: modulus [f] versus reciprocal elongation α^{-1}*

Table (11) lists the ultimate mechanical properties of CNTCOOH. It was observed that the energy required to break the samples has significantly decreased by at least 36% when compared to PLA/TA 10% free of CNTCOOH.

Table 11: Ultimate mechanical properties for PLA-TA/CNTCOOH nanocomposites at different concentrations

Material	α_m	f^*_m (N mm^{-2})	E_m (J mm^{-3})
PLA/TA 10%	3.40 ± 0.13	9.86 ± 0.52	12.41 ± 1.19
CNTCOOH 0.1%	1.22 ± 0.09	9.36 ± 1.15	2.46 ± 1.00
CNTCOOH 0.5%	1.55 ± 0.23	14.26 ± 8.04	7.91 ± 4.04
CNTCOOH 1.0%	1.19 ± 0.05	8.95 ± 5.64	2.17 ± 0.99

For GNP nanocomposites, similar behaviour to CNT and CNTCOOH continued to be observed (Figures 27 and 28). However, GNP nanocomposites showed more enhanced elongation at break as compared to CNT and CNTCOOH nanocomposites. This was mainly attributed to the nature of employed nanofillers. Unlike CNT and CNTCOOH nanofillers, which exhibited nanotube structure that tended to entangle and form more interconnected network, GNP lamellar or flake-like structure enhanced the exfoliation of

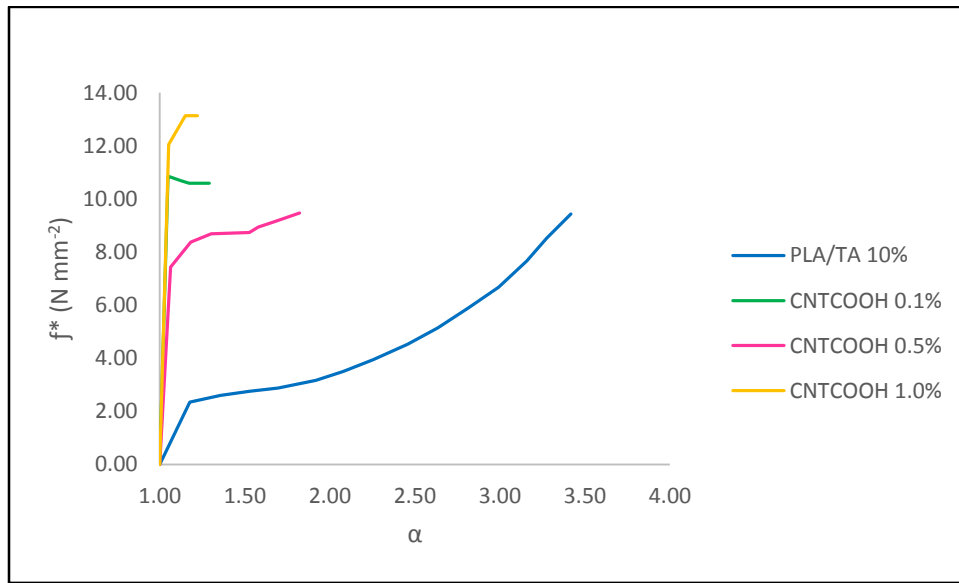the nanofillers and thus, helped the dispersion of the nanofillers within the plasticized PLA matrix.

Figure 27: Stress-strain isotherms for PLA-TA/GNP nanocomposites at different concentrations: nominal force f versus elongation α
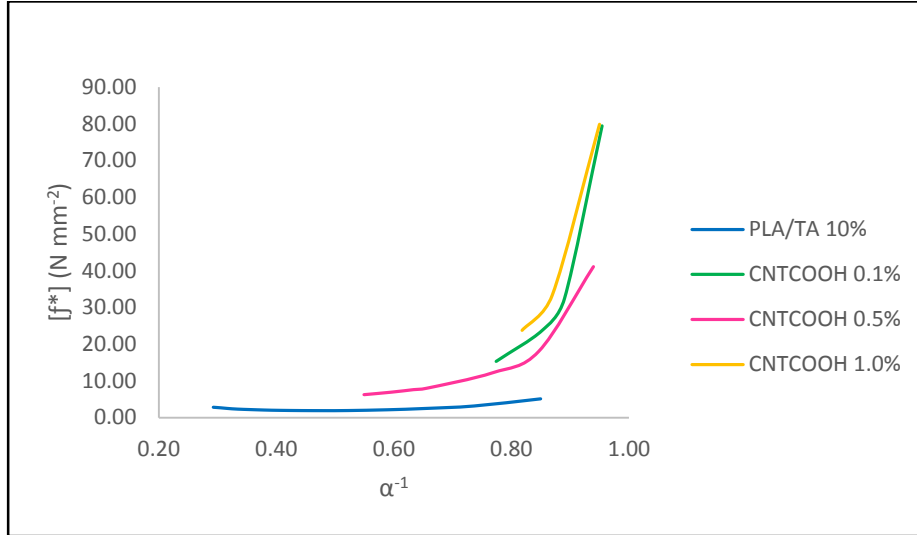

Figure 28: Stress-strain isotherms for PLA-TA/GNP nanocomposites at different concentrations: modulus [f] versus reciprocal elongation α^{-1}*

Table (12) summarizes the ultimate mechanical properties for GNP nanocomposites. From the tabulated results, it was observed that although the maximum elongation has decreased by at least 18% in case of GNP 0.1%, the investigated materials almost maintained the

same values of maximum nominal force at break, and consequently, the energy required to break the samples showed lower values to some extent.

Table 12: Ultimate mechanical properties for PLA-TA/GNP nanocomposites at different concentrations

Material	α_m	$f*_m$ (N mm^{-2})	E_m (J mm^{-3})
PLA/TA 10%	3.40 ± 0.13	9.86 ± 0.52	12.41 ± 1.19
GNP 0.1%	2.77 ± 0.14	8.60 ± 3.42	11.76 ± 3.25
GNP 0.5%	2.38 ± 0.36	7.51 ± 1.15	8.04 ± 0.48
GNP 1.0%	2.71 ± 0.33	9.17 ± 1.37	11.09 ± 1.16

Alternatively, investigating GNPCOOH nanocomposites demonstrated an increase in the elastic modulus at the expense of tensile elongation as observed in other prepared nanocomposites. However, as the case of GNP, it was observed that maximum elongation at break has also decreased but to a much lesser extent (Figure 29).
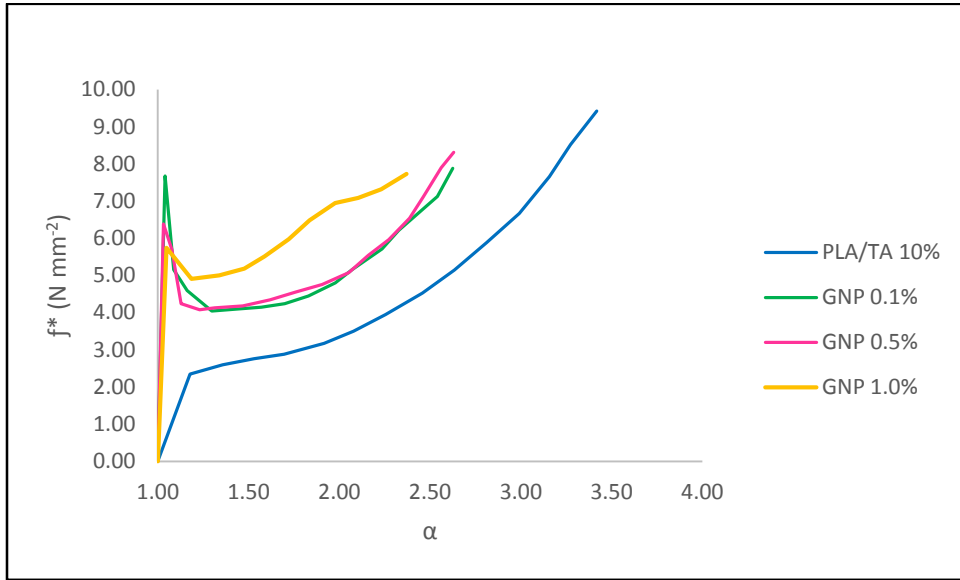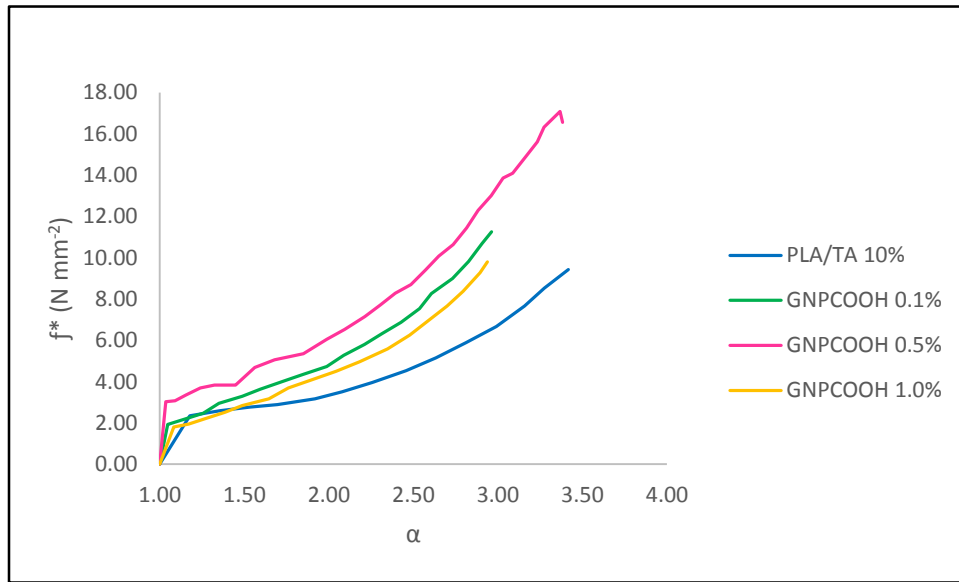

Figure 29: Stress-strain isotherms for PLA-TA/GNPCOOH nanocomposites at different concentrations: nominal force f versus elongation α

The decreased mechanical properties in terms of flexibility for GNPCOOH 1.0% nanocomposites as compared to lower concentrations of GNPCOOH (0.1% and 0.5%) samples may be attributed to the less exfoliated GNP platelets due to the high concentration of the incorporated nano-reinforcement. Furthermore, the energy required to break

GNPCOOH 1.0% was shown to decrease remarkably. GNPCOOH 0.5% nanocomposites exhibited best performance among all investigated samples. GNPCOOH 0.5% showed slight decrease in α_m, and considerable increase in maximum nominal force at break and higher energy required to break the samples indicating enhanced toughness of the GNPCOOH 0.5% nanocomposites accompanied with higher flexibility over that of PLA/TA 10% (Table 13, Figure 30).

Table 13: Ultimate mechanical properties for PLA-TA/GNPCOOH nanocomposites at different concentrations

Material	α_m	f^*_m (N mm^{-2})	E_m (J mm^{-3})
PLA/TA 10%	3.40 ± 0.13	9.86 ± 0.52	12.41 ± 1.19
GNPCOOH 0.1%	3.07 ± 0.13	12.25 ± 0.87	12.71 ± 2.27
GNPCOOH 0.5%	3.18 ± 0.18	12.71 ± 0.69	13.39 ± 5.07
GNPCOOH 1.0%	2.58 ± 0.63	8.24 ± 3.35	6.91 ± 4.62
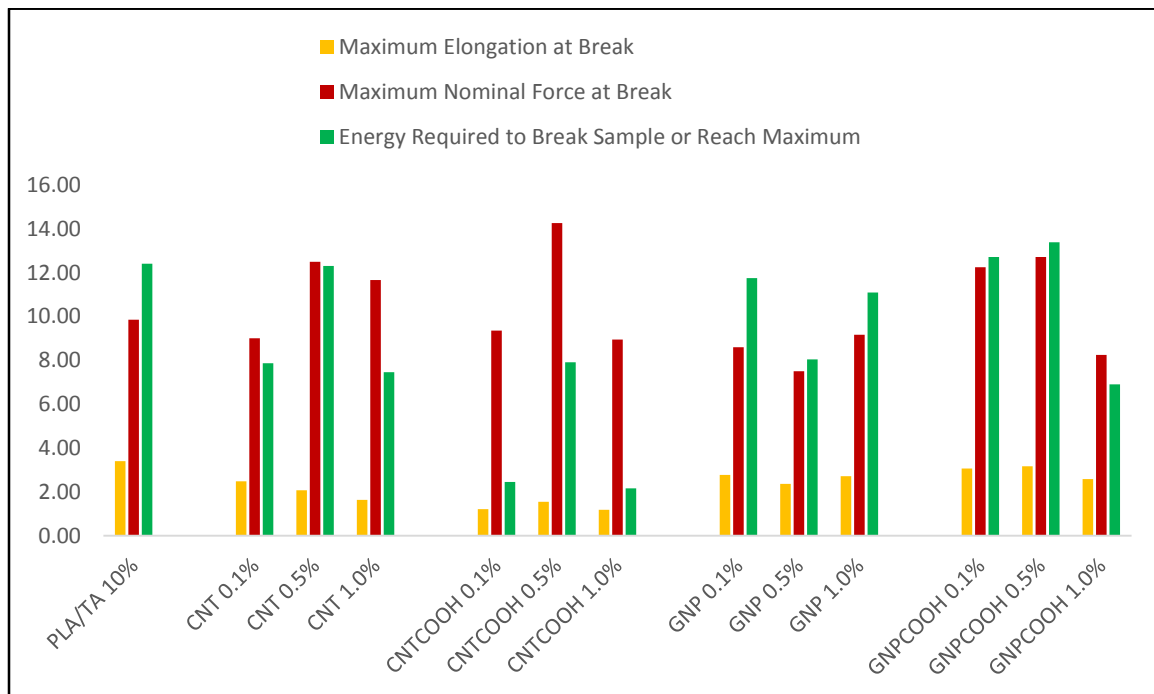
Figure 30: Ultimate mechanical properties for PLA/TA 10% and PLA nanocomposites at different concentrations

This behaviour may be interpreted based on the stress relaxation curve that showed that unlike all other investigated materials, GNPCOOH 0.5% nanocomposites were the only materials that maintained the abnormal behaviour that strengthened the polymer further at

high elongation, and enhanced resistance to stress at these high elongation levels (Figure 31).

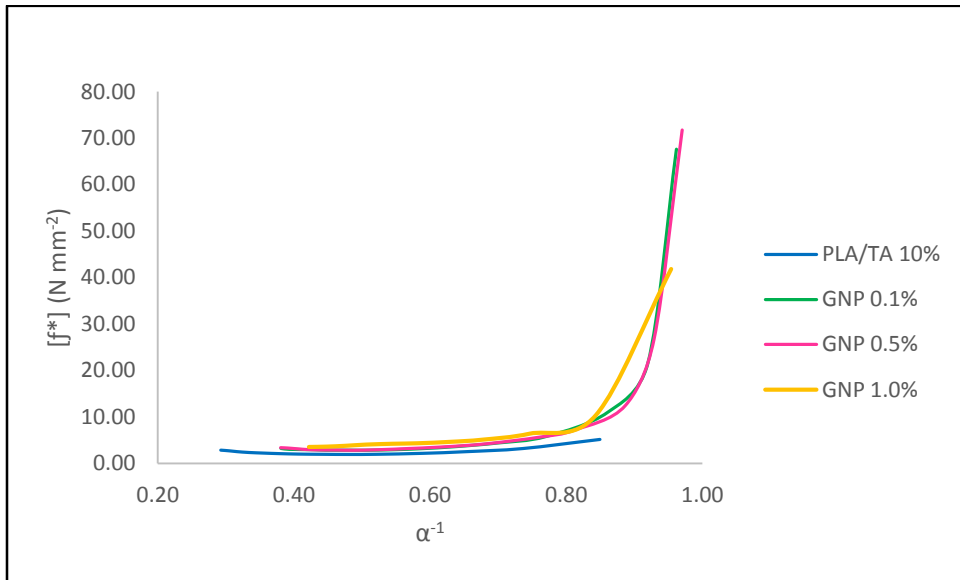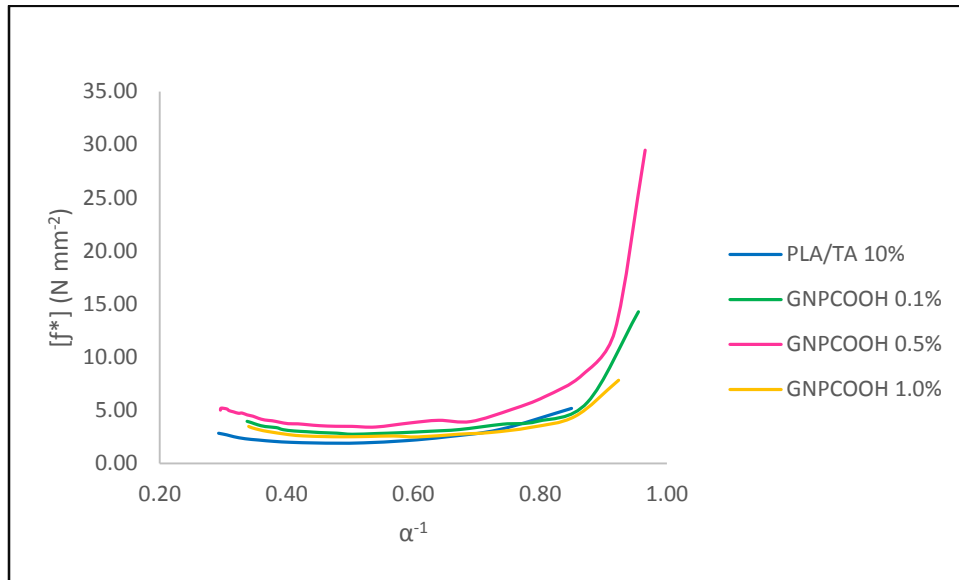*Figure 31: Stress-strain isotherms for PLA-TA/GNPCOOH nanocomposites at different concentrations: modulus [f*] versus reciprocal elongation α^{-1}*

GNPCOOH 0.5% nanocomposites is depicted alone in Figure (32) for better illustration of the upturn behaviour observed for this nanocomposites.
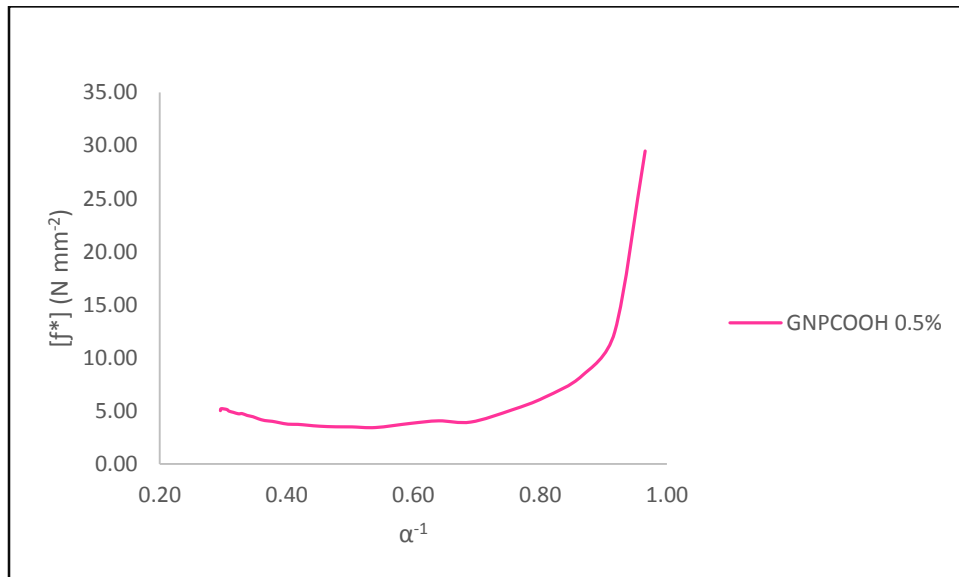
Figure 32: Stress-strain isotherm for PLA-TA/GNPCOOH 0.5% nanocomposites: modulus [f] versus reciprocal elongation α^{-1}*

4.2.2. Differential Scanning Calorimetry Analysis (DSC)

The thermal behaviour of the PLA nanocomposites was assessed using DSC in comparison to that of plasticized PLA as shown in Figure (33 – 36). Table (14) summarizes the thermal characteristics of PLA nanocomposites with different loadings of the nanofillers.

Table 14: Thermal properties of PLA/TA 10% nanocomposites at different concentrations

| Material	T_g (°C)	T_{cc} (°C)	T_m (°C)	ΔH_{cc} (J/g)	ΔH_m (J/g)	X_c (%)
PLA-TA 10%	52.62	102.93	147.86	-9.52	14.73	15.84
CNT 0.1%	56.30	107.43	147.48	-9.04	14.48	15.57
CNT 0.5%	55.43	103.04	147.45	-10.06	13.33	14.33
CNT 1.0%	53.92	101.87	146.96	-11.60	17.07	18.36
CNTCOOH 0.1%	52.80	104.97	147.56	-11.41	15.14	16.28
CNTCOOH 0.5%	57.66	110.97	157.39	-9.65	5.35	5.76
CNTCOOH 1.0%	53.62	102.92	146.51	-16.12	19.51	20.98
GNP 0.1%	54.09	108.92	147.29	-11.39	14.54	15.63
GNP 0.5%	53.12	105.12	146.02	-10.11	13.67	14.70
GNP 1.0%	52.06	111.59	147.10	-7.19	6.77	7.28
GNPCOOH 0.1%	56.63	111.96	147.48	-4.68	8.61	9.26
GNPCOOH 0.5%	57.17	109.48	147.54	-2.84	7.30	7.85
GNPCOOH 1.0%	54.12	109.55	147.18	-4.46	9.39	10.10

In general, it was observed that the glass transition temperature of the nanocomposites has slightly increased as compared to that of PLA/TA 10% as a result of the increase in the various amounts of different nanofillers.

With the increase in the CNT content, the T_g values has decreased slightly possibly due to the agglomerations of CNT at higher loadings. It was also observed that the cold crystallization temperatures for PLA-TA/CNTs nanocomposites were shifted to lower temperatures by increasing CNTs loads (Figure 33). This was attributed to the ability of CNTs to induce crystallization in PLA matrix since CNTs are known to act as a crystal nucleate *(76, 83, 90, 94, 121)*. By increasing CNT concentrations, the surface area available for heterogeneous nucleation in PLA matrix also increases, leading to a decrease in cold crystallization temperatures *(93)*. The well-developed cold crystallization peaks confirm

the efficiency of CNTs role as nucleating agents for PLA crystallization from the amorphous state during second heating cycle *(93)*. The melting temperature T_m was observed to generally remain unchanged at different nanofillers loadings.
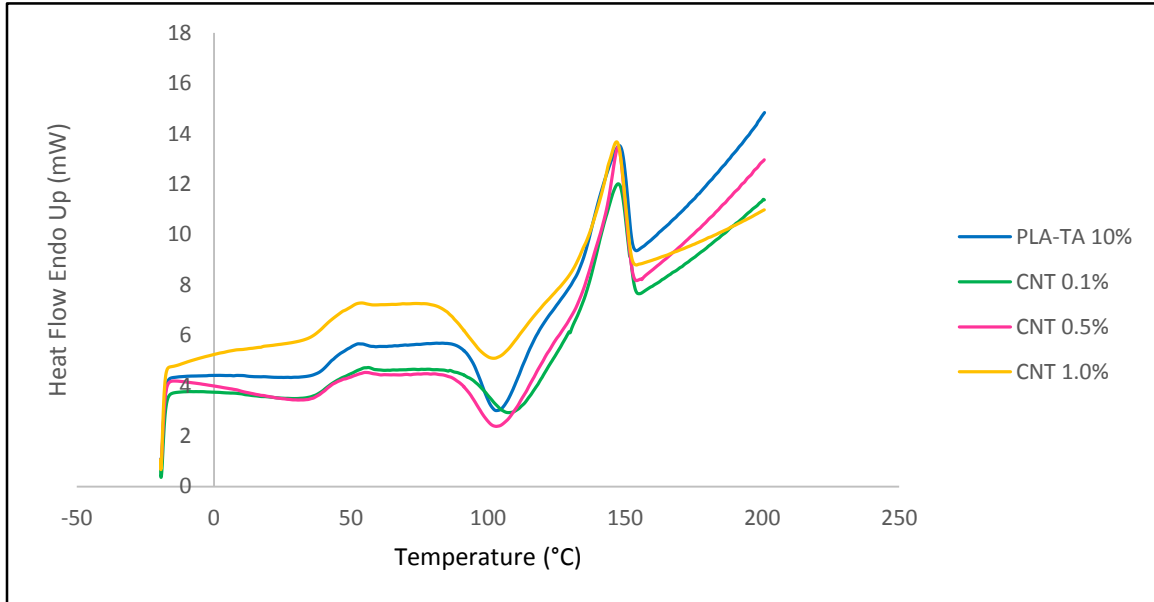
Figure 33: DSC thermograms for PLA-TA/CNT nanocomposites at different concentrations

Similar behaviour has also been observed for the other nanofillers as illustrated in Figures (34 – 36) and Table (14) for CNTCOOH, GNP, and GNPCOOH, respectively.

Figure 34: DSC thermograms for PLA-TA/CNTCOOH nanocomposites at different concentrations

Figure 35: DSC thermograms for PLA-TA/GNP nanocomposites at different concentrations

Figure 36: DSC thermograms for PLA-TA/GNPCOOH nanocomposites at different concentrations

4.2.3. Thermogravimetric Analysis (TGA)

TGA thermograms of PLA nanofillers nanocomposites and their corresponding derivative (DTG) curves are depicted in Figures (37 – 46). The diagrams showed almost similar behavior for all samples. TGA curves showed a major weight loss at the first instance at around 102 – 110 °C owing to water evaporation. Figures (37, 38) revealed that the initial decomposition temperature (T_{onset}) and the decomposition temperature at 50% weight loss for plasticized PLA ($T_{50\%}$) have both slightly decreased compared to neat PLA.
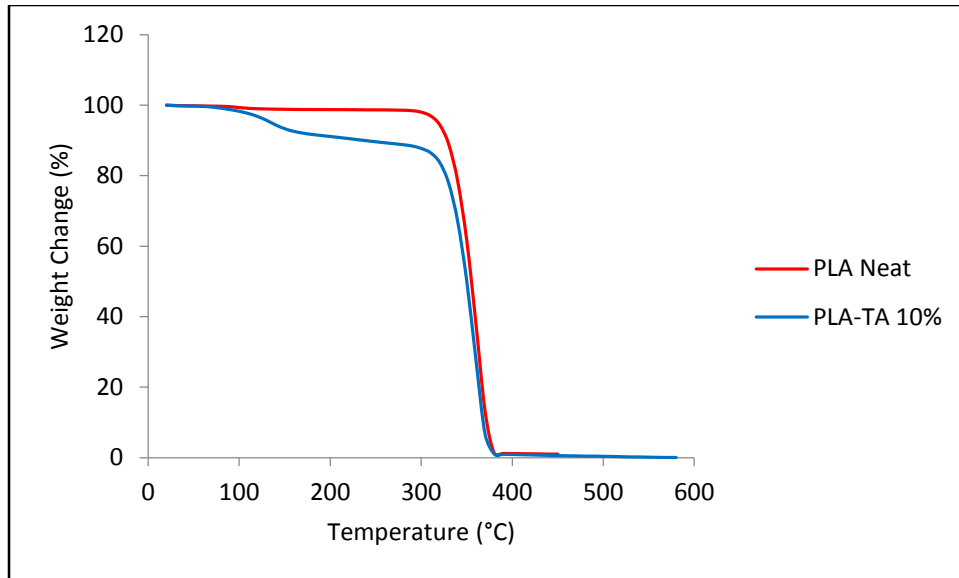
Figure 37: TGA thermograms for neat PLA and PLA/TA 10%

This decrease indicated that the thermal stability of PLA has decreased slightly when triacetin was used to plasticize PLA. This observed trend is probably resulting from the decomposition of the plasticizer molecules into by products that can accelerate the degradation of PLA *(64)*.
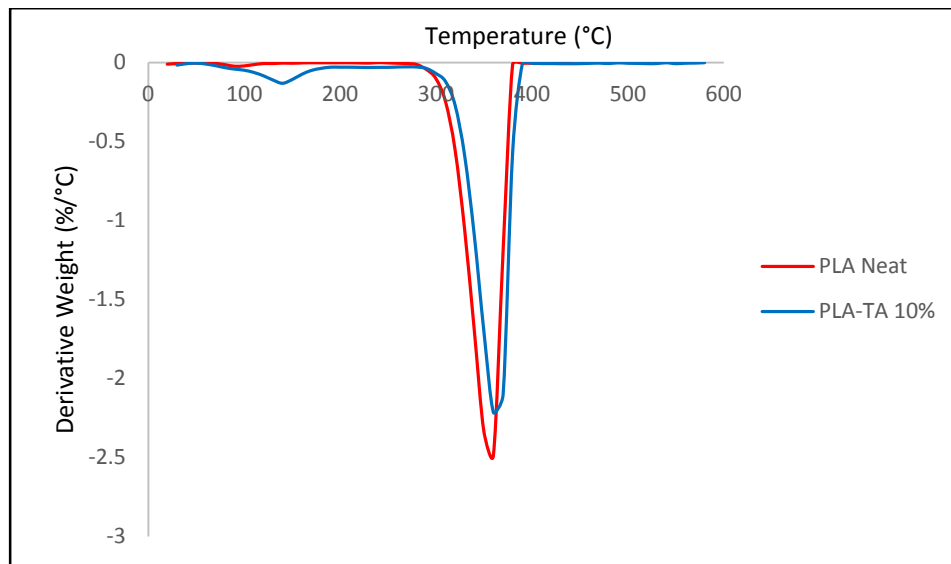
Figure 38: DTG thermograms for neat PLA and PLA/TA 10%

Table 15: Characteristic temperatures for PLA/TA 10% and its nanocomposites at different concentrations

Material	T_{onset} (°C)	$T_{50\%}$ (°C)	T_{max} (°C)
PLA/TA 10%	334.35	349.99	360
CNT 0.1%	348.39	364.05	380
CNT 0.5%	349.41	365.85	380
CNT 1.0%	348.95	365.4	380
CNTCOOH 1.0%	348.74	364.3	380
CNTCOOH 0.5%	349.39	364.96	380
CNTCOOH 1.0%	335.99	351.49	360
GNP 0.1%	335.36	350.88	350
GNP 0.5%	335.89	350.17	360
GNP 1.0%	336.72	351.73	360
GNPCOOH 0.1%	335.46	350.81	360
GNPCOOH 0.5%	335.26	350.95	360
GNPCOOH 1.0%	334.49	349.95	360

By adding different concentrations of pristine CNTs, TGA/DTG patterns were similar to that of plasticized PLA. However, it was observed that T_{onset}, $T_{50\%}$, and T_{max} all have shifted to higher temperatures when CNTs were added indicating that the presence of the nanofillers has actually assisted the thermal stability of the polymeric chains to some extent (Table 15). DTG curves (Figure 40) revealed that T_{max} of TA plasticized PLA/CNT has increased by 20 °C when compared to unfilled PLA. This result indicated that CNTs reached a stage where they effectively started to hamper the evaporation of PLA degraded products by formation of a charred layer, and thus delayed the progress of decomposition process to a perceptible extent *(92)*.

Figure 39: TGA thermograms for PLA-TA/CNT nanocomposites at different concentrations
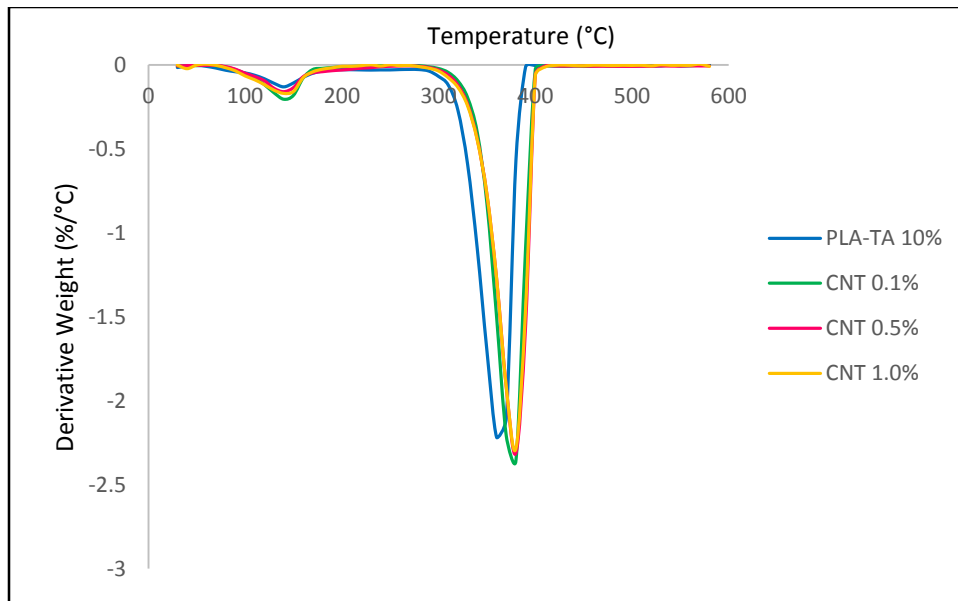
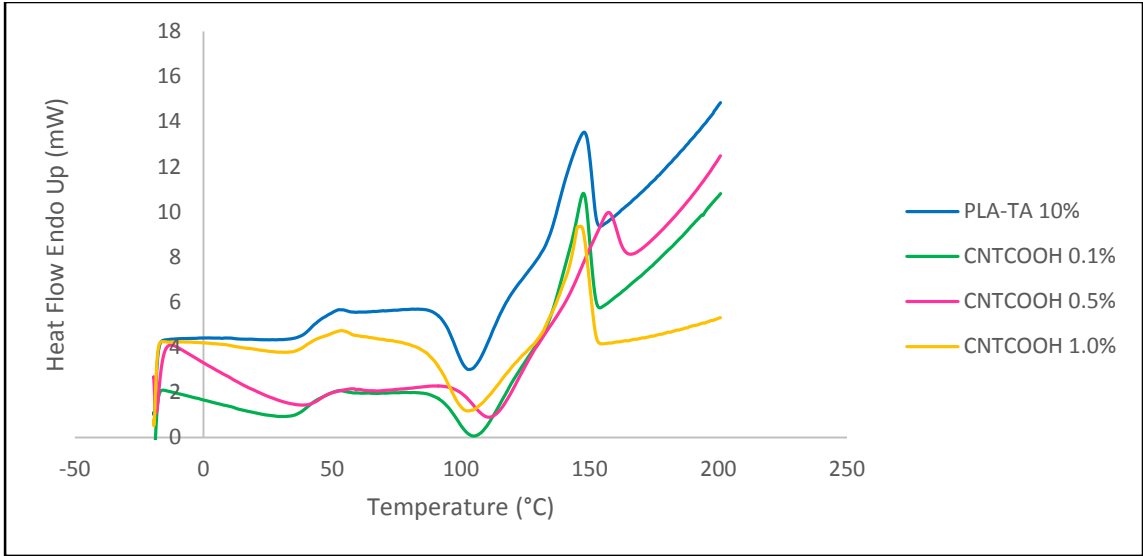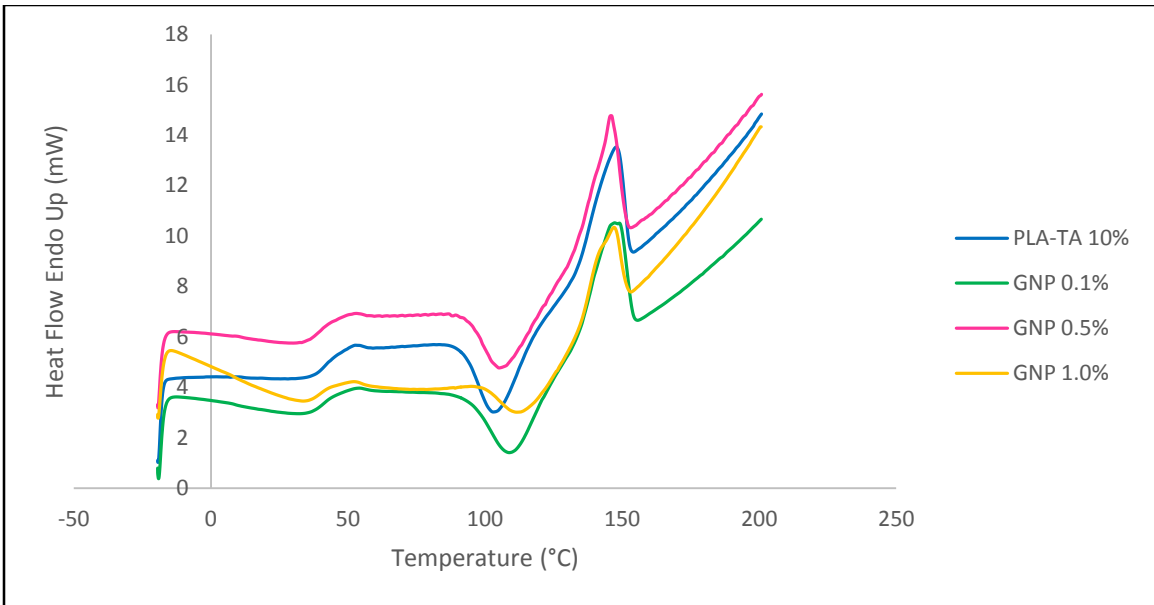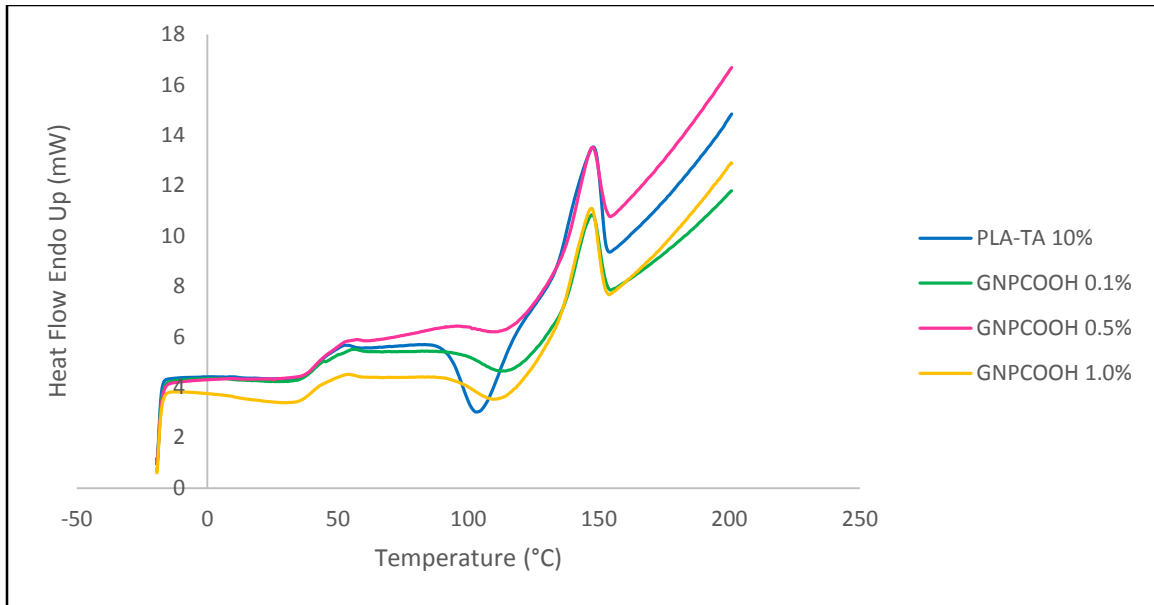*Figure 40: DTG thermograms for PLA-TA/CNT nanocomposites at different concentrations*

For functionalized CNT, as seen from the T_{onset} values for CNTCOOH 1.0%, it was observed that the thermal stability of plasticized PLA was not significantly enhanced as the case in CNTCOOH 0.1% and 0.5% (Figures 41, 42). The reason behind such behaviour may be due to an agglomeration that took place at higher concentrations of CNTCOOH. Thus, a weaker interaction between the nanofillers and the PLA matrix competed with the

68

barrier effect of CNTCOOH nanofillers, hence, the thermal stability remained unchanged. It should be noted, however, that thermal degradation of the aliphatic PLA can take place easily at ester groups backbone by random chain scission, thus resulting in the hydrolysis and breakdown of the polymeric chains. This mechanism can be further enhanced by the presence of acidic or basic species resulting in rapid degradation produced by carboxylic acid found on the surface of the CNT.

Figure 41: TGA thermograms for PLA-TA/CNTCOOH nanocomposites at different concentrations
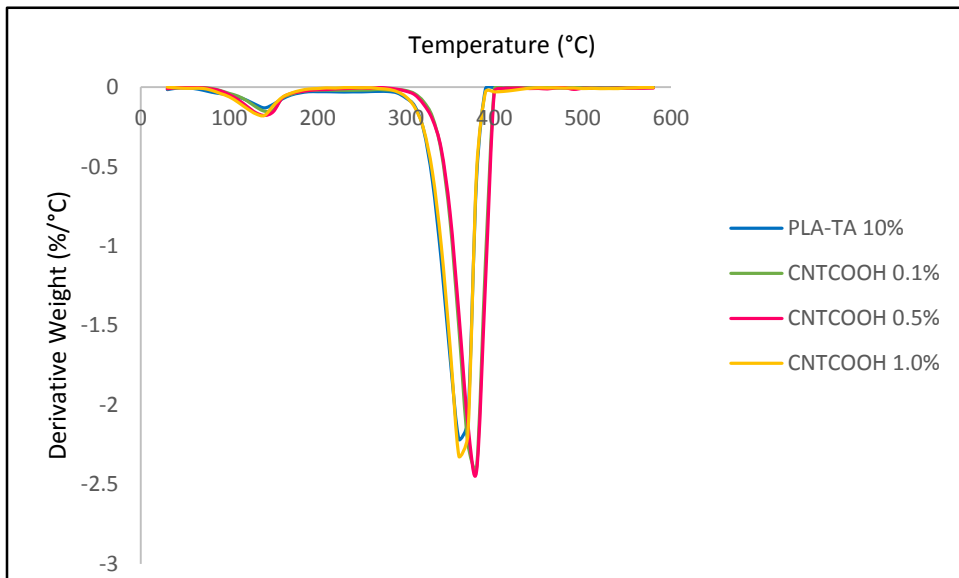
Figure 42: DTG thermograms for PLA-TA/CNTCOOH nanocomposites at different concentrations

Unlike CNT and CNTCOOH nano-reinforcements, GNP and GNPCOOH showed almost no effect on thermal stability of TA plasticized PLA matrix (Figures 43 – 46). T_{onset}, $T_{50\%}$, and T_{max} for GNP and GNPCOOH nanocomposites are tabulated in Table (15).
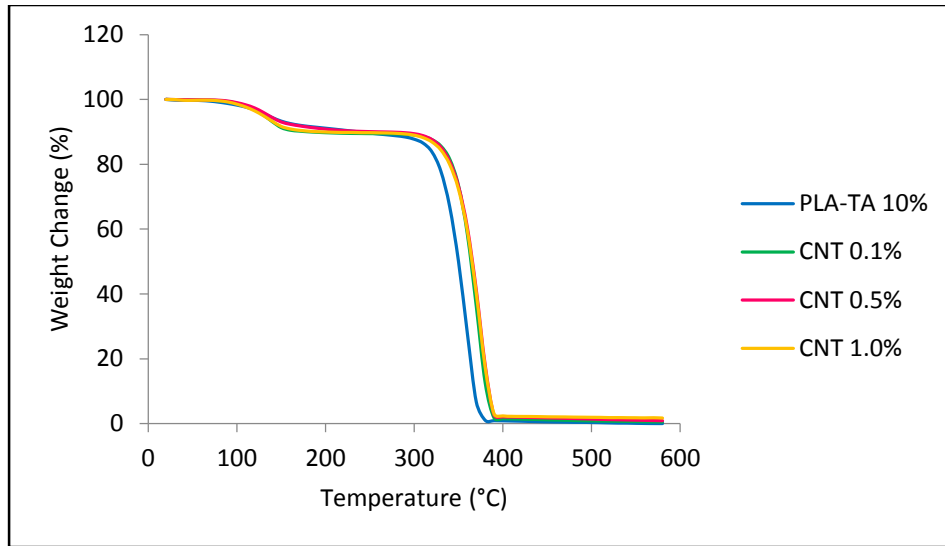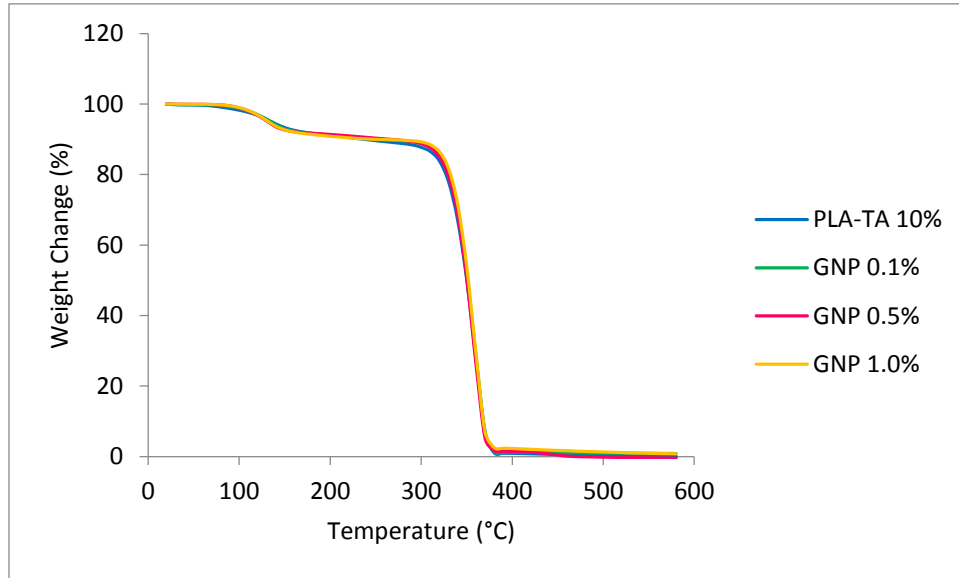

Figure 43: TGA thermograms for PLA-TA/GNP nanocomposites at different concentrations
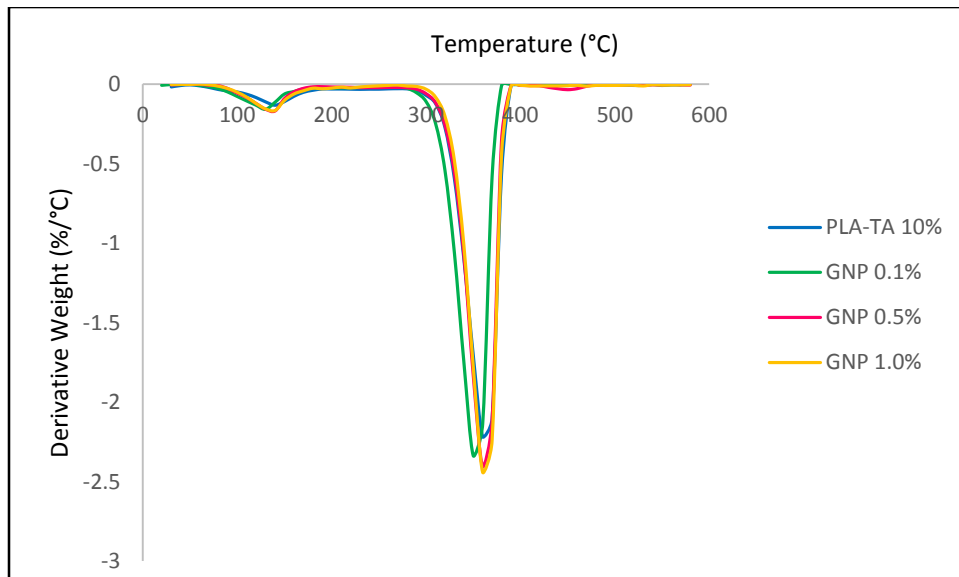
Figure 44: DTG thermogram for PLA-TA/GNP nanocomposites at different concentrations

These results were contradicting with previous studies, which reported that GNP and functionalized GNP had remarkably enhanced the thermal stability of PLA. Researchers studying the effect of GNP and graphene oxides (GO) clarified that the increase in thermal stability when these two nanofillers were incorporated into PLA system was due to the high thermal stability of GNP that tends to degrade at 600 °C *(122)*. Furthermore, it was stated that due to the high aspect ratio and lamellar structure of GNP, this system would prevent the permeation of oxygen by forming a charred layer. This layer also formed an insulating surface that hindered the escape of gaseous molecules during thermal decomposition *(100, 106, 122, 123)*.
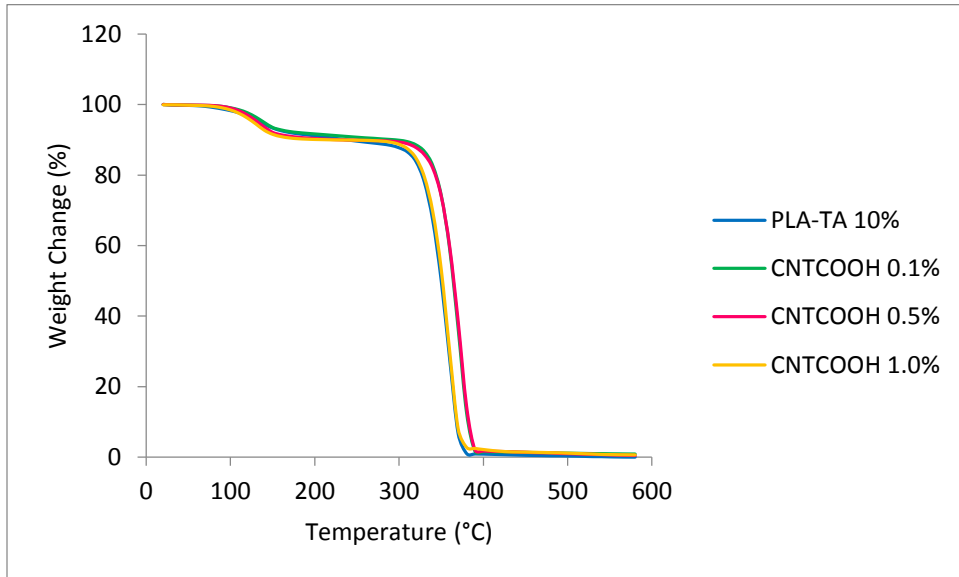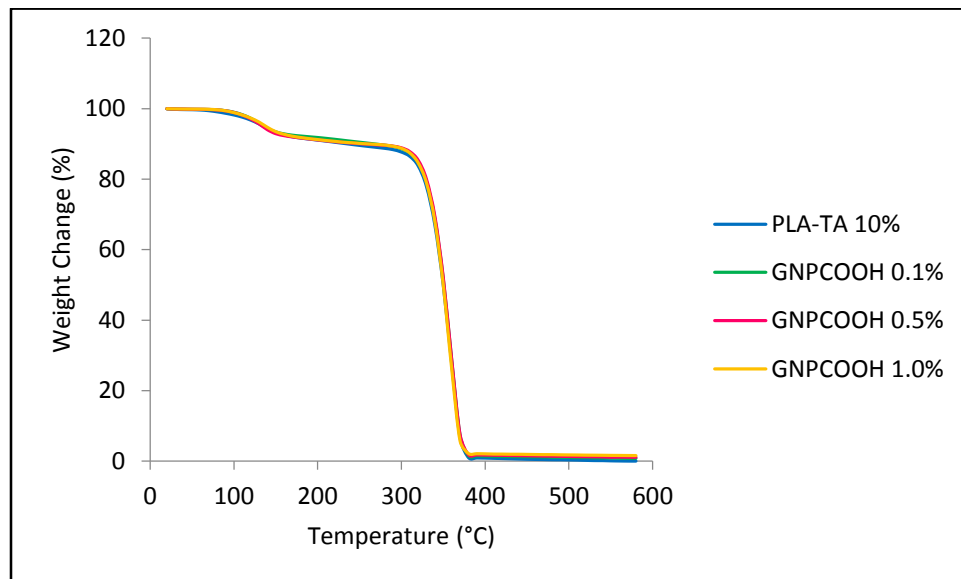

Figure 45: TGA thermograms for PLA-TA/GNPCOOH nanocomposites at different concentrations
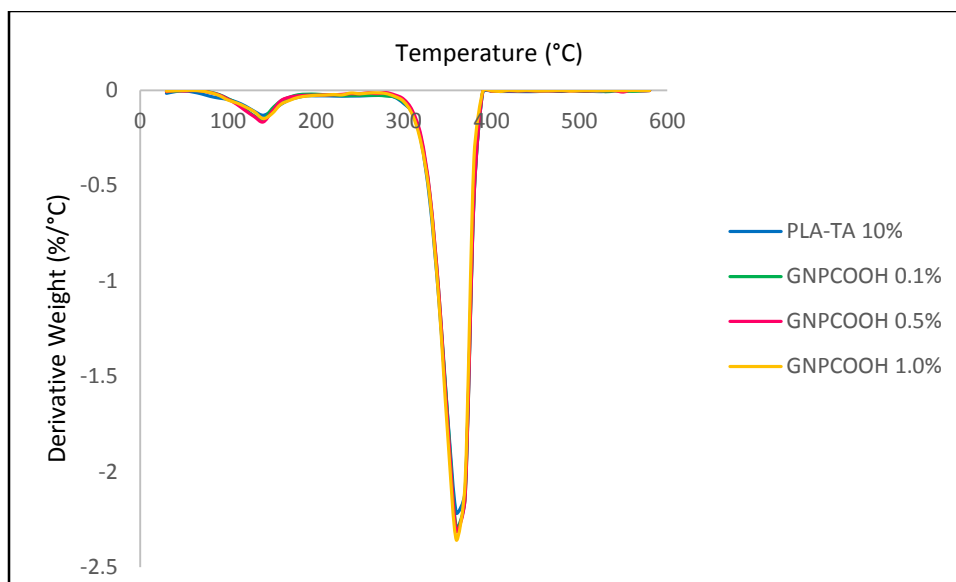
Figure 46: DTG thermograms for PLA-TA/GNPCOOH nanocomposites of different concentrations

To interpret for the results reported herein, it was suggested that the thermal stability was affected by a single factor that exhibited two opposite mechanisms. In other words, the high aspect ratio of GNP and GNPCOOH accompanied by their flake-like structure, which was expected to enhance the thermal stability by formation of char layer was also responsible for reducing the thermal stability. In case of pristine and functionalized GNP nanofillers the platelet-like structure of high aspect ratio has resulted in accumulating heat and acted as heat reservoir and accelerated the thermal decomposition of PLA chains, thus resulting in minute reduction in thermal stability which was offset by the increased polymeric stability resulting from the presence of the nanofillers. The net result is an unchanged or slight increase in thermal stability of PLA chain in case of GNP and GNPCOOH *(97)*.

4.2.4. Mercury Porosimetry Analysis

Figures (47 – 50) represent pore size and pore size distribution with the values for the total porosity (%) are shown in Table (16) for the various investigated nanocomposites.

It was observed that PLA/TA 10% had similar behaviour to neat PLA. In general, pore size for neat PLA and plasticized PLA ranged from 50 – 150 μm with most of the pores in the range of 100 - 120 μm and highest volume of about 0.25 cc/g. The percentage porosity for

72

PLA/TA 10% has been slightly increased as compared to neat PLA, which may be ascribed to the presence of TA plasticizer. The incorporation of different types of nanofillers used in this study showed a tremendous decrease in pore size compared to plasticized PLA. This can be observed for all investigated samples. The total porosity has decreased by at least 80%. The occlusion of pores within the PLA nanocomposites has probably affected their barrier properties. On one hand, the water vapour transmission results showed a decrease in moisture flow rate when nanofillers were added to the system. On the other hand, oxygen permeability test showed unexpected behaviour in spite of the decreased pore size. This suggested that oxygen diffusion followed a different mechanism. This observation is discussed in details in the oxygen permeability section.
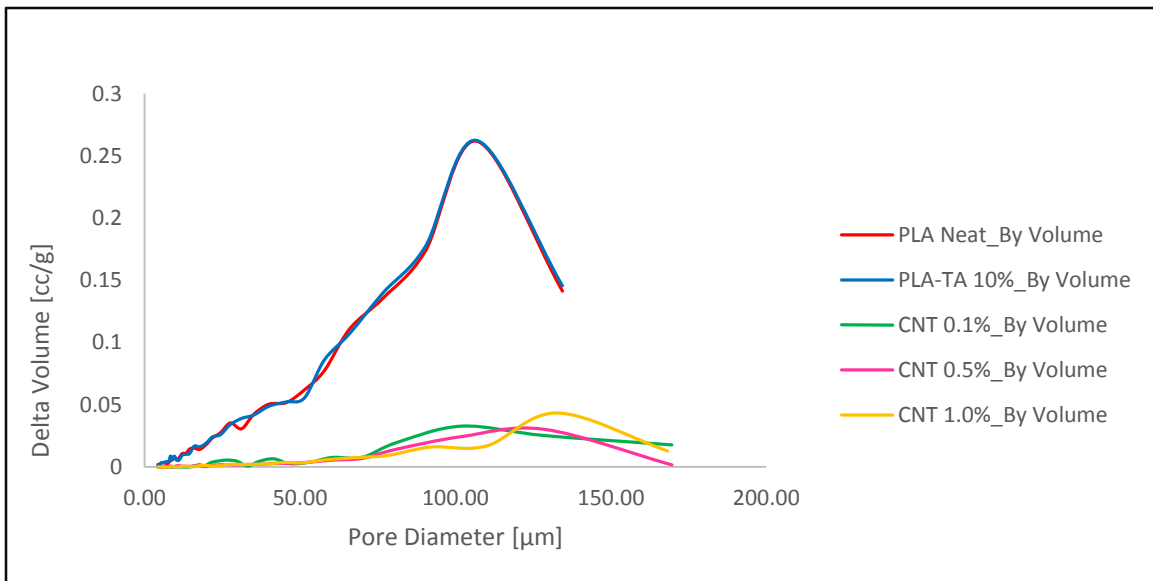
Figure 47: Incremental intrusion volume of mercury versus pore diameter for PLA-TA/CNT nanocomposites at different concentrations
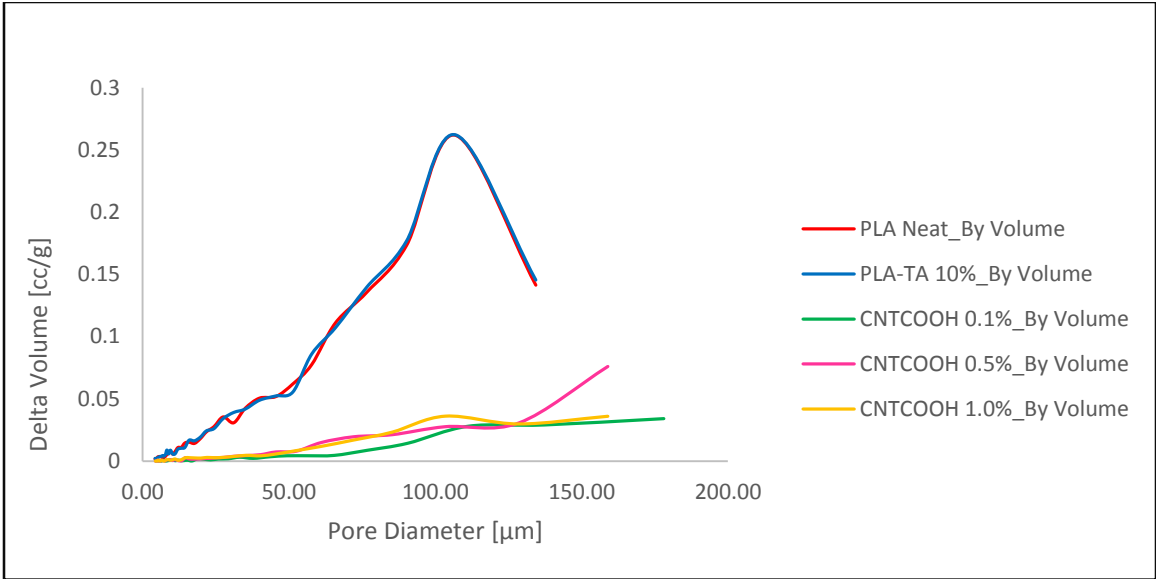
Figure 48: Incremental intrusion volume of mercury versus pore diameter for PLA-TA/CNTCOOH nanocomposites at different concentrations
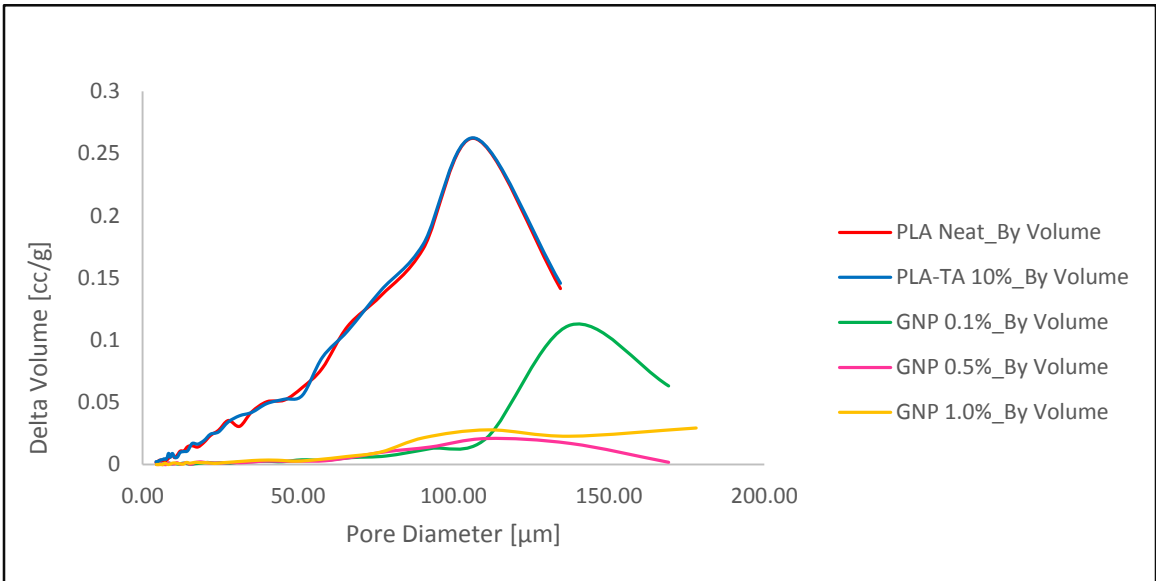
Figure 49: Incremental intrusion volume of mercury versus pore diameter for PLA-TA/GNP nanocomposites at different concentrations

74
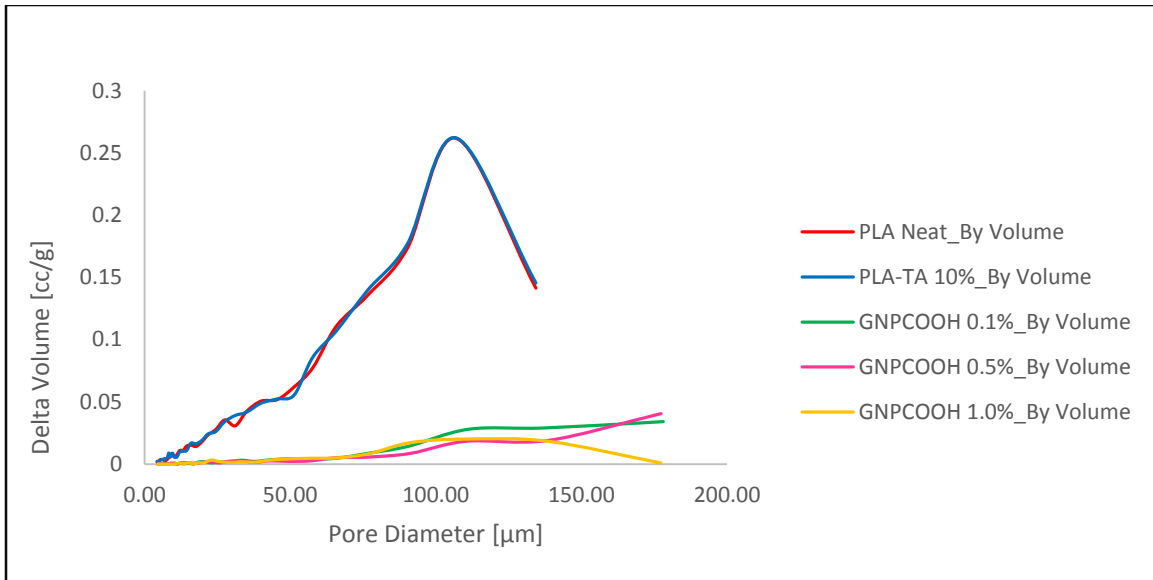
Figure 50: Incremental intrusion volume of mercury versus pore diameter for PLA-TA/GNPCOOH nanocomposites at different concentrations

Table 16: Percentage of total porosity for PLA/TA 10% nanocomposites at different concentrations

Material	Total Porosity (%)
PLA	20.6041
PLA-TA 10%	21.079
CNT 0.1%	2.3132
CNT 0.5%	1.7258
CNT 1.0%	2.0847
CNTCOOH 0.1%	4.1638
CNTCOOH 0.5%	3.6553
CNTCOOH 1.0%	3.1776
GNP 0.1%	3.7696
GNP 0.5%	1.534
GNP 1.0%	2.3131
GNPCOOH 0.1%	2.2462
GNPCOOH 0.5%	1.8277
GNPCOOH 1.0%	1.5066

4.3. Investigation of the Biodegradation of Pristine and Functionalized CNT/ and GNP/ Plasticized PLA Nanocomposites

4.3.1. Natural Biodegradation Test

Figure (51) represents the percentage decrease of samples weight after being buried in plant-based compost for 4 months. During the time of the experiment, temperature, humidity and pH values were measured. The recorded values were 21 °C, 65%, and 6.5 respectively. Biodegradability is considered the main characteristic of biopolymers, however, the time required for degradation to take place differs from one material to another depending on their physical and chemical compositions.
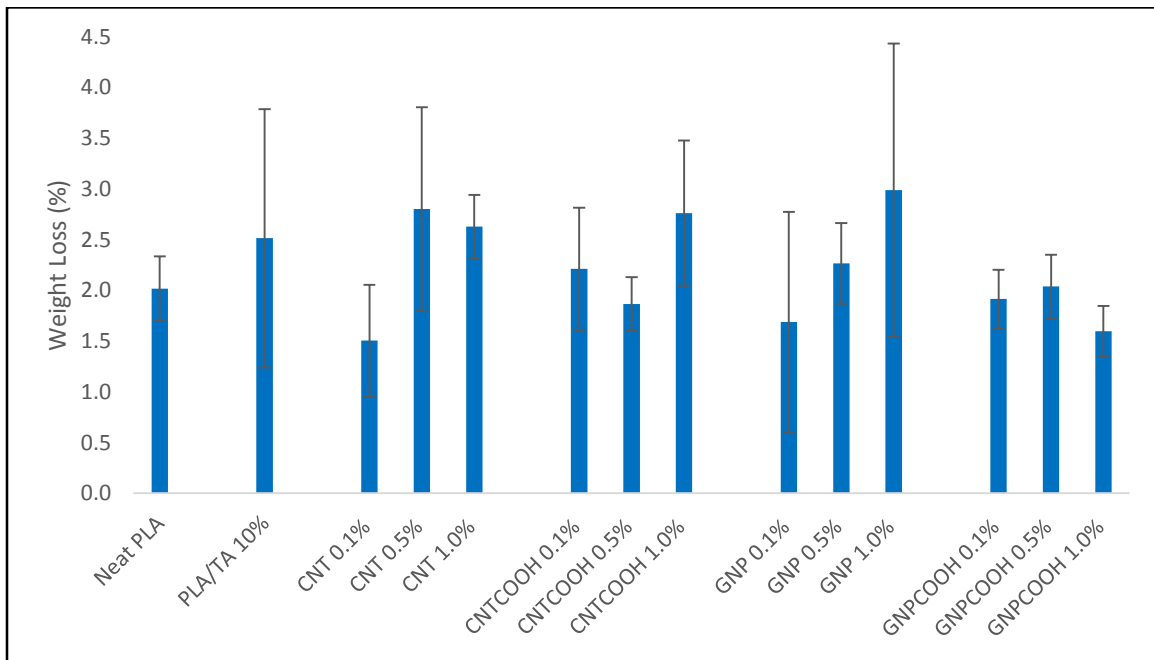
Figure 51: Percentage of weight loss for PLA/TA 10% nanocomposites after 4 months of biodegradation under natural conditions

The relative hydrophilic nature of PLA represented in its polar oxygen atoms influences PLA biodegradation. In order to reach complete biodegradation stage, the first step in decomposition process is the reduction of the molecular weight to less than 10 kDa through hydrolysis. The hydrolysis process takes place through random cleavage mechanism of the ester groups by the aid of water molecules. The hydrolyzed fragments containing lactic acid, oligomers, or other water-soluble products, which are produced from the previous

step are further degraded when consumed by microorganisms. This step results in production of water, carbon dioxide or solid biomass and are considered harmless products *(124)*. This process can be enhanced in acidic or basic media and by controlling the temperature as well as humidity.

Visual inspection showed that buried sample were wrinkled and became more brittle as compared to their original status. PLA is a biodegradable polymer with a slow degradation rate as compared to other biodegradable polymers *(125)*. The hydrolysis of the backbone bonds of PLA, which is enhanced by water absorption is the rate determining step for the biodegradation. At the end of this step, the total mass of the samples may remain largely unchanged but the molecular weight, the mechanical properties and the general integrity of the samples has diminished considerably. This step is usually followed by the absorption of the resultant small polymeric reagents into the soil or by further degradation of these segments by microorganisms.

No specific patterns were observed when different nanofillers were incorporated into PLA matrix. However, this indicated that employed nanofillers had no significant effect on the rate of biodegradation process.

4.3.2. Water Absorption Test

Figure (52) and Table (17) show the results of water absorption for PLA nanocomposites at 25 °C. Visual inspection of samples revealed that samples lost their flexibility after being immersed in distilled water for 24 hours. Hardening of samples was attributed to the hydrolysis process that took place at amorphous domains *(126, 127)*.

All the investigated samples had very low water absorption stemming from the relative low hydrophilicity of PLA. These findings were consistent with the claim that PLA products absorb very limited amounts of water. Addition of triacetin as a plasticizer increased the rate of water diffusion into the biopolymer matrix by about 138%. Although triacetin is hydrophobic, water absorption has increased due to the disruption of the triacetin molecules of the molecular arrangements of PLA, thus creating voids within the PLA matrix. These voids or free volume cavities facilitate water diffusion to the polymer matrix *(128, 129)* .
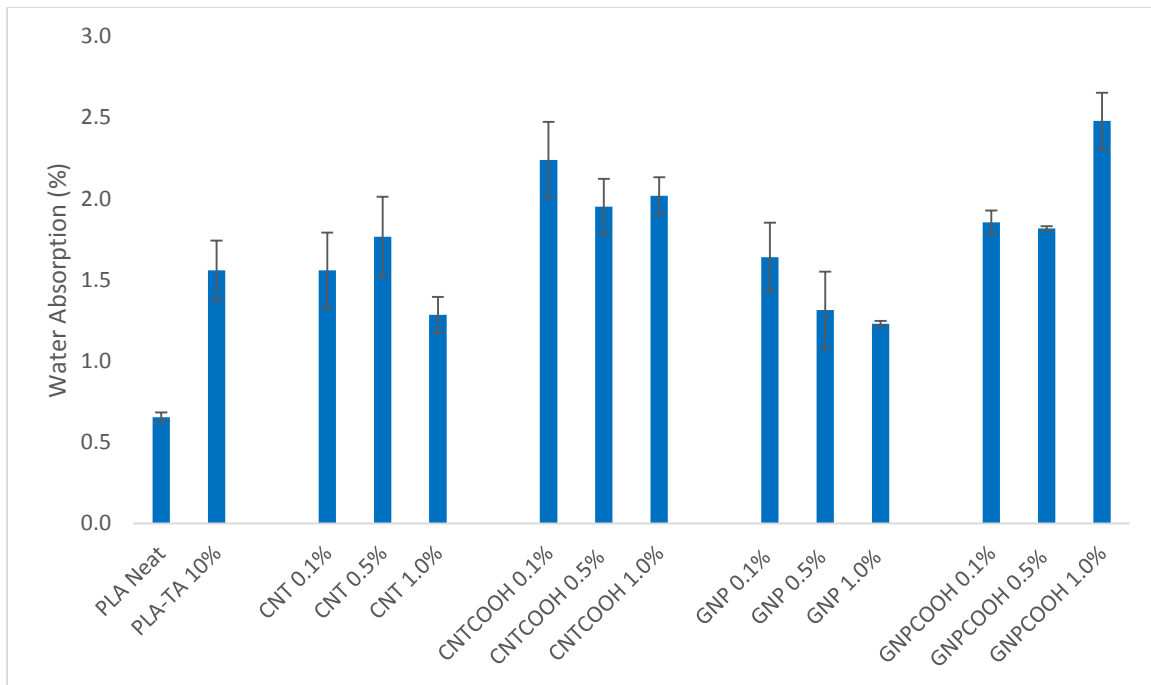
Figure 52: Percentage of water absorption for PLA/TA 10% nanocomposites at different concentrations

Incorporation of pristine CNT had slight effect on water absorption. The observed decrease in water absorption by addition of 1.0 wt% of CNT may be attributed to either the hydrophobic nature of CNT that hindered water uptake, or due to lowering the availability of PLA surface for water absorption *(95)*. Pristine GNP also exhibited the same behaviour of pristine CNT; water absorption showed slight gradual decrease with increased loadings of GNP as compared to plasticized PLA. GNP has clay-like structure; this structure created tortuous paths that hindered moisture uptake due to the high aspect ratio of GNP and enhancing the barrier properties of the nanocomposites *(130, 131)*. On the other hand, the incorporation of functionalized CNT and GNP into PLA/TA 10% matrix showed an increase in water absorption by at least 25% in case of CNTCOOH and 16% for GNPCOOH as compared to plasticized PLA because of the ability of carboxylic groups to form hydrogen bonding through intercalation with the diffused water molecules. i.e. increased the hydrophilicity of the nanofiller particles *(131)*.

Table 17: Percentage of water absorption and water absorption increase for neat PLA and PLA nanocomposites

Material	Water Absorption (%)	Water Absorption Percentage Increase Relative to Neat PLA (%)
Neat PLA	0.655 ± 0.030	N/A
PLA-TA 10%	1.559 ± 0.183	138.036
CNT 0.1%	1.559 ± 0.232	138.042
CNT 0.5%	1.767 ± 0.245	169.694
CNT 1.0%	1.285 ± 0.111	96.245
CNTCOOH 0.1%	2.239 ± 0.234	241.847
CNTCOOH 0.5%	1.952 ± 0.170	197.981
CNTCOOH 1.0%	2.018 ± 0.115	208.047
GNP 0.1%	1.639 ± 0.214	150.226
GNP 0.5%	1.315 ± 0.237	100.795
GNP 1.0%	1.229 ± 0.017	87.707
GNPCOOH 0.1%	1.854 ± 0.073	183.123
GNPCOOH 0.5%	1.818 ± 0.014	177.494
GNPCOOH 1.0%	2.479 ± 0.014	278.416

4.4. Investigation of Barrier Characteristics of the Developed Pristine and Functionalized CNT/ and GNP/ Plasticized PLA Nanocomposites as Potential Food Packaging Materials

4.4.1. Oxygen Permeability Test

For food packaging industry, it is important to have information regarding gas transmission properties in order to develop successful packaging designs for various products *(132)*. Diffusion of air oxygen to the contained food through the packaging material has a significant effect on shelf-life and food quality. Some food items such as fruits and vegetables require the presence of oxygenated atmosphere to help respiration and extend their shelf-life. On the other hand, some other food components such as lipids and vitamins may get deteriorated due to oxidation *(133, 134)*. It must be noted that using plasticizers in improving mechanical properties of polymeric packaging materials can drastically affect the oxygen barrier properties. Glycerol, polyethylene glycol, polypropylene glycol, triacetin, and triethyl citrate are common plasticizers used in food packaging. These plasticizers can incredibly enhance the desirable chain mobility in polymeric matrices. However, it must be noted that this behaviour is accompanied by an increase in oxygen permeability.

The gas permeability of polymer films is controlled by three factors: density packing, polymer chain mobility, and the free volume within the polymeric matrix. Gas permeability can be increased or decreased by introducing substituents that affect the free volumes or molecular chain packing *(135)*. As can be seen from Figure (53), neat PLA and PLA/TA 10% have oxygen permeability within the range of 950 cc.mil/m^2 .d.atm. Polystyrene (PS), polypropylene (PP), polyethylene terephthalate (PET) are known to be the most widely used polymers for food packaging industry thanks to their remarkable mechanical properties as well as their interesting barrier properties *(136)*. They are, however, petroleum based non-renewable nondegradable polymers. Table (18) lists the oxygen barrier values for these petroleum-based polymers and compares them to the result obtained for neat PLA.
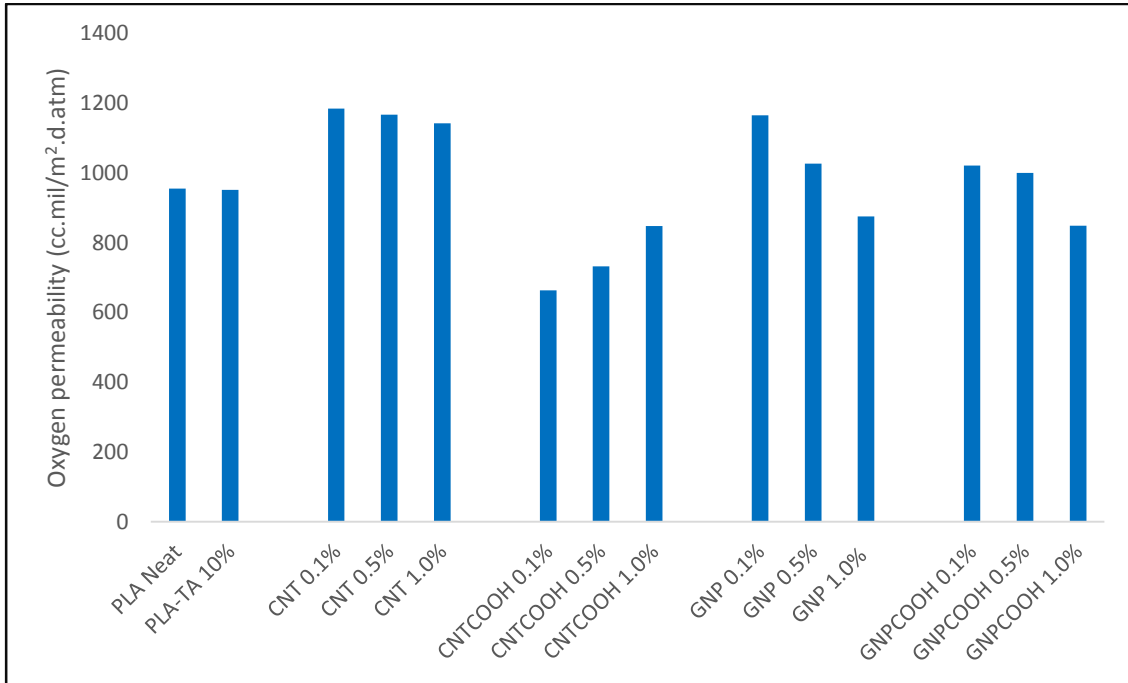
Figure 53: Oxygen permeability results for PLA/TA 10% nanocomposites at different concentrations

Table 18: Oxygen permeability for PS, PP, and PET films

Polymeric Material	Oxygen Permeation (cc.mil/m^2.d.atm)
Polystyrene (PS)	4606 - 6181
Polypropylene (PP)	2323 - 4016
Polyethylene Terephthalate (PET)	118
Poly (lactic Acid) (PLA)	955

Adding different concentrations of CNT nanofillers to plasticized PLA, caused the oxygen permeability to increase by 24.5%, 22.7%, and 20% for CNT 0.1%, CNT 0.5%, and CNT 1.0%, respectively (Table 19). This may be attributed to the nature of carbon nanotube to act as nano-tunnels with smooth interior surfaces that enhance the diffusion of oxygen molecules within the polymeric matrix. On the other hand, data listed in Table (19) showed

that increasing CNT concentration for more than 0.1% caused the oxygen permeability to decrease slightly. Such behaviour was attributed to the increased tortuous paths due to the increased entanglement of CNT at higher concentrations, which overcame the increase in gas permeability *(137)*.

Table 19: Oxygen permeability results for PLA-TA/CNT nanocomposites at different concentrations

Material	Oxygen Permeability (cc.mil/m^2.d.atm)	Percentage Increase (%)
PLA-TA 10%	951.3	N/A
CNT 0.1%	1184.4	24.5
CNT 0.5%	1167	22.7
CNT 1.0%	1142	20.0

For CNTCOOH nanocomposites, the oxygen permeability exhibited a remarkable decrease compared to plasticized PLA, Table (20). Functionalized CNTs were expected to show an increase in gas permeability as the case with CNT since both have the same tunnel structure. However, functionalized CNT possess carboxylic groups at the external surface as well as at the end caps of the nanotubes surface. It was reported that introducing functionalized groups to the terminal ends of the carbon nanotubes blocks these ends and hinders the diffusion of gases. The introduced functional groups may also have certain molecular interaction with the diffusing gaseous molecules *(138)*. It was expected that the increase in CNTCOOH would be associated with further decrease in oxygen permeability based on the aforementioned reasoning. However, higher concentrations of functionalized carbon nanotubes were accompanied by an increase in the oxygen permeability due to the aggregation of the nanofillers particles thus diminishing its barrier efficiency.

Table 20: Oxygen permeability results for PLA-TA/CNTCOOH nanocomposites at different concentrations

Material	Oxygen Permeability (cc.mil/m^2.d.atm)	Percentage Decrease (%)
PLA/TA 10%	951.3	N/A
CNTCOOH 0.1%	663	30.3
CNTCOOH 0.5%	732	23.1
CNTCOOH 1.0%	848	10.9

GNP and GNPCOOH demonstrated similar behaviours. While lower concentrations (0.1% and 0.5%) for both nanofillers displayed an increase in oxygen permeability as compared to PLA/TA 10%, 1.0% concentrations for both nanofillers exhibited a decrease in oxygen permeability as compared to plasticized PLA (Table 21). Pinto *et al.* studied the effect of incorporating GNP and graphene oxide (GO) into PLA matrix.

Table 21: Oxygen permeability results for PLA-TA/GNP and PLA-TA/GNPCOOH nanocomposites at different concentrations

Material	Oxygen Permeability (cc.mil/m^2.d.atm)	Percentage Increase (%)
PLA/TA 10%	951.3	N/A
GNP 0.1%	1165.5	22.5
GNP 0.5%	1027	8.0
GNP 1.0%	875.5	- 8.0
GNPCOOH 0.1%	1021	7.3
GNPCOOH 0.5%	1000	5.1
GNPCOOH 1.0%	848.8	- 10.8

According to their published results, they reported that both, GNP and GO displayed a decrease in oxygen permeability with different concentrations of investigated nanofillers *(103)*. Many researchers interpreted this behaviour based on the assumption that GNP and GO have a lamellar structure with high aspect ratio *(139, 140)*. This system hindered the diffusion of gaseous molecules by generating several layers structure forcing the permeating molecules to flow through a "tortuous path", and hence, decreasing gas

permeability *(139-141)*. This interpretation may apply for the results reported in this study for higher concentrations (1.0%) of GNP and GNPCOOH where oxygen permeability was observed to decrease compared to plasticized PLA. However, for lower concentrations of GNP and GNPCOOH (0.1% and 0.5%) a different mechanism is suggested. The fact that PLA exhibits both hydrophobic and hydrophilic natures based on its structure may – to some extent – decrease its compatibility with the pure hydrophobic GNP. This results in limiting the exfoliation of GNP within the plasticized PLA matrix and leading to the formation of microphase separation. Unoccupied voids are formed around the partially exfoliated GNP, allowing the gaseous molecules to diffuse through the polymeric matrix at higher rates. It was proposed that the same mechanism apply for GNPCOOH. However, the presence of carboxylic groups enhanced the formation of a network of hydrogen bonds with PLA resulting in a slight decrease in gas permeability as compared to PLA-TA/GNP nanocomposites. As mentioned above, further increase in GNP and GNPCOOH content resulted in an obvious decrease in gas permeability due to stacking of GNP and GNPCOOH lamellar structure, which created long diffusion paths due to the aforementioned tortuosity effect of the platelets nanofillers.

4.4.2. Water Vapour Transmission Rate Test (WVTR)

Measuring the barrier properties for polymer nanocomposites for food packaging applications is of great significance. It is reported in the literature that in spite of their importance, more research needs to be conducted particularly in the area of moisture barrier properties *(142)*. Moisture shortens the shelf-life of food as it is considered a detrimental factor for causing microbial infection and contamination of food *(143, 144)*. The "Barrier Property" is defined as the ability of a certain material to reduce gas as well as vapour permeability. Furthermore, water vapour transmission rate is the weight of water vapour transferred through a unit area per unit time under controlled temperature and humidity conditions *(145)*. Water vapour transmission is mainly governed by two parameters, (i) concentration gradient and (ii) vapour pressure on both surfaces of the investigated material *(108)*. Different factors such as physical structure, chemical compositions, and thickness of studied material may affect vapour transmission *(143)*. Although PLA showed many advantages, one of its main drawbacks is poor barrier properties, whether in terms of gas

permeability or water vapour transmission especially when used for food storage *(143)*. In order to improve its barrier properties, different types of nanoparticles including metal oxides, clays, cellulose nanowhiskers, CNT and many other are incorporated into PLA matrix. For example, PLA/CNT nanocomposites was reported to improve water vapour barrier properties by 200% compared to pure PLA *(70)*.

Figures (54 – 58) represent the change in weight (mg) against time (h) for the investigated samples. For all examined materials, it was observed that the gain weight has increased linearly with time. Three samples, namely, CNT 0.5, GNPCOOH 0.5 and GNPCOOH 1.0% exhibited some experimental discrepancies due to development of fine cracks at the film surface due to pressure build up inside the autoclave bottles.
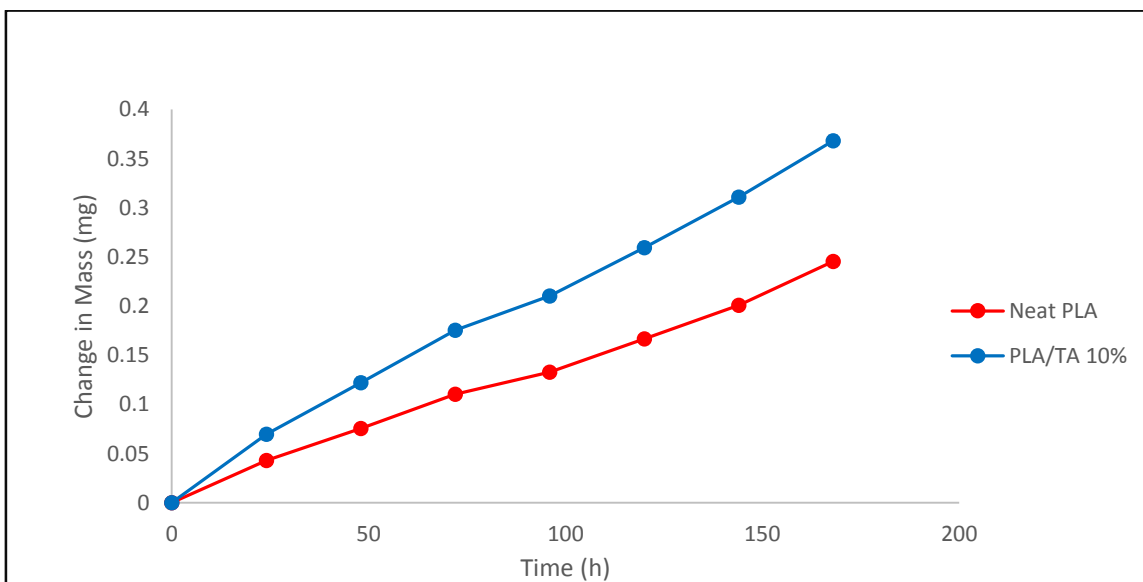
Figure 54: Water vapour transmission results for neat PLA and PLA/TA 10%

Comparing the water vapour transmission for neat PLA and PLA/TA 10% blend indicates an increase in transmission rate for plasticized PLA by about 50%. This significant increase of moisture transmission may be accounted in terms of the plasticizer effect, which instigated the creation of free volume voids within the polymeric matrix. These voids facilitated the transmission of water molecules *(143)*.

On the other hand, the incorporation of the four different types of nanofillers into plasticized PLA in this study along with different concentrations showed a remarkable decrease in water vapour transmission by at least 50%. It is worth mentioning here that the rate transmission was also found to be less than that of neat PLA (curves are not shown). The remarkable decrease in moisture transmission may be attributed to the blocking of pores found in the nanocomposites material by addition of nanofillers; this was also proved through Hg porosimetry measurements. Furthermore, the flow rate in studied sample is also dependent on the hydrophobicity of the nano-reinforcement employed. During vapour transmission, once the saturation levels are reached, water molecules start to diffuse into the other side of the film *(144)*. Since the studied nanofillers are mainly hydrophobic in nature, the process of water absorption and diffusion is normally hindered. Nielsen and Gerlowski suggested that water molecules penetrate through the nanogaps inside the material forming water molecule clusters inside the nanocomposites, and hence hindering further water molecule diffusion and resulting into lower diffusivity *(144)*.
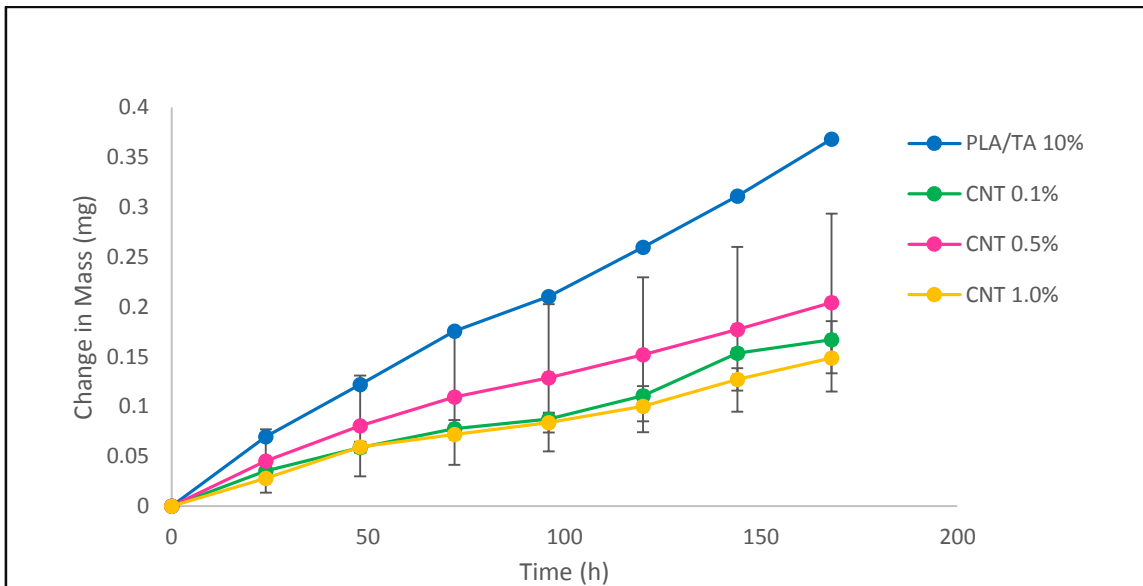
Figure 55: Water vapour transmission results for PLA-TA/CNT nanocomposites at different concentrations

Figure 56: Water vapour transmission results for PLA-TA/CNTCOOH nanocomposites at different concentrations

Figure 57: Water vapour transmission results for PLA-TA/GNP nanocomposites at different concentrations
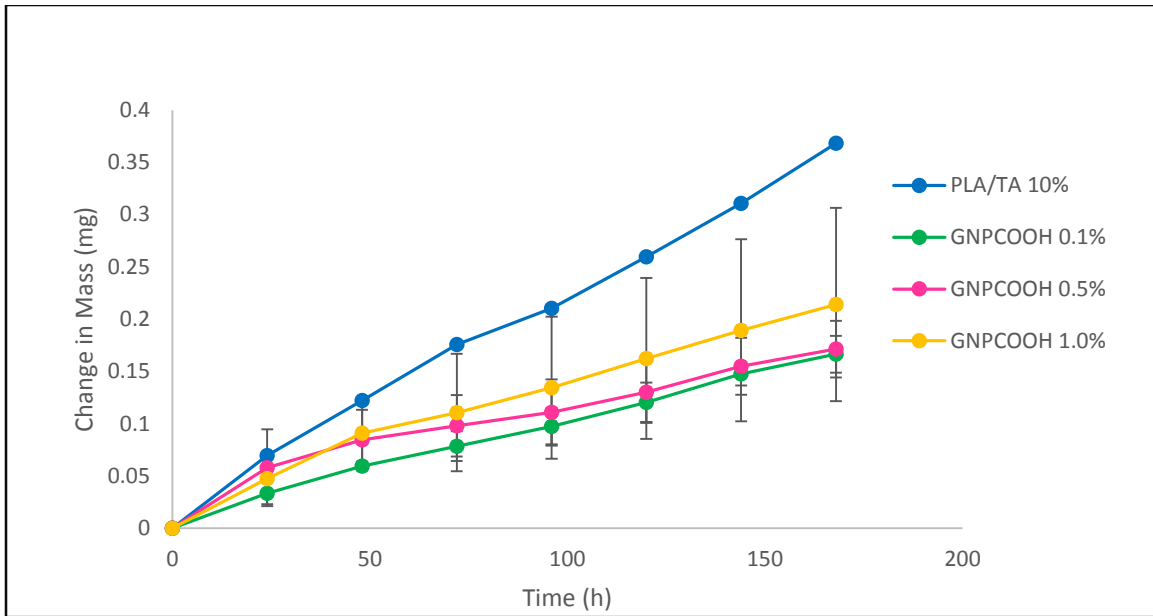
Figure 58: Water vapour transmission results for PLA-TA/GNPCOOH nanocomposites at different concentrations

5. Conclusion and Future Work

The aim of this work is to enhance the physical, chemical, and barrier properties of PLA nanocomposites. PLA is known to have desirable fea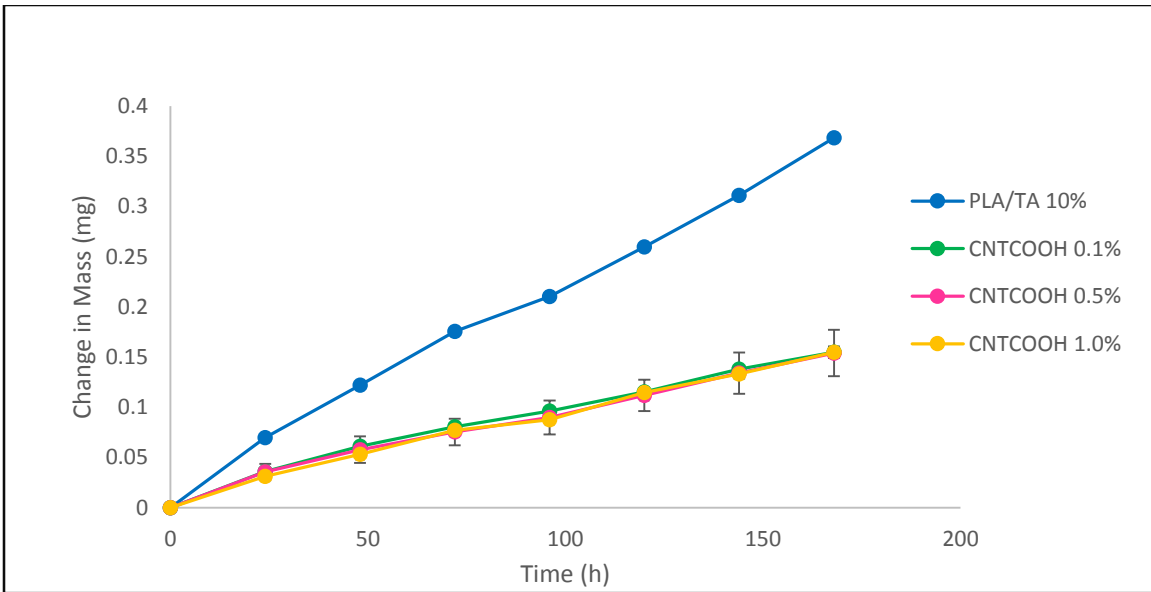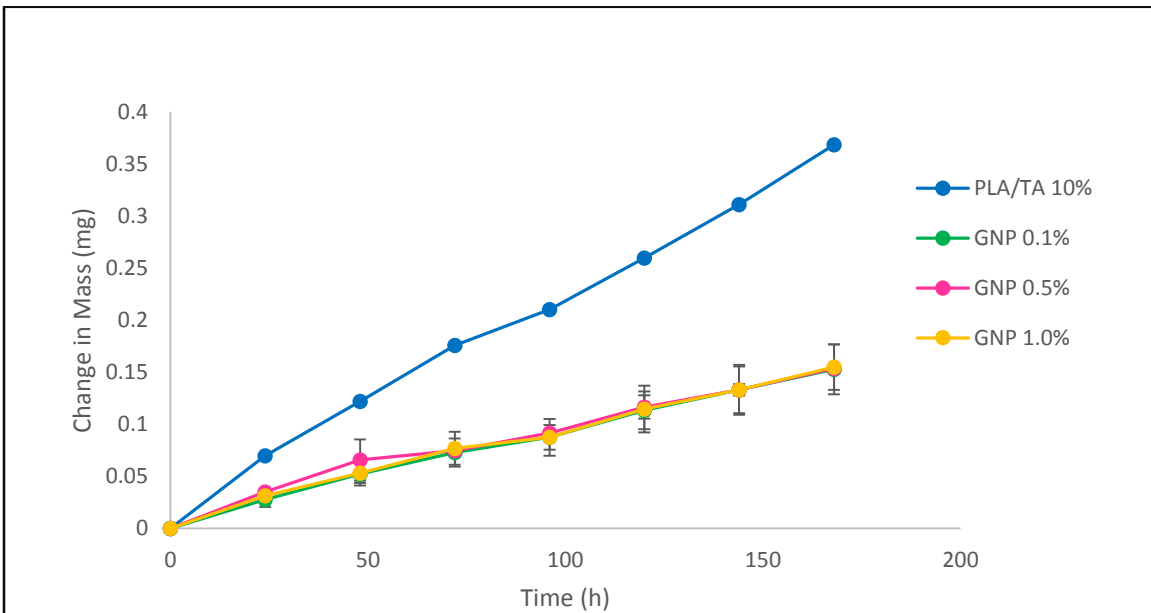tures represented in its biorenewability and biodegradability. However, the brittle nature of PLA hinders its applications, particularly in the field of food packaging where there is no tolerance for film tearing or cracking when subjected to force during manufacturing or application. Thus, the first part of this thesis entailed plasticizing PLA with different plasticizers to reach the best-plasticized system that served as the basis for the PLA nanocomposites by incorporating nanofillers into PLA matrix. The natural plasticizers in the first part included PEG, TBC, and TA. Results obtained from stress – relaxation measurements showed that PEG did not enhance the mechanical properties due to antiplasticization effect. This was also proved by the FT-IR analysis, which revealed a strong hydrogen bonding formation leading to less mobile polymeric chains. High crystallinity of PLA/PEG blends as shown by DSC measurements accounted for the stiffness of PLA prepared films. On the other hand, TBC and TA plasticizers were far more efficient in plasticizing PLA as compared to PEG. This finding was also confirmed by DSC analysis. Although TBC and TA of different concentrations have significantly enhanced the mechanical properties, only PLA/TA 10% was chosen as the base for further investigation of the effect of nano-reinforcement since TA 10% exhibited an interesting behaviour that considerably increased the toughness of the PLA matrix. This unique behaviour indicated that PLA/TA 10% would have high performance due to high energy required for breaking the samples. It is therefore recommended that PLA/TA 10% is to be employed for food packaging applications where high flexibility and toughness are required.

By incorporating nanofillers to PLA/TA 10% blends, the mechanical properties showed a high increase in nominal force associated with considerable decrease in elongation. This was mainly observed for CNT and CNTCOOH nanocomposites due to adsorption of polymeric chains to the surface of the nanofillers. On the other hand, GNP and GNPCOOH maintained the elongation to some extent as compared to that of pristine and functionalized CNT. GNPCOOH 0.5%, based on the obtained results, showed increased toughness and higher energy required to break the samples. Furthermore, it maintained the unique upturn

revealed by PLA/TA 10%. This suggested that GNPCOOH 0.5% is the best combination as compared to other nanocomposites in terms of mechanical properties. TGA analysis revealed that CNT and CNTCOOH except for CNTCOOH 1.0% have slightly enhanced the thermal stability of PLA nanocomposites. On the other hand, GNP and GNPCOOH showed no effect on thermal stability. Mercury porosimetry test showed a considerable decrease in porosity percentage when different nanofillers were incorporated. The biodegradation of PLA nanocomposites under natural conditions revealed that different nanofillers have no specific effect on the rate of PLA degradation although water absorption test showed that functionalized nanofillers showed higher water diffusion as compared to that of pristine PLA. The oxygen permeability of different nanofillers showed interesting behaviours. While CNT and lower concentrations of GNP and GNPCOOH showed an increase in oxygen permeability, CNTCOOH and higher concentrations of GNP and GNPCOOH showed a decrease in oxygen diffusion. Whether oxygen permeability has increased or decreased, both behaviours can have applications for packing different food items such as fruits and vegetables or lipid-containing food items which behave differently in presence of oxygen molecules. Water vapour transmission test also showed an enhancement in barrier properties as it was observed that the rate of moisture diffusion has been significantly decreased by the incorporation of different nanofillers.

Further studies suggested for this work include the study of the flavour/aroma/solvent molecules barrier properties and applying a grease permeability test for PLA nanocomposites. In addition, testing the antimicrobial activity of PLA nanocomposites films would address their resistance to microbial growth, and hence increase the shelf-life for food products. It is also recommended to test whether nanofillers would leach from the PLA packaging material into contained food to assess the health risk of such behaviour if ever existed. Furthermore, PLA-grafted-nanofillers nanocomposites can also be investigated to examine the effect of grafted nanofillers on the mechanical, thermal, and barrier properties in the field of food packaging.

References

1. Rochman, C. M.; Browne, M. A.; Halpern, B. S.; Hentschel, B. T.; Hoh, E.; Karapanagioti, H. K.; Rios-Mendoza, L. M.; Takada, H.; Teh, S.; Thompson, R. C. Policy: Classify plastic waste as hazardous. *Nature* **2013**, *494*, 169-171.

2. Nkwachukwu, O. I.; Chima, C. H.; Ikenna, A. O.; Albert, L. Focus on potential environmental issues on plastic world towards a sustainable plastic recycling in developing countries. *International Journal of Industrial Chemistry* **2013**, *4*, 1-13.

3. Ortega-Rivas, E. In *Protective and Preserving Food Packaging;* Non-thermal Food Engineering Operations; Springer: 2012; pp 325-336.

4. Marsh, K.; Bugusu, B. Food packaging—roles, materials, and environmental issues. *J. Food Sci.* **2007**, *72*, R39-R55.

5. Halden, R. U. Plastics and health risks. *Annu. Rev. Public Health* **2010**, *31*, 179-194.

6. Barnes, D. K.; Galgani, F.; Thompson, R. C.; Barlaz, M. Accumulation and fragmentation of plastic debris in global environments. *Philos. Trans. R. Soc. Lond. B. Biol. Sci.* **2009**, *364*, 1985-1998.

7. Gröndahl, M.; Eriksson, L.; Gatenholm, P. Material properties of plasticized hardwood xylans for potential application as oxygen barrier films. *Biomacromolecules* **2004**, *5*, 1528-1535.

8. Avérous, L.; Pollet, E. In *Biodegradable Polymers;* Avérous, L., Pollet, E., Eds.; Springer London: 2012; pp 13-39.

9. Sorrentino, A.; Gorrasi, G.; Vittoria, V. Potential perspectives of bio-nanocomposites for food packaging applications. *Trends Food Sci. Technol.* **2007**, *18*, 84-95.

10. Ghanbarzadeh, B.; Oleyaei, S. A.; Almasi, H. Nano-Structured Materials Utilized in Biopolymer based Plastics for Food Packaging Applications. *Crit. Rev. Food Sci. Nutr.* **2014**, *55*, 1699-1723.

11. Arias, V.; Höglund, A.; Odelius, K.; Albertsson, A. Polylactides with "green" plasticizers: Influence of isomer composition. *J Appl Polym Sci* **2013**, *130*, 2962-2970.

12. Khare, A.; Deshmukh, S. Studies toward producing eco-friendly plastics. *Journal of plastic film and sheeting* **2006**, *22*, 193-211.

13. Vieira, M. G. A.; da Silva, M. A.; dos Santos, L. O.; Beppu, M. M. Natural-based plasticizers and biopolymer films: A review. *European Polymer Journal* **2011**, *47*, 254-263.

14. Kawasumi, M. The discovery of polymer-clay hybrids. *Journal of Polymer Science Part A: Polymer Chemistry* **2004**, *42*, 819-824.

15. Alexandre, M.; Dubois, P. Polymer-layered silicate nanocomposites: preparation, properties and uses of a new class of materials. *Materials Science and Engineering: R: Reports* **2000**, *28*, 1-63.

16. Brody, A. L.; Bugusu, B.; Han, J. H.; Sand, C. K.; McHugh, T. H. Innovative food packaging solutions. *J. Food Sci.* **2008**, *73*, R107-R116.

17. Marsh, K.; Bugusu, B. Food Packaging—Roles, Materials, and Environmental Issues. *J. Food Sci.* **2007**, *72*, R39-R55.

18. Coles, R.; McDowell, D.; Kirwan, M. J. *Food packaging technology;* CRC Press: 2003; Vol. 5.

19. Williams, H.; Wikström, F.; Otterbring, T.; Löfgren, M.; Gustafsson, A. Reasons for household food waste with special attention to packaging. *J. Clean. Prod.* **2012**, *24*, 141-148.

20. McKown, C. In *In Containers;* Coatings on glass—technology roadmap workshop; 2000; pp 18-19.

21. Ortega-Rivas, E. In *Protective and Preserving Food Packaging;* Non-thermal Food Engineering Operations; Springer: 2012; pp 325-336.

22. Vaclavik, V. A.; Christian, E. W.; Christian, E. W. *Essentials of food science;* Springer: 2008; Vol. 42.

23. Verghese, K.; Lewis, H.; Fitzpatrick, L. *Packaging for Sustainability;* Springer Science & Business Media: 2012; .

24. Ravve, A. *Principles of polymer chemistry;* Springer Science & Business Media: 2012.

25. Wagner, M.; Oehlmann, J. Endocrine disruptors in bottled mineral water: total estrogenic burden and migration from plastic bottles. *Environmental Science and Pollution Research* **2009**, *16*, 278-286.

26. Latini, G. Monitoring phthalate exposure in humans. *Clinica Chimica Acta* **2005**, *361*, 20-29.

27. Halden, R. U. Plastics and health risks. *Annu. Rev. Public Health* **2010**, *31*, 179-194.

28. Skakkebaek, N. E.; Rajpert-De Meyts, E.; Main, K. M. Testicular dysgenesis syndrome: an increasingly common developmental disorder with environmental aspects. *Hum. Reprod.* **2001***, 16*, 972-978.

29. Rahman, M.; Brazel, C. S. The plasticizer market: an assessment of traditional plasticizers and research trends to meet new challenges. *Progress in Polymer Science* **2004***, 29*, 1223-1248.

30. Elango, A.; Shepherd, B.; Chen, T. T. Effects of endocrine disrupters on the expression of growth hormone and prolactin mRNA in the rainbow trout pituitary. *Gen. Comp. Endocrinol.* **2006***, 145*, 116-127.

31. Kamrin, M. A. Bisphenol A: a scientific evaluation. *MedGenMed : Medscape general medicine* **2004***, 6*, 7.

32. Maffini, M. V.; Rubin, B. S.; Sonnenschein, C.; Soto, A. M. Endocrine disruptors and reproductive health: The case of bisphenol-A. *Mol. Cell. Endocrinol.* **2006***, 254*, 179-186.

33. David K. A. Barnes; Galgani, F.; Thompson, R. C.; Barlaz, M. Accumulation and fragmentation of plastic debris in global environments. *Philosophical Transactions of the Royal Society B: Biological Sciences* **2009***, 364*, 1985-1998.

34. Derraik, J. G. B. The pollution of the marine environment by plastic debris: a review. *Marine Pollution Bulletin* **2002***, 44*, 842-852.

35. Eriksen, M.; Maximenko, N.; Thiel, M.; Cummins, A.; Lattin, G.; Wilson, S.; Hafner, J.; Zellers, A.; Rifman, S. Plastic pollution in the South Pacific subtropical gyre. *Mar. Pollut. Bull.* **2013***, 68*, 71-76.

36. Thompson, R. C.; Moore, C. J.; Frederick S. vom Saal; Swan, S. H. Plastics, the environment and human health: current consensus and future trends. *Philosophical Transactions of the Royal Society B: Biological Sciences* **2009***, 364*, 2153-2166.

37. Garlotta, D. A Literature Review of Poly (Lactic Acid). *Journal of Polymers and the Environment* **2001***, 9*, 63-84.

38. Gregory, M. R. Environmental implications of plastic debris in marine settings—entanglement, ingestion, smothering, hangers-on, hitch-hiking and alien invasions. *Philosophical Transactions of the Royal Society B: Biological Sciences* **2009***, 364*, 2013-2025.

39. Mato, Y.; Isobe, T.; Takada, H.; Kanehiro, H.; Ohtake, C.; Kaminuma, T. Plastic resin pellets as a transport medium for toxic chemicals in the marine environment. *Environ. Sci. Technol.* **2001***, 35*, 318-324.

40. Ashton, K.; Holmes, L.; Turner, A. Association of metals with plastic production pellets in the marine environment. *Mar. Pollut. Bull.* **2010**, *60*, 2050-2055.

41. Andrady, A. L. Microplastics in the marine environment. *Mar. Pollut. Bull.* **2011**, *62*, 1596-1605.

42. Teuten, E. L.; Saquing, J. M.; Detlef R. U. Knappe; Barlaz, M. A.; Jonsson, S.; Björn, A.; Rowland, S. J.; Thompson, R. C.; Galloway, T. S.; Yamashita, R.; Ochi, D.; Watanuki, Y.; Moore, C.; Viet, P. H.; Tana, T. S.; Prudente, M.; Boonyatumanond, R.; Zakaria, M. P.; Akkhavong, K.; Ogata, Y.; Hirai, H.; Iwasa, S.; Mizukawa, K.; Hagino, Y.; Imamura, A.; Saha, M.; Takada, H.; Linköpings universitet; Institutionen för tema; Tema vatten i natur och samhälle; Filosofiska fakulteten Transport and release of chemicals from plastics to the environment and to wildlife. *Philosophical Transactions of the Royal Society B: Biological Sciences* **2009**, *364*, 2027-2045.

43. Zhou, Q. Degradation of polylactic acid in the presence of microsize and nanosize fillers, ProQuest, UMI Dissertations Publishing, 2008.

44. Avérous, L.; Pollet, E. In *Biodegradable polymers;* Environmental Silicate Nano-Biocomposites; Springer: 2012; pp 13-39.

45. Najafi Chaloupi, N. Development of polylactide-clay nanocomposites for food packaging applications, ProQuest, UMI Dissertations Publishing, 2012.

46. Rasal, R. M.; Janorkar, A. V.; Hirt, D. E. Poly(lactic acid) modifications. *Progress in Polymer Science* **2010**, *35*, 338-356.

47. Vieira, M. G. A.; da Silva, M. A.; dos Santos, L. O.; Beppu, M. M. Natural-based plasticizers and biopolymer films: A review. *European Polymer Journal* **2011**, *47*, 254-263.

48. Ren, J.; SpringerLink (Online service) *Biodegradable Poly(Lactic Acid): Synthesis, Modification, Processing and Applications;* Springer Berlin Heidelberg: Berlin, Heidelberg, 2011; .

49. Labrecque, L. V.; Kumar, R. A.; Dav, V.; Gross, R. A.; McCarthy, S. P. Citrate esters as plasticizers for poly(lactic acid). *J Appl Polym Sci* **1997**, *66*, 1507-1513.

50. Arias, V.; Höglund, A.; Odelius, K.; Albertsson, A.; KTH; Skolan för kemivetenskap (CHE); Fiber- och polymerteknik Polylactides with "green" plasticizers: Influence of isomer composition. *J Appl Polym Sci* **2013**, *130*, 2962-2970.

51. Białecka-Florjańczyk, E.; Florjańczyk, Z. In *Solubility of Plasticizers, Polymers and Environmental Pollution-Chapter 22;* Elsevier B.V: 2007; pp 397-408.

52. Menczel, J. D.; Prime, R. B. *Thermal analysis of polymers: fundamentals and applications;* John Wiley: Hoboken, N.J, 2009.

53. Cao, N.; Yang, X.; Fu, Y. Effects of various plasticizers on mechanical and water vapor barrier properties of gelatin films. *Food Hydrocoll.* **2009**, *23*, 729-735.

54. Cheng, L. H.; Karim, A. A.; Seow, C. C. Effects of Water-Glycerol and Water-Sorbitol Interactions on the Physical Properties of Konjac Glucomannan Films. *J. Food Sci.* **2006**, *71*, E62-E67.

55. Baltacioğlu, H.; Balköse, D. Effect of zinc stearate and/or epoxidized soybean oil on gelation and thermal stability of PVC-DOP plastigels. *J Appl Polym Sci* **1999**, *74*, 2488-2498.

56. Vanstrom, J. R. Mechanical characterization of commercial biodegradable plastic films, ProQuest, UMI Dissertations Publishing, 2012.

57. Dicker, M. P. M.; Duckworth, P. F.; Baker, A. B.; Francois, G.; Hazzard, M. K.; Weaver, P. M. Green composites: A review of material attributes and complementary applications. *Composites Part A* **2014**, *56*, 280.

58. Gruber, P. R. Cargill Dow LLC. *J. Ind. Ecol.* **2003**, *7*, 209-213.

59. Martin, O.; Avérous, L. Poly(lactic acid): plasticization and properties of biodegradable multiphase systems. *Polymer* **2001**, *42*, 6209-6219.

60. Ljungberg, N.; Wesslén, B.; Kemiska institutionen; Gemensamma institutioner för naturvetenskapliga och tekniska fakulteterna; Common departments, the faculties of Science and Engineering; Polymer and Materials Chemistry (LTH); Department of Chemistry; Center for Chemistry and Chemical Engineering; Lunds universitet; Kemicentrum; Polymer- och Materialkemi (LTH); Lund University The effects of plasticizers on the dynamic mechanical and thermal properties of poly(lactic acid). *J Appl Polym Sci* **2002**, *86*, 1227-1234.

61. Ljungberg, N.; Andersson, T.; Wesslén, B.; Kemiska institutionen; Gemensamma institutioner för naturvetenskapliga och tekniska fakulteterna; Common departments, the faculties of Science and Engineering; Polymer and Materials Chemistry (LTH); Department of Chemistry; Center for Chemistry and Chemical Engineering; Lunds universitet; Kemicentrum; Polymer- och Materialkemi (LTH); Lund University Film extrusion and film weldability of poly(lactic acid) plasticized with triacetine and tributyl citrate. *J Appl Polym Sci* **2003**, *88*, 3239-3247.

62. Ljungberg, N.; Wesslén, B.; Kemiska institutionen; Gemensamma institutioner för naturvetenskapliga och tekniska fakulteterna; Common departments, the faculties of Science and Engineering; Polymer and Materials Chemistry (LTH); Department of Chemistry; Center for Chemistry and Chemical Engineering; Lunds universitet;

Kemicentrum; Polymer- och Materialkemi (LTH); Lund University Tributyl citrate oligomers as plasticizers for poly (lactic acid): thermo-mechanical film properties and aging. *Polymer* **2003**, *44*, 7679-7688.

63. Ljungberg, N.; Wesslén, B.; Kemiska institutionen; Gemensamma institutioner för naturvetenskapliga och tekniska fakulteterna; Common departments,the faculties of Science and Engineering; Polymer and Materials Chemistry (LTH); Department of Chemistry; Center for Chemistry and Chemical Engineering; Lunds universitet; Kemicentrum; Polymer- och Materialkemi (LTH); Lund University Tributyl citrate oligomers as plasticizers for poly (lactic acid): thermo-mechanical film properties and aging. *Polymer* **2003**, *44*, 7679-7688.

64. Hassouna, F.; Raquez, J.; Addiego, F.; Dubois, P.; Toniazzo, V.; Ruch, D. New approach on the development of plasticized polylactide (PLA): Grafting of poly(ethylene glycol) (PEG) via reactive extrusion. *European Polymer Journal* **2011**, *47*, 2134-2144.

65. Choi, K.; Choi, M.; Han, D.; Park, T.; Ha, C. Plasticization of poly(lactic acid) (PLA) through chemical grafting of poly(ethylene glycol) (PEG) via in situ reactive blending. *European Polymer Journal* **2013**, *49*, 2356-2364.

66. Neethirajan, S.; Jayas, D. S. Nanotechnology for the Food and Bioprocessing Industries. *Food and Bioprocess Technology* **2011**, *4*, 39-47.

67. Sozer, N.; Kokini, J. L. Nanotechnology and its applications in the food sector. *Trends Biotechnol.* **2009**, *27*, 82-89.

68. Falguera, V.; Quintero, J. P.; Jiménez, A.; Muñoz, J. A.; Ibarz, A. Edible films and coatings: Structures, active functions and trends in their use. *Trends Food Sci. Technol.* **2011**, *22*, 292-303.

69. Sekhon, B. S. Food nanotechnology - an overview. *Nanotechnology, science and applications* **2010**, *3*, 1.

70. Azeredo, H. M. C. d. Nanocomposites for food packaging applications. *Food Res. Int.* **2009**, *42*, 1240-1253.

71. Baksi, S.; Biswas, S. Nanocomposites–An Overview. *THE SCITECH JOURNAL* **2014**, *1*.

72. Alexandre, M.; Dubois, P. Polymer-layered silicate nanocomposites: preparation, properties and uses of a new class of materials. *MATERIALS SCIENCE & ENGINEERING R-REPORTS* **2000**, *28*, 1-63.

73. Arora, A.; Padua, G. W. Review: nanocomposites in food packaging. *J. Food Sci.* **2010**, *75*, R43-R49.

74. Rhim, J.; Lee, J.; Hong, S. Increase in water resistance of paperboard by coating with poly(lactide). *Packaging Technology and Science* **2007**, *20*, 393-402.

75. Zhao, R.; Torley, P.; Halley, P. J. Emerging biodegradable materials: starch- and protein-based bio-nanocomposites. *J. Mater. Sci.* **2008**, *43*, 3058-3071.

76. Moon, S.; Jin, F.; Lee, C.; Tsutsumi, S.; Hyon, S. In *In Novel Carbon Nanotube/Poly (L-lactic acid) Nanocomposites; Their Modulus, Thermal Stability, and Electrical Conductivity;* Macromolecular symposia; Wiley Online Library: 2005; Vol. 224, pp 287-296.

77. Sinha Ray, S. *Clay-Containing Polymer Nanocomposites;* Elsevier: 2013.

78. Choudhary, V.; Gupta, A. Polymer/carbon nanotube nanocomposites. *Carbon Nanotubes-Polymer Nanocomposites* **2011**, 65-90.

79. Balasubramanian, K.; Burghard, M. Chemicaly functionalized carbon nanotubes. *Small (Weinheim an der Bergstrasse, Germany)* **2005**, *1*, 180.

80. Breuer, O.; Sundararaj, U. Big Returns From Small Fibers: A Review of Polymer/Carbon Nanotube Composites. *Polymer Composites* **2004**, *25*, 630-645.

81. Sathyanarayana, S.; Hübner, C. Thermoplastic Nanocomposites with Carbon Nanotubes. *Structural Nanocomposites: Perspectives for Future Applications* **2013**, 19-60.

82. Hussain, F.; Hojjati, M.; Okamoto, M.; Gorga, R. E. Review article: Polymer-matrix Nanocomposites, Processing, Manufacturing, and Application: An Overview. *J. Composite Mater.* **2006**, *40*, 1511-1575.

83. Zhang, D.; Kandadai, M. A.; Cech, J.; Roth, S.; Curran, S. A. Poly(L-lactide) (PLLA)/multiwalled carbon nanotube (MWCNT) composite: characterization and biocompatibility evaluation. *The journal of physical chemistry.B* **2006**, *110*, 12910.

84. Kobashi, K.; Villmow, T.; Andres, T.; Pötschke, P. Liquid sensing of melt-processed poly (lactic acid)/multi-walled carbon nanotube composite films. *Sensors Actuators B: Chem.* **2008**, *134*, 787-795.

85. Bourbigot, S.; Fontaine, G.; Gallos, A.; Bellayer, S. Reactive extrusion of PLA and of PLA/carbon nanotubes nanocomposite: processing, characterization and flame retardancy. *Polym. Adv. Technol.* **2011**, *22*, 30-37.

86. Kuan, C.; Kuan, H.; Ma, C. M.; Chen, C. Mechanical and electrical properties of multi-wall carbon nanotube/poly (lactic acid) composites. *Journal of Physics and Chemistry of Solids* **2008**, *69*, 1395-1398.

87. Kuan, C.; Kuan, H.; Chen, C.; Lin, K.; Chiang, C.; Peng, H. Multi-walled carbon nanotube reinforced poly (l-lactic acid) nanocomposites enhanced by water-crosslinking reaction. *Journal of Physics and Chemistry of Solids* **2008***, 69*, 1399-1402.

88. Wu, D.; Wu, L.; Zhou, W.; Zhang, M.; Yang, T. Crystallization and biodegradation of polylactide/carbon nanotube composites. *Polymer Engineering & Science* **2010***, 50*, 1721-1733.

89. Kim, H.; Chae, Y. S.; Kwon, H. I.; Yoon, J. Thermal degradation behaviour of multi-walled carbon nanotube-reinforced poly(L-lactide) nanocomposites. *Polym. Int.* **2009***, 58*, 826-831.

90. Dong, Q.; Li, Y.; Han, C.; Zhang, X.; Xu, K.; Zhang, H.; Dong, L. Poly(l-lactide)/poly(d-lactide)/multiwalled carbon nanotubes nanocomposites: Enhanced dispersion, crystallization, mechanical properties, and hydrolytic degradation. *J Appl Polym Sci* **2013***, 130*, 3919-3929.

91. Mai, F.; Habibi, Y.; Raquez, J.; Dubois, P.; Feller, J.; Peijs, T.; Bilotti, E. Poly/carbon nanotube nanocomposites with integrated degradation sensing. *Polymer* **2013***, 54*, 6818.

92. Wu, L.; Wu, D.; Zhang, M.; Zhao, Y. Viscoelasticity and thermal stability of polylactide composites with various functionalized carbon nanotubes. *Polym. Degrad. Stab.* **2008***, 93*, 1577-1584.

93. Mina, M. F.; Beg, M. D.; Islam, M. R.; Nizam, Abu KMM Alam A; Younus, R. M. Characterization of Biodegradable Nanocomposites with Poly (Lactic Acid) and Multi-Walled Carbon Nanotubes. *World Academy of Science, Engineering and Technology* **2013***, 73*, 1019-1024.

94. Mina, M. F.; Beg, M. D. H.; Islam, M. R.; Nizam, A.; Alam, A. K. M. M.; Yunus, R. M. Structures and properties of injection-molded biodegradable poly(lactic acid) nanocomposites prepared with untreated and treated multiwalled carbon nanotubes. *Polymer Engineering & Science* **2014***, 54*, 317-326.

95. Chrissafis, K.; Paraskevopoulos, K. M.; Jannakoudakis, A.; Beslikas, T.; Bikiaris, D. Oxidized multiwalled carbon nanotubes as effective reinforcement and thermal stability agents of poly(lactic acid) ligaments. *J Appl Polym Sci* **2010***, 118*, 2712-2721.

96. Potts, J. R.; Dreyer, D. R.; Bielawski, C. W.; Ruoff, R. S. Graphene-based polymer nanocomposites. *Polymer* **2011***, 52*, 5-25.

97. Chieng, B. W.; Ibrahim, N. A.; Wan Yunus, W. M. Z.; Hussein, M. Z.; Loo, Y. Y. Effect of graphene nanoplatelets as nanofiller in plasticized poly(lactic acid)

nanocomposites: Thermal properties and mechanical properties. *Journal of Thermal Analysis and Calorimetry* **2014***, 118*, 1551-1559.

98. Kuilla, T.; Bhadra, S.; Yao, D.; Kim, N. H.; Bose, S.; Lee, J. H. Recent advances in graphene based polymer composites. *Progress in Polymer Science* **2010***, 35*, 1350-1375.

99. Narimissa, E.; Gupta, R. K.; Choi, H. J.; Kao, N.; Jollands, M. Morphological, mechanical, and thermal characterization of biopolymer composites based on polylactide and nanographite platelets. *Polymer Composites* **2012***, 33*, 1505-1515.

100. Kim, I.; Jeong, Y. G. Polylactide/exfoliated graphite nanocomposites with enhanced thermal stability, mechanical modulus, and electrical conductivity. *Journal of Polymer Science Part B: Polymer Physics* **2010***, 48*, 850-858.

101. Pinto, A. M.; Cabral, J.; Tanaka, D. A. P.; Mendes, A. M.; Magalhães, F. D. Effect of incorporation of graphene oxide and graphene nanoplatelets on mechanical and gas permeability properties of poly(lactic acid) films. *Polym. Int.* **2013***, 62*, 33-40.

102. Pinto, A. M.; Moreira, S.; Gonçalves, I. C.; Gama, F. M.; Mendes, A. M.; Magalhães, F. D. Biocompatibility of poly (lactic acid) with incorporated graphene-based materials. *Colloids and Surfaces B: Biointerfaces* **2013***, 104*, 229-238.

103. Pinto, A. M. Effect of biodegradation on PLA/graphene-nanoplatelets composites mechanical properties and biocompatibility.

104. Chieng, B. W.; Ibrahim, N. A.; Yunus, W. M. Z. W.; Hussein, M. Z.; Giita Silverajah, V. S. Graphene Nanoplatelets as Novel Reinforcement Filler in Poly(lactic acid)/Epoxidized Palm Oil Green Nanocomposites: Mechanical Properties. *International journal of molecular sciences* **2012***, 13*, 10920-10934.

105. Chieng, B.; Ibrahim, N.; Yunus, W.; Hussein, M. Poly(lactic acid)/Poly(ethylene glycol) Polymer Nanocomposites: Effects of Graphene Nanoplatelets. *Polymers* **2013***, 6*, 93-104.

106. Chieng, B. W.; Ibrahim, N. A.; Wan Md Zin Wan Yunus; Hussein, M. Z.; Then, Y. Y.; Loo, Y. Y. Effects of Graphene Nanoplatelets and Reduced Graphene Oxide on Poly(lactic acid) and Plasticized Poly(lactic acid): A Comparative Study. *Polymers* **2014***, 6*, 2232-2246.

107. Li, X.; Xiao, Y.; Bergeret, A.; Longerey, M.; Che, J. Preparation of polylactide/graphene composites from liquid-phase exfoliated graphite sheets. *Polymer Composites* **2014***, 35*, 396-403.

108. Pankaj, S.; Bueno-Ferrer, C.; Misra, N.; O'Neill, L.; Jimenez, A.; Bourke, P.; Cullen, P. Characterization of polylactic acid films for food packaging as affected by

dielectric barrier discharge atmospheric plasma. *INNOVATIVE FOOD SCIENCE & EMERGING TECHNOLOGIES* **2014***, 21*, 107-113.

109. Grigale-Sorocina, Z.; Kalnins, M.; Dzene, A.; Tupureina, V. Biodegradable Plasticized Poly (lactic acid) Films. *Rigas Tehniskas Universitates Zinatniskie Raksti* **2010***, 21*, 97.

110. Felton, L. A.; McGinity, J. W. *Aqueous polymeric coatings for pharmaceutical dosage forms;* CRC Press: 2008.

111. Madkour, T.; Hagag, F.; Mamdouh, W.; Azzam, R. Molecular-level modeling and experimental investigation into the high performance nature and low hysteresis of thermoplastic polyurethane/multi-walled carbon nanotube nanocomposites. *Polymer* **2012***, 53*, 5788-5797.

112. Cui, M.; Liu, L.; Guo, N.; Su, R.; Ma, F. Preparation, Cell Compatibility and Degradability of Collagen-Modified Poly(lactic acid). *MOLECULES* **2015***, 20*, 595-607.

113. El-Hadi, A. M. The effect of additives interaction on the miscibility and crystal structure of two immiscible biodegradable polymers. *Polímeros* **2014***, 24*, 9-16.

114. Alcantar, N. A.; Aydil, E. S.; Israelachvili, J. N. Polyethylene glycol–coated biocompatible surfaces. *J. Biomed. Mater. Res.* **2000***, 51*, 343-351.

115. Xiong, X.; Yi, C.; Han, Q.; Shi, L.; Li, S. I2/ionic liquid as a highly efficient catalyst for per-O-acetylation of sugar under microwave irradiation. *Chinese Journal of Catalysis* **2015***, 36*, 237-243.

116. Yuksel, N.; Baykara, M.; Shirinzade, H.; Suzen, S. Investigation of triacetin effect on indomethacin release from poly(methyl methacrylate) microspheres: Evaluation of interactions using FT-IR and NMR spectroscopies. *Int. J. Pharm.* **2011***, 404*, 102-109.

117. Mina, M. F.; Beg, M. D.; Islam, M. R.; Nizam, Abu KMM Alam A; Younus, R. M. Characterization of Biodegradable Nanocomposites with Poly (Lactic Acid) and Multi-Walled Carbon Nanotubes.

118. Ahmed, J.; Varshney, S. K.; Auras, R.; Hwang, S. W. Thermal and Rheological Properties of L-Polylactide/Polyethylene Glycol/Silicate Nanocomposites Films. *J. Food Sci.* **2010***, 75*, N97-N108.

119. Kulinski, Z.; Piorkowska, E. Crystallization, structure and properties of plasticized poly(l-lactide). *Polymer* **2005***, 46*, 10290-10300.

120. Nijenhuis, A.; Colstee, E.; Grijpma, D.; Pennings, A. High molecular weight poly (L-lactide) and poly (ethylene oxide) blends: Thermal characterization and physical properties. *Polymer* **1996***, 37*, 5849-5857.

121. Pötschke, P.; Andres, T.; Villmow, T.; Pegel, S.; Brünig, H.; Kobashi, K.; Fischer, D.; Häussler, L. Liquid sensing properties of fibres prepared by melt spinning from poly(lactic acid) containing multi-walled carbon nanotubes. *Composites Sci. Technol.* **2010***, 70*, 343-349.

122. Murariu, M.; Dechief, A. L.; Bonnaud, L.; Paint, Y.; Gallos, A.; Fontaine, G.; Bourbigot, S.; Dubois, P. The production and properties of polylactide composites filled with expanded graphite. *Polym. Degrad. Stab.* **2010***, 95*, 889-900.

123. Cao, Y.; Feng, J.; Wu, P. Preparation of organically dispersible graphene nanosheet powders through a lyophilization method and their poly(lactic acid) composites. *Carbon* **2010***, 48*, 3834-3839.

124. Ndazi, B. S.; Polymerteknologi; Skolan för kemivetenskap (CHE); KTH; Fiber- och polymerteknik Characterization of hydrolytic degradation of polylactic acid/rice hulls composites in water at different temperatures. *eXPRESS Polymer Letters* **2011***, 5*, 119-131.

125. Yuzay, I. E.; Auras, R.; Soto-Valdez, H.; Selke, S. Effects of synthetic and natural zeolites on morphology and thermal degradation of poly(lactic acid) composites. *Polym. Degrad. Stab.* **2010***, 95*, 1769-1777.

126. Ndazi, B. S.; Polymerteknologi; Skolan för kemivetenskap (CHE); KTH; Fiber- och polymerteknik Characterization of hydrolytic degradation of polylactic acid/rice hulls composites in water at different temperatures. *eXPRESS Polymer Letters* **2011***, 5*, 119-131.

127. Ndazi, B. S.; Polymerteknologi; Skolan för kemivetenskap (CHE); KTH; Fiber- och polymerteknik Characterization of hydrolytic degradation of polylactic acid/rice hulls composites in water at different temperatures. *eXPRESS Polymer Letters* **2011***, 5*, 119-131.

128. Tsou, C.; Suen, M.; Yao, W.; Yeh, J.; Wu, C.; Tsou, C.; Chiu, S.; Chen, J.; Wang, R.; Lin, S.; Hung, W.; De Guzman, M.; Hu, C.; Lee, K. Preparation and Characterization of Bioplastic-Based Green Renewable Composites from Tapioca with Acetyl Tributyl Citrate as a Plasticizer. *Materials* **2014***, 7*, 5617-5632.

129. Zhu, J.; Li, X.; Huang, C.; Chen, L.; Li, L. Plasticization effect of triacetin on structure and properties of starch ester film. *Carbohydr. Polym.* **2013***, 94*, 874.

130. Lee, J. H.; Lee, J. H.; Rhee, K. Y. Effects of moisture absorption and surface modification using 3-aminopropyltriethoxysilane on the tensile and fracture

characteristics of MWCNT/epoxy nanocomposites. *Appl. Surf. Sci.* **2010**, *256*, 7658-7667.

131. Kim, H.; Whisler, D.; Chen, Z.; Bisagni, C.; Kawai, M.; Krueger, R. *Proceedings of the American Society for Composites 2014-Twenty-ninth Technical Conference on Composite Materials;* DEStech Publications, Inc: 2014; .

132. Yuniarto, K.; Welt, B. A.; PURWANTO, A.; Purwadaria, H. K.; Abdellatief, A.; Sunarti, T. C.; Purwanto, S. Effect of Plasticizer on Oxygen Permeability of Cast Polylactic acid (PLA) Films Determined using Dynamic Accumulation Method. *Journal of Applied Packaging Research* **2014**, *6*, 5.

133. Ghanbarzadeh, B.; Oromiehie, A. R.; Musavi, M.; Falcone, P. M.; D-Jomeh, Z. E.; Rad, E. R. Study of mechanical properties, oxygen permeability and AFM topography of zein films plasticized by polyols. *Packaging Technology and Science* **2007**, *20*, 155-163.

134. Sothornvit, R.; Krochta, J. Plasticizer effect on oxygen permeability of β-lactoglobulin films. *J. Agric. Food Chem.* **2000**, *48*, 6298-6302.

135. Ge, L.; Zhu, Z.; Li, F.; Liu, S.; Wang, L.; Tang, X.; Rudolph, V. Investigation of Gas Permeability in Carbon Nanotube (CNT)− Polymer Matrix Membranes via Modifying CNTs with Functional Groups/Metals and Controlling Modification Location. *The Journal of Physical Chemistry C* **2011**, *115*, 6661-6670.

136. Fukushima, K.; Fina, A.; Geobaldo, F.; Venturello, A.; Camino, G. Properties of poly(lactic acid) nanocomposites based on montmorillonite, sepiolite and zirconium phosphonate. *EXPRESS POLYMER LETTERS* **2012**, *6*, 914-926.

137. Kim, S.; Pechar, T. W.; Marand, E. Poly(imide siloxane) and carbon nanotube mixed matrix membranes for gas separation. *Desalination* **2006**, *192*, 330-339.

138. co-giovannigolemme; Mariagiovannabuonomenna *Advanced Materials for Membrane Preparation;* Bentham Science Publishers: US, 2012.

139. Kuila, T.; Bose, S.; Mishra, A. K.; Khanra, P.; Kim, N. H.; Lee, J. H. Effect of functionalized graphene on the physical properties of linear low density polyethylene nanocomposites. *Polym. Test.* **2012**, *31*, 31-38.

140. Kwon, K.; Chang, J. -. Comparison of the properties of polyimide nanocomposites containing three different nanofillers: organoclay, functionalized graphene, and organoclay/functionalized graphene complex. *J. Composite Mater.* **2014**.

141. Kim, H.; Miura, Y.; Macosko, C. W. Graphene/polyurethane nanocomposites for improved gas barrier and electrical conductivity. *Chemistry of Materials* **2010**, *22*, 3441-3450.

142. Kim, J.; Hu, C.; Woo, R. S. C.; Sham, M. Moisture barrier characteristics of organoclay–epoxy nanocomposites. *Composites Sci. Technol.* **2005**, *65*, 805-813.

143. Abdulkhani, A.; Hosseinzadeh, J.; Ashori, A.; Dadashi, S.; Takzare, Z. Preparation and characterization of modified cellulose nanofibers reinforced polylactic acid nanocomposite. *Polym. Test.* **2014**, *35*, 73-79.

144. Bhatia, A.; Gupta, R.; Bhattacharya, S.; Choi, H. Analysis of Gas Permeability Characteristics of Poly(Lactic Acid)/Poly(Butylene Succinate) Nanocomposites. *JOURNAL OF NANOMATERIALS* **2012**, *2012*.

145. Shogren, R. Water vapor permeability of biodegradable polymers. *J. Environ. Polymer Degradation* **1997**, *5*, 91-95.